24 Fluorescence Correlation Spectroscopy

In the previous chapter we described fluorescence imaging and spectroscopy on single molecules. Individual fluorophores can be studied if the observed volume is restricted and the fluorophores are immobilized on a surface. With present technology it is difficult to track freely diffusing single molecules. Single-molecule detection (SMD) on surfaces is a powerful technique because it avoids ensemble averaging and allows single events to be observed. If a dynamic process such as a chemical reaction is being studied, there is no need to synchronize the population because the individual kinetic events can be observed. However, SMD has its limitations. The most stable fluorophores typically emit 10^5 to 10^6 photons prior to irreversible photodestruction. Because of the modest detection efficiency of optical systems, and the need for high emissive rates for detection of the emission over background, single molecules can only be observed for a brief period of time—1 second or less—which may be too short to observe many biochemical processes. When the fluorophore is bleached the experiment must be started again with a different molecule. Additionally, SMD requires immobilization on a surface, which can affect the functioning of the molecule and slow its access to substrates and/or ligands because of unstirred boundary layers near the surface.

Fluorescence correlation spectroscopy (FCS) is also a method based on observation of a single molecule or several molecules. In contrast to SMD, FCS does not require surface immobilization and can be performed on molecules in solution. The observed molecules are continuously replenished by diffusion into a small observed volume. FCS thus allows continuous observation for longer periods of time and does not require selection of specific molecules for observation. FCS is based on the analysis of time-dependent intensity fluctuations that are the result of some dynamic process, typically translation diffusion into and out of a small volume defined by a focused laser beam and a confocal aperture. When the fluorophore diffuses into a focused light beam, there is a burst of emitted photons due to multiple excitation-emission cycles from the same fluorophore. If the fluorophore diffuses rapidly out of the volume the photon burst is short lived. If the fluorophore diffuses more slowly the photon burst displays a longer duration. Under typical conditions the fluorophore does not undergo photobleaching during the time it remains in the illuminated volume, but transitions to the triplet state frequently occur. By correlation analysis of the time-dependent emission, one can determine the diffusion coefficient of the fluorophore. In this case "time-dependent" refers to the actual time and not to a time delay or time-dependent decay following pulsed excitation.

FCS has many applications because a wide variety of processes can result in intensity fluctuations. In addition to translation diffusion, intensity fluctuations can occur due to ligand–macromolecule binding, rotational diffusion, internal macromolecule dynamics, intersystem crossing, and excited-state reactions. The data are interpreted in terms of correlation functions. Different equations are needed to describe each process, and usually two or more processes affect the data at the same time. It is also necessary to account for the size and shape of the observed volume. As a result the theory and equations for FCS are rather complex.

FCS was first described in the early 1970s in a series of classic papers.[1–4] An extensive description of FCS and its applications can be found in a recent monograph.[5] These papers describe the theory for FCS and recognize its potential for measurement of diffusion and reaction kinetics. The theory showed that FCS would allow measurement of kinetic constants even when the system was in equilibrium, if the reversible process caused spectral changes. The FCS data will contain information on the reaction rates because a reaction at equilibrium still proceeds in both directions, so that the spectral properties will continue to fluctuate. However, the early FCS measurements were plagued by low sig-

nal-to-noise (S/N) ratios for a variety of reasons, including a large number of observed molecules, intensity changes in the laser light sources, low-quantum-yield fluorophores, and low-efficiency detectors.[6] In contrast to fluorescence intensity measurements, where it is easier to measure solutions with higher fluorophore concentrations, FCS measurements are best performed when observing a small number of fluorophores (<10). In order to detect a small number of fluorophores with a focused laser beam the sample needed to be dilute, typically near 1 nM. Since the samples are diluted, the unwanted background due to fluorescent impurities and scatter needed to be suppressed by confocal optics and effective filtering. Because of all these requirements FCS was not widely used for 20 years. By the early 1990s a number of technical advances made FCS a practical technology, including confocal optics, high-efficiency avalanche photodiode (APD) detectors, stable lasers, and multiphoton excitation and commercially available instruments.[6] As a result there has been a rapid increase in the applications of FCS to biochemical analysis.[7–16] FCS is now being used to detect protein association reactions, DNA hybridization, immunoassays, binding to membrane receptors, gene expression, and diffusion of labeled intracellular proteins, to name a few.

24.1. PRINCIPLES OF FLUORESCENCE CORRELATION SPECTROSCOPY

FCS is typically performed using freely diffusing molecules. Excitation is usually accomplished with a laser focused to a diffraction-limited spot. A confocal pinhole is used to reject signal from outside the desired volume. Using these optical conditions, the observed volume is an ellipsoid that is elongated along the optical axis. The concentration of the fluorophores needs to be in a range where just a few molecules are present in the observed volume.

To illustrate the principle of FCS consider a cylindrical volume 0.08 μm in diameter and 2 μm in length (Figure 24.1) that is slightly larger than for a typical FCS instrument. The volume of this cylinder is 1 fl = 10^{-15} liters. If the fluorophore concentration is 1 nM, then the observed volume contains an average of 0.6 molecules. The average number of fluorophores in the volume is determined by the bulk concentration and remains constant in a stationary experiment. However, random diffusion of the fluorophores results in time-dependent changes, called fluctuations, in the number of fluorophores in the volume. Fluctuations in occupancy number in this small volume result in intensity

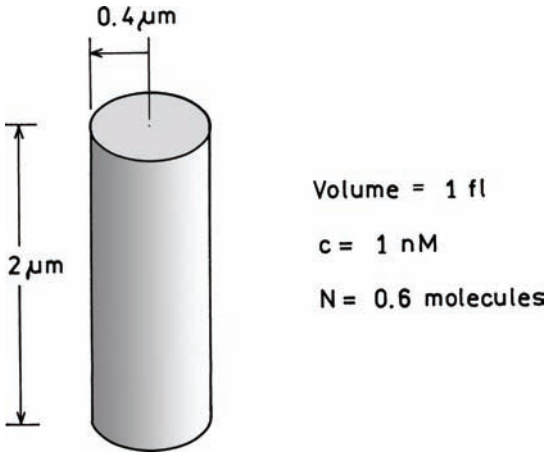

Figure 24.1. Typical volume in an FCS experiment.

fluctuations in the fluorescence intensity. The theory for FCS provides the basis for extracting molecular information from the molecules by analysis of the rates and amplitudes of the intensity fluctuations.

The theory of FCS is based on Poisson statistics. For random discrete events the number of fluorophores in the volume can be described by the Poisson distribution

$$P(n,N) = \frac{N^n}{n!}e^{-N} \qquad (24.1)$$

In this expression $P(n,N)$ is the probability of n fluorophores being present in the volume when the average number of molecules in the volume is N. Using eq. 24.1 one can calculate that for $N = 0.6$ there is a 55% probability that the volume contains no fluorophores, a 33% probability that the volume contains 1 fluorophore, and a 10% probability that the volume contains 2 fluorophores (Figure 24.2). The fluorescence intensity from this volume will fluctuate as the fluorophores diffuse into and out of the volume.

The changes in occupation number of the volume will result in changes in the intensity (Figure 24.3). If the diffusion is slow the fluorophores will move slowly into and out of the volume. If the diffusion is faster the occupation number and intensity will change more rapidly. This time-dependent intensity is analyzed statistically to determine the amplitude and frequency distribution of fluctuations. The intensity at a given time $F(t)$ is compared with the intensity at a slightly later time $F(t + \tau)$. If diffusion is slow, $F(t)$ and $F(t + \tau)$ are likely to be similar (top panel). If diffusion is fast, $F(t)$ and $F(t + \tau)$ are likely to be different (lower

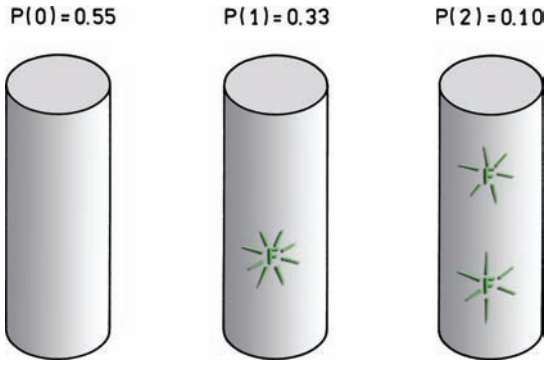

Figure 24.2. Poisson distribution of a 1-nM fluorophore solution in a 1-fl volume, $N = 0.6$.

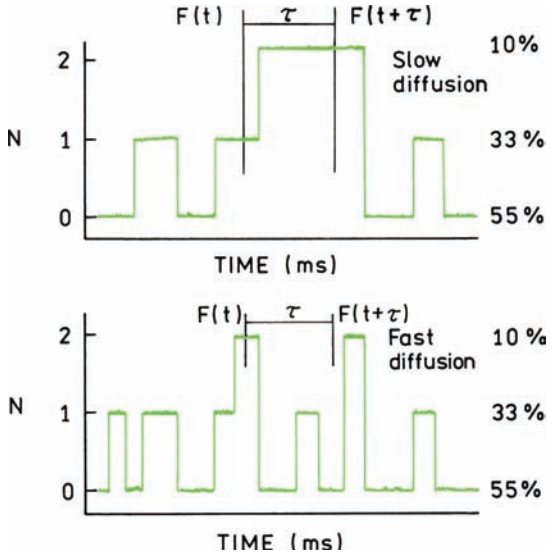

Figure 24.3. Fluctuations in the number of fluorophores (N) in the observed volume of 1 fl with $c = 1$ nM. The intensity axis is in units of the intensity from a single fluorophore.

panel). In an FCS instrument a dedicated correlation board is usually used to calculate the correlation between $F(t)$ and $F(t + \tau)$ for a range of delay times τ. This results in an autocorrelation function $G(\tau)$ that contains information on the diffusion coefficient and occupation number of the observed volume. The dependence of the correlation function on the rate of diffusion makes FCS valuable for measuring a wide range of binding interactions, such as protein–ligand binding and DNA hybridization. Note that the correlation time τ in an FCS measurement is not related to the lifetime of the fluorophore.

An important feature of FCS is a measurement of the number of diffusing species in the observed volume. In principle, this measurement does not rely on an external calibration or the quantum yields of the fluorophores. In practice, calibrations are performed using known solutions. The important point is the amplitude of the autocorrelation function at $\tau = 0$ reveals the average number of molecules being observed. Sometimes a proportionality constant is used to adjust this number. FCS can thus be used to detect changes in particle density due to association or cleavage reactions. In contrast to single molecule detection, the observed molecules are continually replaced by diffusion, so that photobleaching is less of a problem. Additionally, since only a few molecules are observed, FCS provides high sensitivity. Intensity fluctuations can also occur due to blinking of the fluorophores upon transition to the triplet state, structural changes in biomolecules, and the rate of lateral translation in flowing samples. There are also more advanced types of FCS, such as dual-color cross-correlation FCS, which selectively detects species that contain two fluorophores, such as DNA oligomers labeled with two different fluorophores.

FCS can provide information about reaction kinetics even when the reaction is in equilibrium. Consider a simple reaction $F + M \rightleftharpoons F^*M$, where F is a fluorophore that is nonfluorescent in solution but fluorescent (F^*) when bound to a macromolecule (M). The reaction kinetics would usually be studied by starting the reaction from a nonequilibrium condition, such as mixing separate solutions of F and M in a stopped-flow instrument. Upon mixing the intensity would change as the reaction approached equilibrium. When the reaction reaches equilibrium the fluorescence intensity will remain constant and no additional information is obtained by continuing to measure the intensity. In contrast, FCS can measure the reaction kinetics under equilibrium conditions. If a small number of molecules are observed the intensity will fluctuate as the fluorophore binds to and dissociates from the macromolecules. The rate of intensity fluctuations contains information on the sum of the forward and reverse reaction rates.

Because of the ability of FCS to determine the number of observed particles, and to determine the rates of diffusion, and other dynamic processes, there has been a rapid expansion of FCS technology into a wide range of applications, including high-throughput screening, DNA analysis, and detection of small numbers of intracellular species. In the following section we describe the theory and practice of FCS with examples to illustrate the potential of this technology.

24.2. THEORY OF FCS

The equations for FCS are moderately complex, and there are many subtle points that result from the unique aspects of the measurements. Different authors use slightly different terminology for FCS. Hence it is valuable to review the theory to provide a basis for understanding the data and the factors that influence the measured correlation functions.

The autocorrelation function of the fluorescence intensity is given by the product of the intensity at time t, $F(t)$, with the intensity after a delay time τ, $F(t + \tau)$, averaged over a large number of measurements.[17–21] The time t refers to the actual time as the intensities are observed. Data collection times range from seconds to minutes. The delay time τ is the difference in real time between measurement of $F(t)$ and $F(t+ \tau)$, typically in the range from 10^{-2} to 10^{2} ms. If the intensity fluctuations are slow compared to τ, then $F(t)$ and $F(t+ \tau)$ will be similar in magnitude. That is, if $F(t)$ is larger than the average intensity $<F>$, then $F(t + \tau)$ is likely to be larger than $<F>$. If the intensity fluctuations are fast relative to τ, then the value of $F(t)$ and $F(t + \tau)$ will not be related. The value of the autocorrelation for a time delay τ is given by the average value of the products

$$R(\tau) = <F(t)F(t + \tau)>$$

$$= \frac{1}{T}\int_0^T F(t)F(t + \tau)dt \qquad (24.2)$$

where T is the data accumulation time. The factor $1/T$ normalizes the value of the products $F(t)F(t + \tau)$ for the data accumulation time. This mathematical process is typically performed using dedicated correlation boards that perform the needed operations in real time as the fluctuating intensity is observed. With modern electronics it is now also possible to record the time (t)-dependent intensities for the duration of the data collection (T) and then perform the calculations. Additional information can be obtained from the complete list of time-dependent intensities, so it seems likely that this approach will eventually be standard in FCS experiments.

The quantities of interest are the fluctuations in $F(t)$ around the mean value

$$\delta F(t) = <F> - F(t) \qquad (24.3)$$

The autocorrelation function for the fluorescence intensities, normalized by average intensity squared, is given by

$$G'(\tau) = \frac{<F(t)F(t + \tau)>}{<F><F>}$$

$$= 1 + \frac{<\delta F(0)\delta F(\tau)>}{<F>^2} \qquad (24.4)$$

In this expression we have replaced t with 0. The delay time τ is always relative to a datapoint at an earlier time so that only the difference τ is relevant. It is important to remember the meaning of t and τ in FCS, which is different from their meaning in time-resolved fluorescence. In time-resolved fluorescence t refers to the time after the excitation pulse and τ refers to the decay time. In FCS t refers to real time and τ refers to a time difference between two intensity measurements. In the FCS literature there are occasional inaccuracies in the words used to describe the correlation functions in eqs. 24.2 and 24.4. Equation 24.2 is the autocorrelation function of the fluorescence intensities. The term $\delta F(t)$ in eq. 24.3 is the variance, so that the last term on the right side of eq. 24.4 is actually the autocovariance of $F(t)$, but is conventionally referred to as the "autocorrelation function." A more accurate term is "the autocorrelation function of the fluorescence fluctuations."[17] Another confusing point is the definition of the autocorrelation function. Some authors use eq. 24.4 and other authors use

$$G(\tau) = \frac{<\delta F(0)\delta F(\tau)>}{<F>^2} \qquad (24.5)$$

which is the autocorrelation function of fluorescence fluctuations. We will use eq. 24.5 since this avoids inclusion of one (1) in all the subsequent equations. For simplicity we will refer to eq. 24.5 as the correlation or autocorrelation function.

In order to interpret the FCS data we need a theoretical model to describe the fluctuations. The data are typically the number of photon counts in a given time interval, typically about a microsecond, which are due to a small number of fluorophores. The intensity is dependent on the number of photons detected from each fluorophore in a given period of time. For FCS it is convenient to use a parameter called the brightness, which is given by

$$B = q\sigma Q \qquad (24.6)$$

where q is the quantum efficiency for detection of the emitted photons, σ is the cross-section for absorption, and Q is the quantum yield for emission of the fluorophore. The brightness is the number of photons per second for a single fluorophore observed for a given set of optical conditions. Unlike the quantum yield, the brightness is not a molecular property of the fluorophore, but depends on the precise optical conditions including the light intensity, light collection efficiency of the instrument, and the counting efficiency of the detector. The measured intensity from the sample, typically in kHz, is given by the integral of the fluorophore concentration over the observed volume:

$$F(t) = B \int \mathrm{CEF}(r) I(r) C(r,t) dV \qquad (24.7)$$

In this expression CEF(r) is the collection efficiency function of the instrument as a function of position (r). The integral extends over the entire observed space. The position r is more properly described as a vector ($\vec{r}$) but for simplicity we assume r is a vector. The excited fluorophores will be distributed in a three-dimensional volume, in the x-y plane and along the optical z-axis. $I(r)$ is the excitation intensity at each position r, and $C(r,t)$ is the distribution of fluorophores. Equation 24.7 looks complex, but it has a simple meaning. The intensity depends on the concentration and spatial distribution of the excitation and detection efficiency, and the brightness of the fluorophores. The observed intensity also depends on the excited and observed volumes, which is accounted for by the integral. It is usually not necessary to consider these factors separately, so that the instrument is described as having a detection profile:

$$p(r) = \mathrm{CEF}(r) I(r) = \mathrm{MDE}(r) \qquad (24.8)$$

which is also referred to as the molecular detection efficiency MDE(r).

Figure 24.4 shows a typical FCS instrument. A laser is focused on the sample. The emission is selected with a dichroic filter. The out-of-focus light is rejected with a pinhole, which is typically large enough to pass all light from a region slightly larger than the illuminated spot.[10] The intensity profile of the focused laser is assumed to be Gaussian. For this configuration, the brightness profile can be approximated by a three-dimensional Gaussian (Figure 24.5):

$$p(r) = I_0 \exp\left[-2(x^2 + y^2)/s^2\right] \exp(-2z^2/u^2) \qquad (24.9)$$

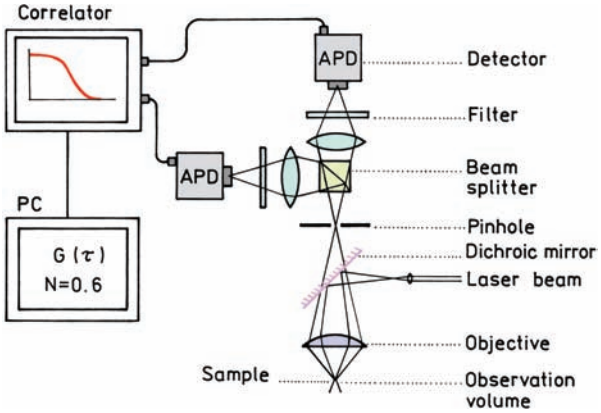

Figure 24.4. Typical instrumentation for FCS. Revised from [17].

The surface of the volume is not sharply defined. The radius s and half-length u refer to distances at which the profile decreases to e^{-2} of its maximal value I_0.

Equation 24.7 gives the time-dependent intensity. We now need to calculate the autocorrelation function due to concentration fluctuations throughout the observed volume. This function is more complex than for a fluorophore diffusing in and out of a volume with a sharp boundary (Figure 24.1). As the fluorophore diffuses it enters regions where the count rate per fluorophore is higher or lower

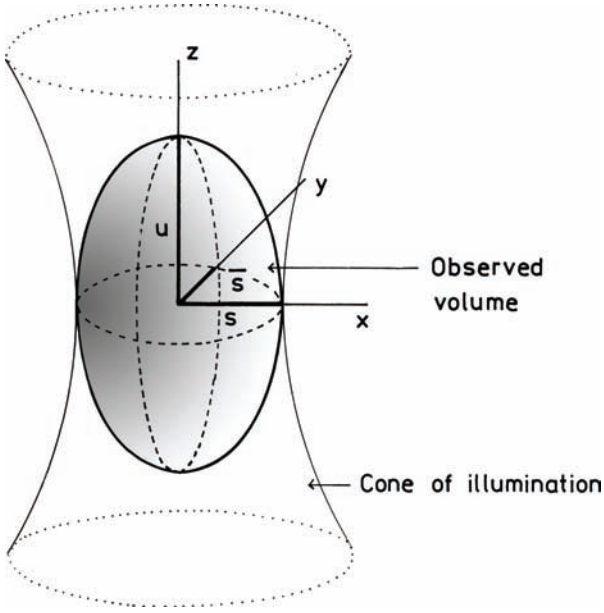

Figure 24.5. Ellipsoidal observed volume with focused single photon excitation and confocal detection.

based on the detection profile $p(r)$. The autocorrelation function for the intensity fluctuation is given by

$$G(\tau) = \frac{B^2 \int\int p(r)p(r') <\delta C(r,0)\delta C(r',\tau)> dV d'V}{\left[BC\int p(r)dV\right]^2} \quad (24.10)$$

where r is the position of the fluorophore at $t = 0$ and r' is its position at $t = \tau$. This formidable expression can be understood as follows. The denominator contains the average intensity, which is given by the product of the brightness B, mean concentration C, and the detection profile of the instrument integrated over the observed volume. The concentration term and brightness appear outside the integral because Q is independent of position, and only the average concentration is needed to calculate the average intensity. The detection profile $p(r)$ accounts for the excitation and detection efficiency. The numerator calculates the intensity fluctuations from the concentration fluctuations at each point in the sample, which is then integrated over the observed volume. When the fluorophore moves from r to a new location r', its brightness becomes proportional to the detection profile at this position $p(r')$. The integral extends over the observed volume for all the fluorophores present in the volume. The term B^2 is again outside the integral because the intrinsic brightness of the fluorophore does not depend on position. Remarkably, the correlation function (but not the S/N ratio) is independent of fluorophore brightness, which cancels in eq. 24.10. This makes sense because we are measuring the correlation between fluorophore locations, which should not depend on the brightness of the fluorophore.

It is instructive to consider the number of fluorophores in a typical FCS experiment. A diffraction-limited volume will typically have a diameter of 0.5 µm and a total length of 2 µm. For this size and shape the effective volume is 0.35 fl. The effective volume is not equal to the geometric volume of an ellipsoid because the detection profile does not have sharp boundaries. Figure 24.6 shows calculations of the number of fluorophores in this volume. Occupation numbers of 2 to 20 are expected for fluorophore concentrations from 9.6 to 96 nM. The width of the distribution is given by $\sqrt{N}$ and increases with the occupation number, as characteristic for a Poisson distribution.

Equation 24.10 is not limited to diffusion and can be used to derive a correlation function for any process that results in the intensity fluctuations. Chemical or photochemical processes that change the brightness of a fluorophore can also be studied. In place of $\delta C(r,\tau)$ eq. 24.10 is then used with a different r' model to derive the expected autocorrelation function.

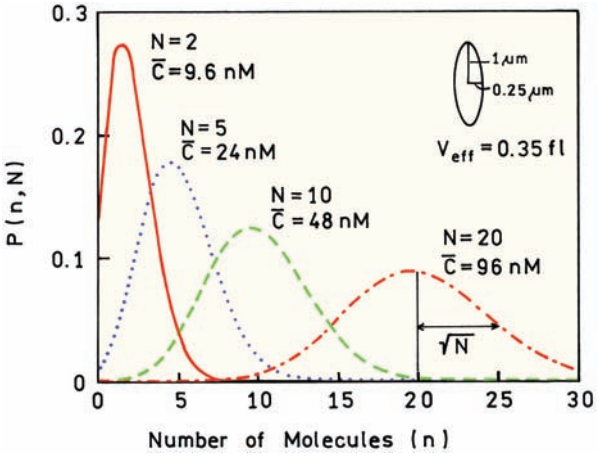

Figure 24.6. Poisson distribution in an ellipsoidal volume for various fluorophore concentrations. The volume of a geometric ellipsoid with $s = 0.25$ µm and $u = 1.0$ µm is 0.26 fl.

24.2.1. Translational Diffusion and FCS

Perhaps the most common application of FCS is to measure translational diffusion. The rate of diffusion depends on the size of the molecule and its interactions with other molecules. The correlation function for diffusion in three dimensions is given by[18]

$$<\delta C(r,0)\delta C(r',\tau)>$$

$$= \bar{C}(4\pi D\tau)^{3/2}\exp\left[-|r - r'|^2/4D\tau\right] \quad (24.11)$$

where D is the diffusion coefficient. Insertion of eq. 24.11 in 24.10, using the Gaussian detection profile (eq. 24.9) and some complex mathematics, yields the correlation function for three-dimensional diffusion:

$$G(\tau) = G(0)\left(1 + \frac{4D\tau}{s^2}\right)^{-1}\left(1 + \frac{4D\tau}{u^2}\right)^{-1/2}$$

$$= G(0)D(\tau) \quad (24.12)$$

where $G(0)$ is the amplitude at $\tau = 0$. For future convenience we define $D(\tau)$ as the portion of the correlation function

which contains the diffusion coefficient. This expression is also written as

$$G(\tau) = G(0)\left(1 + \frac{\tau}{\tau_D}\right)^{-1}\left(1 + \left(\frac{s}{u}\right)^2 \frac{\tau}{\tau_D}\right)^{-1/2}$$

$$= G(0)D(\tau) \qquad (24.13)$$

where the diffusion time is

$$\tau_D = s^2/4D \qquad (24.14)$$

The origin of eq. 24.14 is understood by recalling that the mean distance a molecule diffuses in a time τ is proportional to $\sqrt{D\tau}$. The form of eq. 24.12 is a result of the shape of the detection profile (eq. 24.9) being integrated with the concentration correlation function. Different detection profiles will result in different forms of eq. 24.12.

Figure 24.7 shows the correlation functions expected for a single freely diffusing species, that is, a homogeneous population, with diffusion coefficients ranging from 10^{-5} to 10^{-7} cm^2/s. We assumed the observed volume was an ellipsoid with radius $s = 0.25$ µm and half-length $u = 1$ µm. The correlation function $G(\tau)$ is usually plotted using a logarithmic τ axis. The amplitude of $G(\tau)$ decreases as τ increases. $G(\tau)$ approaches zero because at long times the fluorophores have no memory of their initial position. The value of τ_D is usually determined by least-squares fitting of the simulated curve with the measured data. A diffusion coefficient of 10^{-6} cm^2/s results in $\tau_D = 0.156$ ms. As the diffusion coefficient decreases the correlation function shifts to longer τ values, which reflects slower intensity fluctuations as the fluorophores diffuse more slowly into and out of the observed volume. As we will discuss below, a 100-fold change in diffusion coefficient would require a 10,000-fold change in molecular weight, so that the curves in Figure 24.7 are more shifted than is typical in an FCS experiment. The autocorrelation function is also expected to depend on the fluorophore concentration.

The autocorrelation function is that it provides a measurement of the average number of molecules N in the observed volume, even if the bulk concentration is not known. The number of molecules is given by the inverse of the intercept at $\tau = 0$, $G(0) = 1/N$. Hence the amplitude of the correlation function is larger for a smaller number of molecules. This is the reason why FCS was relatively unused in the 1970s and 1980s. Without confocal optics to

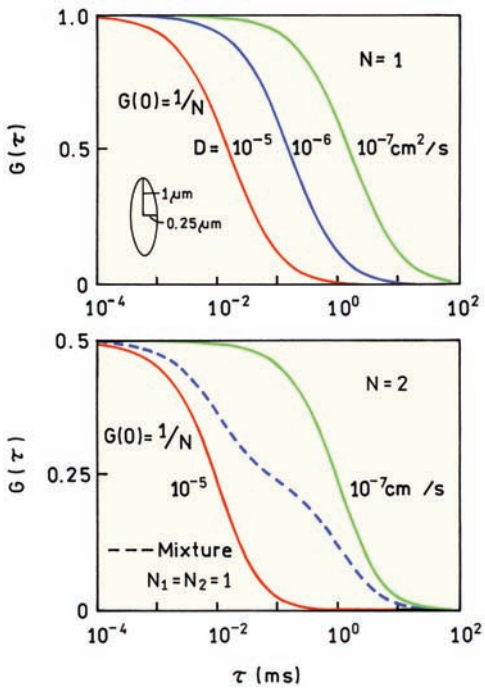

Figure 24.7. Simulated autocorrelation functions for diffusion in three dimensions (eq. 24.12) for diffusion coefficients of 10^{-5} to 10^{-7} cm^2/s (top) and for a mixture of two diffusing species (bottom). The observed volume was assumed to be an ellipsoid with $s = 0.25$ µm and $u = 1$ µm.

reduce the observed volume the number of molecules was large and the amplitudes of the correlation functions were too small for reliable measurements, even with long data acquisition times. Another important feature of $G(\tau)$ for a single species is that $G(\tau)$ does not depend on the brightness of the fluorophore. The brightness B affects the S/N of the measurement and the ability to see the fluorophore over the background. However, the correlation function itself is independent of the brightness and $G(0)$ depends only on the average number of observed fluorophores.

At first glance it is difficult to see from eqs. 24.5 and 24.10 why the value of $G(0)$ is equal to $1/N$. Since N is proportional to $\bar{c}$ the denominator contains a factor N^2. The numerator also has two concentration terms as a product, suggesting a factor of N^2 in the numerator. However, for a Poisson distribution the variance is proportional to the square root of the mean, so that δC is proportional to $\sqrt{N}$. Hence the numerator contains a factor N, and the ratio gives $G(0) = 1/N$.

One might think that if $G(\tau)$ reveals the number of fluorophores then it should be possible to determine the fluorophore concentration. This is only partially correct. The

number of fluorophores in the effective volume observed by the instrument is given by

$$N = \overline{C} V_{\text{eff}} \tag{24.15}$$

If V_{eff} was precisely known then $\overline{c}$ could be calculated. In FCS we have an estimate of V_{eff}, but we do not know an exact volume. The effective volume is dependent on the exact shape of the detection function $p(r)$. If the observed volume is described by 24.9 then

$$V_{\text{eff}} = \pi^{3/2} s^2 u \tag{24.16}$$

This effective volume is different from the geometric volume of an ellipsoid, which is given by $(4/3)\pi s^2 u$. For the ellipsoid shown in Figure 24.7 the effective volume is $V_{\text{eff}} =$ 0.35 fl and the geometric volume is 0.26 fl. The effective volume is different for other shapes, such as for a flat cylinder, a highly elongated volume, or when using two-photon excitation. While the shape of V_{eff} is not known precisely the number of observed fluorophores is known. For this reason volume is defined in an unusual way. The value of V_{eff} is that volume which contains N fluorophores at a known concentration.

It is also important to understand the meaning of τ_D obtained from the autocorrelation function. The diffusion coefficient D is a molecular property with a defined value that is independent of any instrumental parameters. Since τ_D depends on D one is inclined to think that τ_D is also a molecular parameter and independent of the instrument. However, τ_D depends on the radius of the observed volume. This means that the recovered value of D depends on accurate knowledge of the shape of V_{eff}. For this reason FCS instruments are frequently calibrated with fluorophores with known diffusion coefficients. The width and length of the volume are adjusted until the known diffusion coefficient is recovered and the measured correlation function matches the calculated correlation function. In principle, there is no need to calibrate the concentration or instrument sensitivity because the value of $N = G(0)^{-1}$ is determined without any assumptions, except that the solution contains only a single type of fluorophore with the same spectral and diffusive properties. Solutions with known concentrations are used for calibration procedures. Since FCS measurements are often used to measure relative diffusion coefficients of two species, the results can be useful even if the absolute values of the diffusion coefficients are somewhat inaccurate.

24.2.2. Occupation Numbers and Volumes in FCS — Advanced Topic

There are some differences in how authors use the $G(0)$ intercept to calculate N. Instead of $G(0) = 1/N$, some authors use $G(0) = \gamma/N$, where γ is a geometric factor that depends on the detection profile. For a Gaussian volume, γ is sometimes set equal to $1/\sqrt{8} = 0.35$. For a volume with a Gaussian profile for the width and a Lorentzian profile for the length, the factor is $\gamma = 0.076$. This difference arises from how the sample volume is defined. The volume of a Gaussian-shaped sample is obtained by integration of eq. 24.9 to yield $V_G = \pi^{3/2} s^2 u/\sqrt{8}$. The γ factor for a Gaussian-Lorentzian shape is obtained in a similar way. The γ factor is used if the sample volume is taken as the integrated volume. If the effective volume of a Gaussian shape is defined by eqs. 24.15 and 24.16 then $G(0) = 1/N$. For this chapter we will use $V_{\text{eff}} = \pi^{3/2} s^2 u$ and $G(0) = 1/N$.

24.2.3. FCS for Multiple Diffusing Species

The use of FCS to measure binding reactions depends on the shape of the autocorrelation function for a sample with two diffusion coefficients. Assume the ligand is labeled with the fluorophore and that the labeled ligand binds to a protein. In solution the ligand has a diffusion coefficient D_1, and the protein-bound ligand has a diffusion coefficient D_2. If the free and bound fluorophores have equal brightness, that is, the absorption spectra and quantum yield of the labeled ligand do not change upon binding, the autocorrelation function is given by

$$G(\tau) = \frac{1}{N^2}\left[N_1 D_1(\tau) + N_2 D_2(\tau)\right] \tag{24.17}$$

where N_1 and N_2 are the number of free and bound fluorophores and $N = N_1 + N_2$ is the total number of fluorophores. The diffusive parts of the autocorrelation function are given by eq. 24.12 with diffusion coefficients D_1 and D_2. Note that D_i refers to a diffusion coefficient and $D_i(\tau)$ refers to the part of the autocorrelation function that contains the diffusion coefficients.

The lower panel in Figure 24.7 shows simulated autocorrelation functions for a mixture of diffusing fluorophores with $D_1 = 10^{-5}$ cm^2/s and $D_2 = 10^{-7}$ cm^2/s. In this case we assumed the total number of diffusing fluorophores to be $N = 2$. When both species are present the heterogeneity in the diffusion coefficients can be seen in the shape of

the autocorrelation function (dashed line). This change in shape serves as the basis for measuring association reactions between biomolecules. Autocorrelation functions are calculated for various assumed diffusion coefficients and functional amplitudes until the calculated function matches the measured function. This procedure is analogous to that used to resolve multi-exponential decays from time-resolved measurements. Note that the value of $G(0)$ is 0.5 because we assumed an average of two fluorophores are in the effective volume for these simulations. Equation 24.17 only applies if the two species do not exchange between the free and bound forms during the timescale of the experiment, which is the diffusion time τ_D. If the ligand binds and dissociates within the time it is in the observed volume, only a single diffusion coefficient will be observed. If the ligand moves from the free to bound form on a timescale comparable to the diffusion time, the correlation function cannot be written as a sum of two correlation functions with different diffusion coefficients.

Fluorophores frequently display changes in quantum yield or brightness (eq. 24.6) upon binding to a biomolecule. In this case the two species still contribute to the autocorrelation function, but do not contribute in direct proportion to their relative concentrations or quantum yields. For a sample with two different quantum yields, Q_1 and Q_2, with brightness B_1 and B_2, and diffusion coefficients D_1 and D_2, the correlation function is given by

$$G(\tau) = \frac{N_1 B_1^2 D_1(\tau) + N_2 B_2^2 D_2(\tau)}{(N_1 B_1 + N_2 B_2)^2} \qquad (24.18)$$

with $D_i(\tau)$ defined as in eq. 24.12. For several different species this expression becomes

$$G(\tau) = \frac{\Sigma N_i B_i^2 D_i(\tau)}{(\Sigma N_i B_i)^2} \qquad (24.19)$$

Notice that each species contributes to the autocorrelation function proportional to the square of its quantum yield or brightness. This means that the autocorrelation function is strongly weighted by the brightest species in the sample. For instance, suppose the sample contains one molecule with $Q_1 = 1.0$ and one molecule with $Q_2 = 0.1$. The fraction of the signal due to Q_1 will be about 99%.

The presence of two or more species with different brightness complicates interpretation of $G(0)$. The $\tau = 0$ intercept reflects an apparent number of observed molecules according to

$$N_{app} = \frac{(\Sigma N_i B_i)^2}{\Sigma N_i B_i^2} \qquad (24.20)$$

For the sample containing one molecule with $Q_1 = 1$ and one molecule with $Q_2 = 0.1$, the apparent number of molecules will not be 2, but will be 1.20.

24.3. EXAMPLES OF FCS EXPERIMENTS

24.3.1. Effect of Fluorophore Concentration

Figure 24.8 shows autocorrelation functions for rhodamine 6G (R6G) in 70% sucrose.[22] The sucrose was used to decrease the diffusion coefficient of R6G and shift the curves to longer values of τ. The amplitudes of $G(\tau)$ are strongly dependent on the concentration of R6G. These data illustrate the effect of occupation number on the autocorrelation functions. As the R6G concentration increases the $G(\tau)$ amplitude decreases. At an R6G concentration of 0.62 nM the $G(0)$ intercept shows there are an average of 5 molecules in the observed volume. At an R6G concentration of 20 nM about 150 molecules contribute to the autocorrelation function, which results in the low amplitude. Notice that the number of R6G molecules is known even if the effective volume is not known. By comparison with Figure

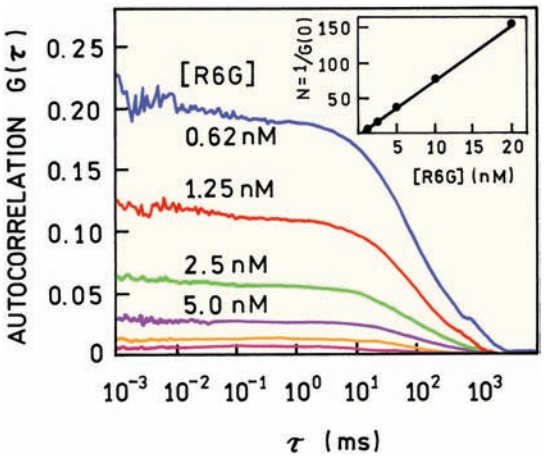

Figure 24.8. Fluorescence autocorrelation function for rhodamine 6G (R6G) in 70% sucrose. From top to bottom the R6G concentrations were 0.62, 1.25, 2.5, 5, 10, and 20 nM. The insert shows the measured average number of molecules. Redrawn from [22].

24.6 one can determine that the effective volume was probably larger than 0.35 fl.

While the amplitude of $G(\tau)$ depends on the R6G concentration, the curves all display the same correlation time. This is expected because the diffusion coefficient of R6G should not depend on its concentration, at least at low concentrations used for FCS. By fitting these curves to eq. 24.12 one can recover the diffusion time without any assumptions. The diffusion time can be used to calculate the R6G diffusion coefficient (eq. 24.14), but this requires knowledge of the dimensions of the ellipsoid. This dependence shows that the value of τ_D is not a molecular parameter and that assumptions are needed to calculate the diffusion coefficient.

24.3.2. Effect of Molecular Weight on Diffusion Coefficients

Since the autocorrelation function depends on the rate of diffusion, it seems natural to use FCS to determine molecular weights. It is known that the translational diffusion coefficient of a molecule is related to its size by

$$D = \frac{kT}{6\pi\eta r} \tag{24.21}$$

where k is Boltzmann's constant, T is the temperature, η is the viscosity of the solvent, and R is the hydrodynamic radius. The radius is related to the molecular weight MW of the molecule with a specific gravity $\bar{\nu}$ by

$$V = \mathrm{MW}\bar{\nu} = \frac{4}{3}\pi R^3 \tag{24.22}$$

$$R = \left(\frac{3\mathrm{MW}\bar{\nu}}{4\pi}\right)^{1/3} \tag{24.23}$$

where V is the volume. These equations show that the radius and diffusion coefficient are weakly dependent on the molecular weight. For instance, a 10-fold increase in the molecular weight will only result in a $(10)^{1/3}$ = 2.15-fold change in the diffusion coefficient. The association of two proteins of equal size will double the molecular weight and cause only a 1.26-fold or 26% increase in the diffusion coefficient. For this reason it is difficult to measure the association of two similar size proteins by FCS. In many applications of FCS a system is selected because it provides a large change in effective molecular weight of the diffusing species.

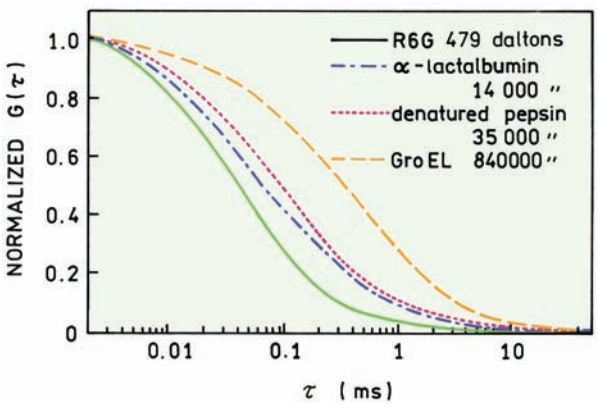

Figure 24.9. Effect of molecular weight on the autocorrelation functions of proteins labeled with tetramethylrhodamine-5-isothiocyanate (TRITC). The effective volume was determined by assuming the diffusion coefficient of R6G was 2.8 x 10^{-6} cm^2/s. Revised from [23].

Figure 24.9 shows experimental curves for R6G and three proteins with very different molecular weights.[23] This figure also contains the autocorrelation function for R6G. The data for R6G were used to determine the effective volume using a known diffusion coefficient of 2.8 x 10^{-6} cm^2/s for R6G (MW = 479). Autocorrelation functions are shown for three proteins: α-lactalbumin (MW = 14,000), denatured pepsin (MW = 35,000), and the chaperonin GroEL (MW = 840,000). The midpoint of the curves shifts 2.5-fold from 0.08 to 0.2 ms. The molecular weight increases from 14,000 to 840,000, which predicts a $(60)^{1/3}$-, or approximately fourfold increase in the diffusion coefficient. These curves show that the autocorrelation functions are dependent on molecular weight, but that substantial changes in molecular weight are needed to result in detectable changes in the diffusion time. In the case of binding interactions it is possible to couple one of the reactants to polymeric nanoparticles so as to increase the change in molecular weight upon binding, as has been done for FCS immunoassays.[24]

It is interesting to recall that the rotational correlation time (θ) of a molecule is directly proportional to the volume (V) or molecular weight of a molecule:

$$\theta = \frac{\eta V}{kT} = \frac{\eta \mathrm{MW}\bar{\nu}}{kT} = \frac{1}{6D_R} \tag{24.24}$$

where D_R is the rotational diffusion coefficient. Anisotropy measurements are preferred when the binding reaction results in a modest change in molecular weight.

24.4. APPLICATIONS OF FCS TO BIOAFFINITY REACTIONS

The dependence of the autocorrelation functions on the diffusion coefficients has resulted in the use of FCS to measure binding reactions, including binding of small ligands to proteins,[25–26] protein–protein interactions,[27–28] DNA hybridization,[29–30] polymerase chain reactions,[31–33] DNA–protein interactions,[34–35] and interactions with receptors.[36–38] Additional references are listed following the main reference section.

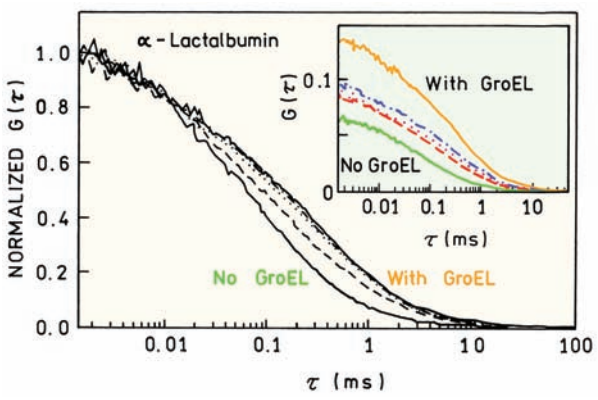

Figure 24.10. Normalized autocorrelation curves for reduced TRITC-labeled α-lactalbumin (α-LA) upon titration with GroEL. The insert shows the un-normalized curves. Revised from [23].

24.4.1. Protein Binding to the Chaperonin GroEL

The use of FCS to measure binding reactions is illustrated by studies of protein binding to GroEL. Chaperonin GroEL is a large multi-subunit protein (MW = 840,000) that promotes folding of denatured proteins or folding of peptide chains as they are extended during protein synthesis. The subunits form a cylindrical cavity that appears to interact with the hydrophobic regions of unfolded proteins. FCS was used to study the interactions of partially denatured α-lactalbumin (α-LA) with GroEL.[23] The partially denatured protein was obtained by reducing the four disulfide bonds of α-LA, followed by labeling with TRITC. Upon addition of GroEL the autocorrelation functions of labeled α-LA shifted to longer times (Figure 24.10). This shift is readily detectable because of the relative sizes of α-LA (14,000) and GroEL (840,000). Titration of α-LA with GroEL resulted in dilution of the sample, which caused an increase in amplitude for the more dilute solutions of α-LA (insert). For these experiments the concentration of α-LA was about 100 nM, which resulted in the low amplitudes of the autocorrelation curves (not shown).

Data of the type shown in Figure 24.10 can be used to recover the fractional binding of α-LA to GroEL. If the brightness of labeled α-LA does not change upon binding to GroEL the autocorrelation function is given by

$$G(\tau) = \frac{1}{N}\left[(1 - y)D_F(\tau) + yD_B(\tau)\right] \qquad (24.25)$$

where the subscripts refer to α-LA free (F) in solution or bound (B) to GroEL. $D_F(\tau)$ and $D_B(\tau)$ are diffusive parts of the autocorrelation function (eq. 24.12) with diffusion coefficients D_F and D_B. The fraction of total α-LA bound to GroEL is given by y. This fraction can be used to calculate the binding constant for the reaction. However, there are several parameters to be recovered from the data: the two diffusion times, the fraction bound, and possibly the $\tau = 0$ intercept. For this analysis the diffusion times of the individual proteins were measured for α-LA or GroEL (Figure 24.9), and these values used as fixed parameters. This allowed analysis of the data in terms of just two parameters: the fraction bound and the total number of diffusing molecules (eq. 24.17).

24.4.2. Association of Tubulin Subunits

FCS can be used to study the self-assembly or aggregation of proteins. One example is the association of tubulin to form microtubules that are important components in the mitotic machinery of cells. A variety of natural products are known that interact with tubulin to disrupt cell division. Such natural products apparently evolved as part of the competition between organisms for survival. These compounds are often small peptides or depsipeptides and are of interest for use as antineoplastic drugs. These compounds interact with the α,β-dimer of tubulin, which is referred to as tubulin. In some cases the compounds depolymerize the microtubules, and in other cases they prevent depolymerization or cause formation of unique aggregates. FCS was used to study the sizes of tubulin aggregates induced by these compounds.[38] The TAMRA-labeled tubulin dimer was observed upon addition of cryptophycin (Figure 24.11). This addition resulted in an approximate 2.5-fold

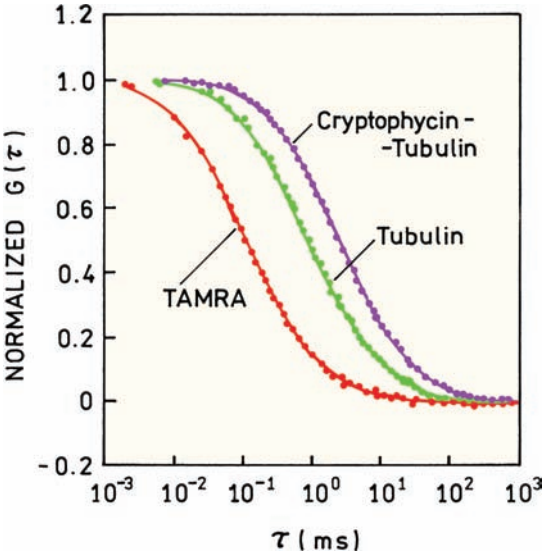

Figure 24.11. Effect of cryptophycin on the normalized autocorrelation function of TAMRA-labeled tubulin dimer. Revised and reprinted with permission from [38]. Copyright © 2003, American Chemical Society.

increase in the diffusion time of tubulin. Such a large increase in τ_D indicates that tubulin must aggregate into larger particles than dimers. This increase in τ_D was roughly consistent with the increase in hydrodynamic radius expected for self-association to an octamer.[38]

24.4.3. DNA Applications of FCS

As might be expected, FCS has been applied to DNA analysis. Surprisingly, a relatively small number of papers have appeared on hybridization of oligomers of similar size.[30] A large number of papers have appeared where one of the DNA strands was much larger than the other or using dual-color FCS, which is discussed later in this chapter. FCS has also been used to study the interaction of DNA with proteins,[39–42] DNA condensation,[43–44] or binding of DNA oligomers to larger RNA targets.[45]

FCS can be effectively used to monitor DNA hybridization when there is a large change in diffusion coefficient.[46–48] Figure 24.12 shows the normalized autocorrelation functions for a rhodamine-labeled 18-mer during hybridization with M13 DNA, which contains about 7250 base pairs (specifically M13mp18). Because of the large change in effective molecular weight the shift in $G(\tau)$ is dramatic. There was no change in brightness of the labeled oligomer upon binding to M13, so that the fractions bound and free could be calculated using eq. 24.17.

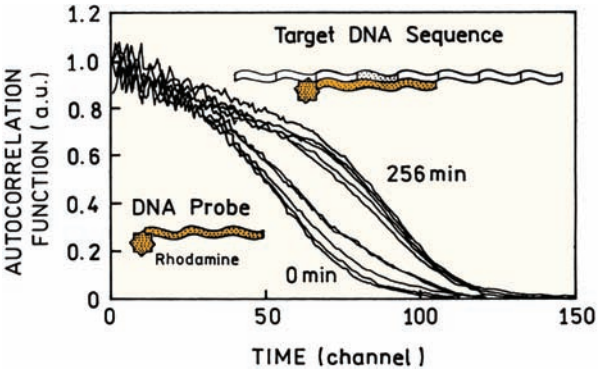

Figure 24.12. Hybridization of a rhodamine-labeled 18-mer to M13 DNA containing the appropriate complementary sequence. M13 DNA has about 7250 bases. Revised from [47].

FCS has also been used to study degradation of DNA by enzymes. One example is shown in Figure 24.13 for double-stranded DNA with a 500-base-pair oligomer.[47–48] The 500-mer was randomly labeled at low density with a tetramethylrhodamine-labeled nucleotide, TMR-dUTP. The oligomer was progressively digested from the 3' end by T7 exonuclease. As the reaction proceeds the amplitude of $G(\tau)$ decreases, reflecting the increased number of diffusing species. Examination of the normalized curves (insert) shows a progressive shift to shorter diffusion times as the DNA is progressively degraded. This shift is expected given the small size of a labeled nucleotide relative to a 500-base-pair oligomer. In principle the $\tau = 0$ intercepts of $G(\tau)$ can be used to recover the number of diffusing species. However, for such an analysis it is necessary to know the relative brightness of each species (eq. 24.20). For the case shown in Figure 24.13 there are two dominant species: free TMR-d-UTP and the residual section of the 500-mer. The relative brightness of the species will be approximately proportional to the number of fluorophores per particle. In the initial stages of the reaction one could probably assume just two species: a dim monomer that contains one TMR and a bright oligomer that contains many TMRs. As the reaction proceeds it will become progressively more difficult to resolve the population of the various sized DNA fragments.

FCS was also used to measure the appearance of labeled DNA fragments during polymerase chain reaction (PCR) and to characterize the size of the fragments.[31] The fluorophore TMR-dUTP was incorporated into the PCR products. FCS analysis was performed following removal of the free TMR-dUTP, which otherwise would decrease the amplitude of $G(\tau)$. Incorporation of TMR-dUTP into a 217-mer was easily observed from the shift in $G(\tau)$ (Figure

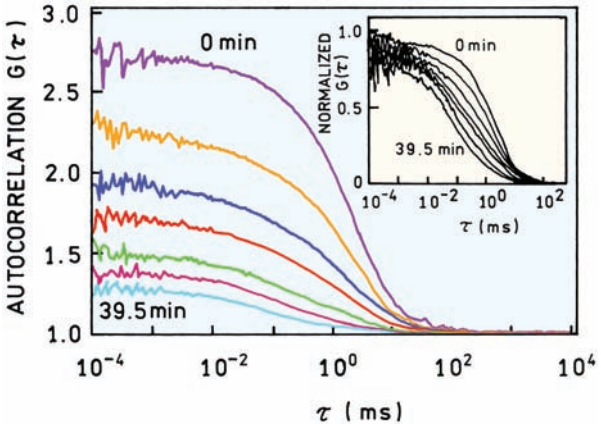

Figure 24.13. Autocorrelation functions for double-stranded DNA, 500 base pairs long, randomly labeled with tetramethyrhodamine-4-dUTP in the presence of T7 DNA polymerase, acting as an exonuclease. Revised from [47].

24.14). The PCR reaction was used to synthesize labeled DNA with different lengths. In the case of DNA fragments it is possible to obtain information on their length from the diffusion times (Figure 24.15). This was possible because increasing the molecular weight of DNA results in elongating a relatively stiff rod in one dimension, rather than filling a three-dimensional volume. For such molecules the diffusion time increases nearly linearly with length (L) according to[49–50]

$$\tau_D = \frac{3\pi\eta s^2}{4kT}\frac{L}{\ln p + \gamma} \qquad (24.26)$$

where L is the length of the rod, p is the length/diameter ratio, and γ is an end-group correction. The important point

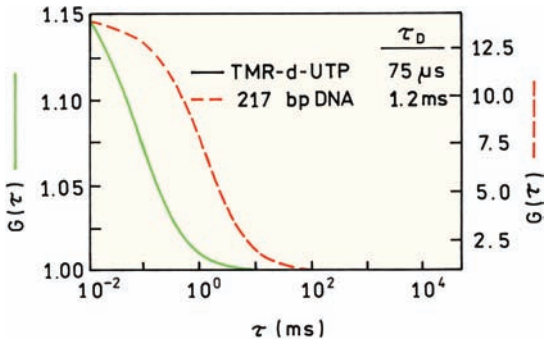

Figure 24.14. Normalized autocorrelation curves for TMR-dUTP and when incorporated into a 217-mer by PCR. Revised and reprinted with permission from [31]. Copyright © 1998, American Chemical Society.

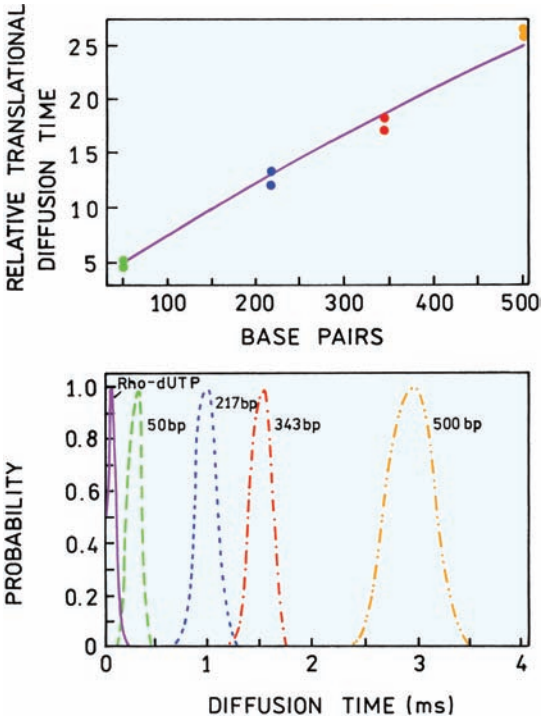

Figure 24.15. Effect of DNA length on FCS diffusion times. Revised and reprinted with permission from [31]. Copyright © 1998, American Chemical Society.

is that τ_D should increase roughly in proportion to the number of bases in the oligomer.

DNA oligomers of known length were used to create a calibration curve of diffusion time versus the number of base pairs. The autocorrelation curves for the fragments (Figure 24.14) were used to recover the distribution of diffusion times for the oligomers. This was accomplished by fitting the data to

$$G(\tau) = \frac{1}{N}\int_0^\infty P(\tau_D)\,G(\tau_D)\,d\tau_D \qquad (24.27)$$

where $G(\tau)$ is given by eq. 24.12 and $P(\tau_D)$ is the normalized probability for value of τ_D. The meaning of this integral is that the observed correlation function is the sum of a large number of such functions, weighted by the relative probability of τ_D in the sample. This analysis is similar to the analysis of intensity decays in terms of lifetime distributions. The recovered correlation times for these fragments increase significantly with the number of base pairs. The distribution (Figure 24.15, lower panel) shows good resolution of τ_D, but it would be difficult to recover more than sev-

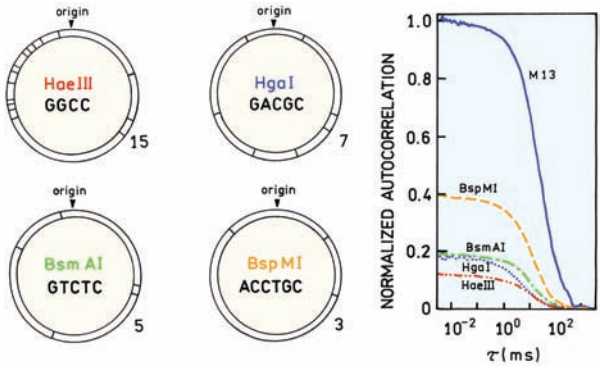

Figure 24.16. Cleavage of rhodamine-labeled M13 DNA by four restriction enzymes. The number of cleavage sites is shown under each circle. Revised from [51].

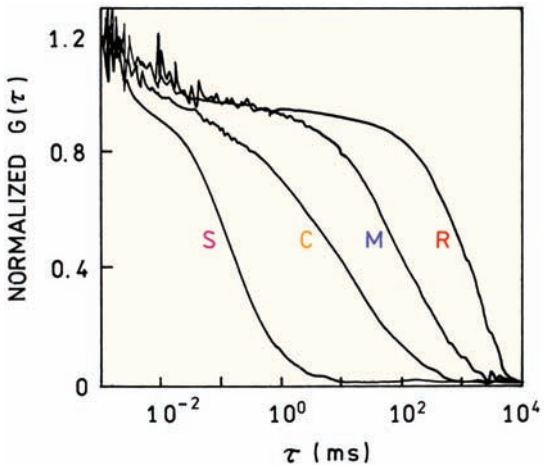

Figure 24.17. Autocorrelation curves for rhodamine derivatives in solution (S), in the cytoplasm (C), and bound to the membranes (M) of rat basophilic leukemia cells (RBL). A lipophilic rhodamine derivative was used to bind to the membranes. Also shown is the curve for Cy3-labeled IgE bound to the IgE receptor on the membrane (R). The pinhole was 100 μm in diameter. Revised from [62].

eral τ_D values in a mixed sample if the lengths were more similar. The distributions were obtained from measurements on a single species, with a single brightness, so that resolution of multiple τ_D values can be expected to be more difficult for a mixture of species with different brightness.

In addition to monitoring the length of DNA oligomers, FCS can be used to roughly estimate the number of fragments formed during DNA cleavage.[51] Figure 24.16 shows the $G(\tau)$ curves for M13 DNA (7250 base pairs) after cleavage by several restriction enzymes. From the known sequence and enzyme specificity one can predict the number of fragments formed by each enzyme. The $G(0)$ values from autocorrelation curves are largest for BspMI, which generates only 3 fragments, and smallest for HaeIII, which generates 15 fragments. Of course, the $G(0)$ values give only an apparent number of diffusing species since the fragments are of unequal length and their contributions to $G(\tau)$ are weighted according to eq. 24.18.

24.5. FCS IN TWO DIMENSIONS: MEMBRANES

FCS is not limited to three-dimensional samples, but can also be used to study cell membranes.[52–61] FCS is especially useful for studies of membranes because diffusion is limited to two dimensions. Also, the typically viscous nature of membranes result in a wide range of diffusion times for membrane-localized fluorophores. The wide range of diffusion times possible with cells or cell membranes is shown in Figure 24.17. The correlation curves are for rhodamine derivatives in solution (S), in the cytoplasm (C), and bound to the membranes of a rat leukemia cell (M). Also shown is the curve for Cy3-labeled IgE bound to the IgE receptor. The diffusion times span four orders of magnitude. Hence we expect the autocorrelation curves to contain information about diffusive transport in membranes. To obtain a similar change in diffusion times for a three-dimensional solution the molecular weight would need to change by a factor of 10^{12}.

Recall that the correlation function eq. 24.12 was derived assuming a three-dimensional Gaussian volume (eq. 24.9). In a membrane the fluorophores are constrained in a two-dimensional plane. In this case the observed volume can be described by a planar two-dimensional Gaussian distribution:

$$p(r) = I_0 \exp\left[-2(x^2 + y^2)/s^2\right] \qquad (24.28)$$

For this geometry the correlation function for a freely diffusing species is

$$G(\tau) = G(0)(1 + \tau/\tau_D)^{-1} = G(0)\left(1 + \frac{4D\tau}{s^2}\right)^{-1} \qquad (24.29)$$

where s is the radius of the disk and the diffusion time is given by $\tau_D = s^2/4D$ (eq. 24.14). Intuitively this expression is similar to eq. 24.12, except that the exit pathway out of the plane is no longer available to the molecule, and the square-root term is no longer present.

It is informative to examine the properties of the correlation function in two and three dimensions: $G_{2D}(\tau)$ and

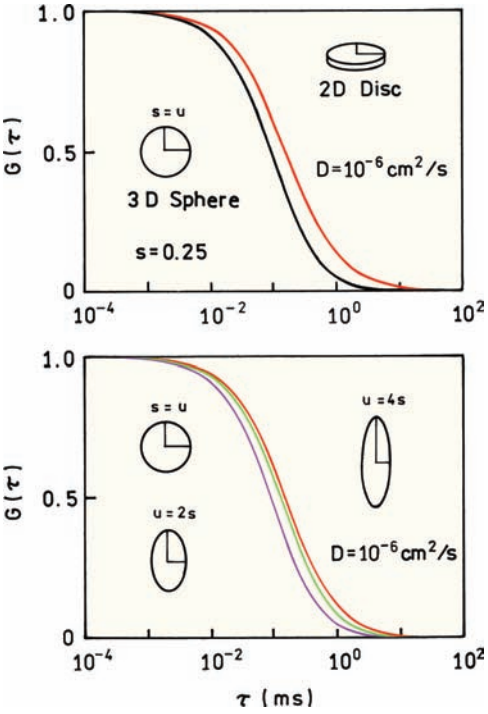

Figure 24.18. Simulated autocorrelation functions for a sphere in three dimensions and a disk in two dimensions (top), and for spherical and elongated 3-dimensional shapes (bottom). $D = 10^{-6}$ cm²/s and $s = 0.25$ μm.

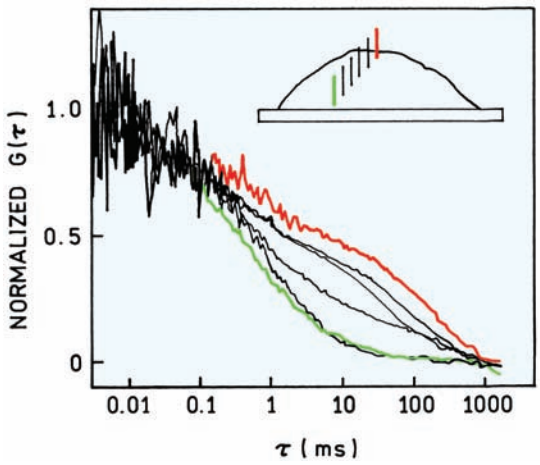

Figure 24.19. Diffusion of a lipid-containing GFP at various positions with an RBL cell as indicated on the insert. Revised from [62].

$G_{3D}(\tau)$, respectively. Figure 24.18 (top) shows the correlation function for a sphere and a disk, plotted for the same diffusion coefficient of 10^{-6} cm²/s. The disk shows a modest shift to longer times due to the restricted diffusion path. In this model it is assumed the fluorophore cannot diffuse out of the plane. Frequently in the FCS literature one finds that $G_{2D}(\tau)$ is used when $G_{3D}(\tau)$ seems appropriate and vice versa. This occurs because there are only minor differences between the correlation functions once the shape of the volume is considered. The lower panel shows simulated autocorrelation functions for a sphere and two progressively elongated shapes. When the ellipsoid has an aspect ratio of 4 the autocorrelation is virtually indistinguishable from $G_{2D}(\tau)$. This result is due to the elongated volume in $G_{3D}(\tau)$ and the modest contribution of the last term on the right in eq. 24.12.[21] Note also that these curves were drawn with a fixed diffusion coefficient. If the value of D is allowed to vary, as in the case when analyzing experimental data, then the curves would shift along the τ axis to the position of maximum overlap. In this case it would become even more difficult to distinguish between $G_{2D}(\tau)$ and $G_{3D}(\tau)$.

While the shapes of the autocorrelation functions are not strongly dependent on two versus three dimensions, the autocorrelation function for membranes can be dramatically different from free diffusion in solution. The effect of a cell membrane on diffusion of a lipophilic GFP derivative is shown in Figure 24.19.[62] This GFP molecule contained a bound palmitoyl chain to provide binding affinity for the membranes. As the focal volume was moved up from the cytoplasm to the cell membrane the autocorrelation function showed increased amplitude at long times. The $G(\tau)$ curves could be modeled using two diffusion times according to

$$G(\tau) = \frac{\overline{C}_{2D} D_{2D}(\tau) + \overline{C}_{3D} D_{3D} \tau}{V_{eff}(\overline{C}_{2D} + \overline{C}_{3D})^2} \qquad (24.30)$$

$$D_{2D}(\tau) = \left(1 + \frac{4D_B(\tau)}{s^2}\right)^{-1} \qquad (24.31)$$

$$D_{3D}(\tau) = \left(1 + \frac{4D_F\tau}{s^2}\right)^{-1}\left(1 + \frac{4D_F\tau}{u^2}\right)^{-1/2} \qquad (24.32)$$

where D_B and D_F are the diffusion coefficients of membrane-bound and free GFP, respectively. Equation 24.30 can be obtained from eq. 24.18 by noting $N_i = C_i V_{eff}$. Notice that this expression has different diffusion coefficients for the free and bound forms of the fluorophore. These different diffusion coefficients account for the shape of $G(\tau)$ in Figure 24.19 as compared to the simulations in Figure 24.18, where the shapes of $G_{2D}(\tau)$ and $G_{3D}(\tau)$ are similar. The long timescale of FCS measurements, extending to seconds, has

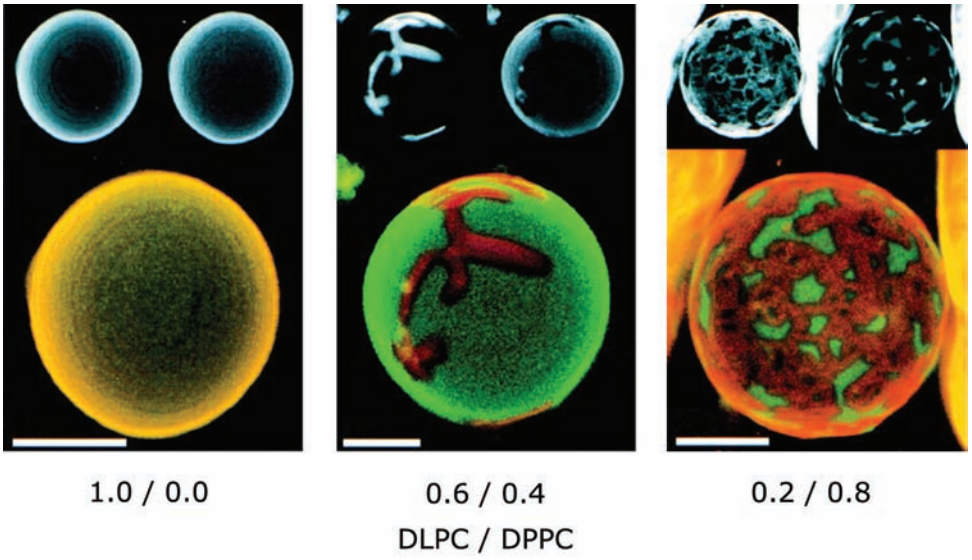

Figure 24.20. Confocal fluorescence images of giant unilamellar vesicles (GUVs) labeled with a cyanine (DiI-C_{20}) or a Bodipy (Bodipy-PC)-labeled lipid. The lipid compositions are shown under the images. In the upper black and white images DiI-C_{20} is on the left and Bodipy-PC on the right. The bars indicate 10 μm. Revised from [67].

revealed the phenomenon of anomalous subdiffusion of membrane-bound proteins where the $G(\tau)$ curve is spread out over a larger range of τ values.[63–66]

24.5.1. Biophysical Studies of Lateral Diffusion in Membranes

The ability of FCS to measure widely different diffusion coefficients has been useful in studies of lateral diffusion in membranes. Giant unilamellar vesicles (GUVs) about 35 μM in diameter were used to allow observation of specific regions of the membranes. Figure 24.20 shows confocal fluorescence microscopy images of GUVs that were labeled with two lipophilic dyes: DiI-C_{20} and Bodipy-PC.[67] For these images the GUVs were composed of two phospholipids: dilauroyl phosphatidylcholine (DLPC) and dipalmitoyl phosphatidylcholine (DPPC). At room temperature DLPC bilayers are in the fluid state and DPPC bilayers in the solid state. Because of the difference in length of the acyl side chain, C12 for lauroyl and C16 for palmitoyl, bilayers containing both lipids show lateral phase separation. This does not mean that each phase is composed only of DLPC or DPPC but rather that two phases exist: a fluid phase rich in DLPC and a solid phase rich in DPPC.

The images in Figure 24.20 were taken through two different emission filters to select for the shorter-wavelength emission of Bodipy-PC (shown as green) or the longer-wavelength emission of DiI-C_{20} (shown as red). To obtain the confocal images the GUVs were labeled with both probes at relatively high concentrations. When the GUV contains only DLPC both probes are distributed homogeneously (left). When the GUVs contain a mixture of DLPC and DPPC one finds liquid domains rich in Bodipy-PC and solid domains rich in DiI-C_{20}. As the mole fraction of DPPC increases the extent of the solid phase containing DiI-C_{20} increases (middle and right). GUVs similar to those shown in Figure 24.20 were studied by FCS. For FCS the GUVs were labeled with only one probe DiI-C_{20} at a lower concentration to allow observation of only a few probe molecules. For this system we expect the diffusion to be two dimensional with different diffusion coefficients in each phase. Assuming the probe brightness is the same in both phases the autocorrelation function becomes

$$G(\tau) = \frac{\overline{C}_F D_F(\tau) + \overline{C}_S D_S(\tau)}{V_{eff}(\overline{C}_F + \overline{C}_S)^2} \qquad (24.33)$$

where F and S refer to the fluid and solid phases, respectively, and the diffusion correlation function in each phase is given by

$$D_i(\tau) = \left(1 + \frac{4D_i\tau}{s^2}\right)^{-1} \qquad (24.34)$$

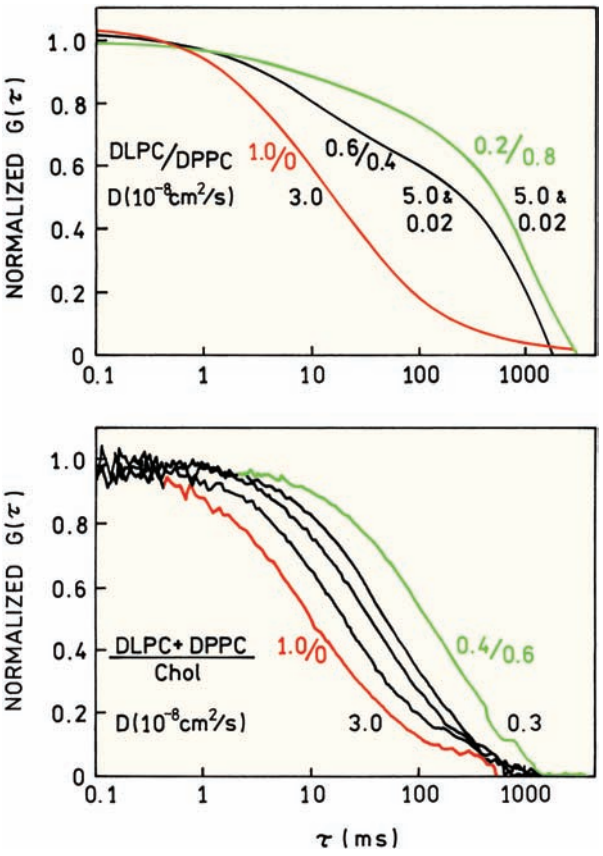

Figure 24.21. Autocorrelation functions of DiI-C_{20} in GUVs with the indicated molar ratios of DLPC to DPPC (top) and phospholipid (DLPC + DPPC) to cholesterol (bottom). The observed volume is about 1 μm in diameter. Revised from [67].

Figure 24.21 (top) shows the autocorrelation function for DiI-C_{20} in GUVs with different amounts of DLPC and DPPC. In GUVs containing only DLPC, fitting to eq. 24.23 yielded a single diffusion coefficient of 3 x 10^{-8} cm^2/s.

The autocorrelation functions become more complex for GUVs containing both DLPC and DPPC. For a DLPC/DPPC ratio between 0.6 to 0.4 it is easy to see the contribution of more than one diffusion coefficient to the shape of the autocorrelation function. As the amount of DPPC increases the diffusion appears to be more homogeneous, but fitting the data still required two diffusion coefficients. The measurements on GUVs containing both DLPC and DPPC were repeated several times and averaged, so that the correlation function contains contributions from both phases. If the observation volume is focused on one phase then one expects to see only the diffusion coefficient(s) characteristic of that phase. The effect of cholesterol on the GUVs is shown in the lower panel. As the mole fraction of cholesterol increases the diffusion coefficient decreases (Figure 24.21, bottom). The autocorrelation function shifts aggressively to longer diffusion times without a dramatic change in shape. This result indicates that only a single phase state is present in the bilayers that contain cholesterol.

24.5.2. Binding to Membrane-Bound Receptors

Cell membranes contain receptors for a wide variety of molecules. Since FCS provides information on long timescales, it is logical to use FCS to measure the slow diffusion of membrane-bound proteins. One example is the receptor for the C-peptide of insulin, which is now known to have physiological activity. Insulin is composed of two peptide chains that are linked by two disulfide bonds. When insulin is first synthesized it appears as a single longer inactive peptide called proinsulin.[68] Insulin is activated by cleaving off a small peptide called the C-peptide. The released C-peptide is physiologically active and causes increased glomerular filtration rates.[69–70] This suggests there is a cell surface receptor for the C-peptide.

FCS was used to detect specific binding of the C-peptide to human renal tubular cells.[71–73] This was accomplished using rhodamine-labeled C-peptide and by focusing the observed volume on the cell membrane (Figure 24.22, insert). The upper panel shows the intensity fluctuations for the labeled peptide when free in solution (left) and when bound to the cell membrane (right). The rate of fluctuation is much faster for the free as compared to the membrane-bound peptide. The autocorrelation functions show that the diffusion time increased nearly 1000-fold when bound to the membranes. The specificity of binding was shown by adding unlabeled C-peptide, which shifted the curve back to that typical of the free peptide (dashed line).

The data can be analyzed in two ways. One approach is to use a mixture of the correlation functions for 2D and 3D diffusion. In this case the fitting function is

$$G(\tau) = \frac{1}{N}\left[(1 - y)G_{3D}(\tau) + yG_{2D}(\tau)\right] \quad (24.35)$$

where the $G(\tau)$ function for 2D and 3D are defined in eqs. 24.31 and 24.32, respectively. The terms $(1 - y)$ and y represent the fractions of labeled peptide that are free and bound, respectively. Another approach is to recover the probability distribution for the diffusion times τ_D:

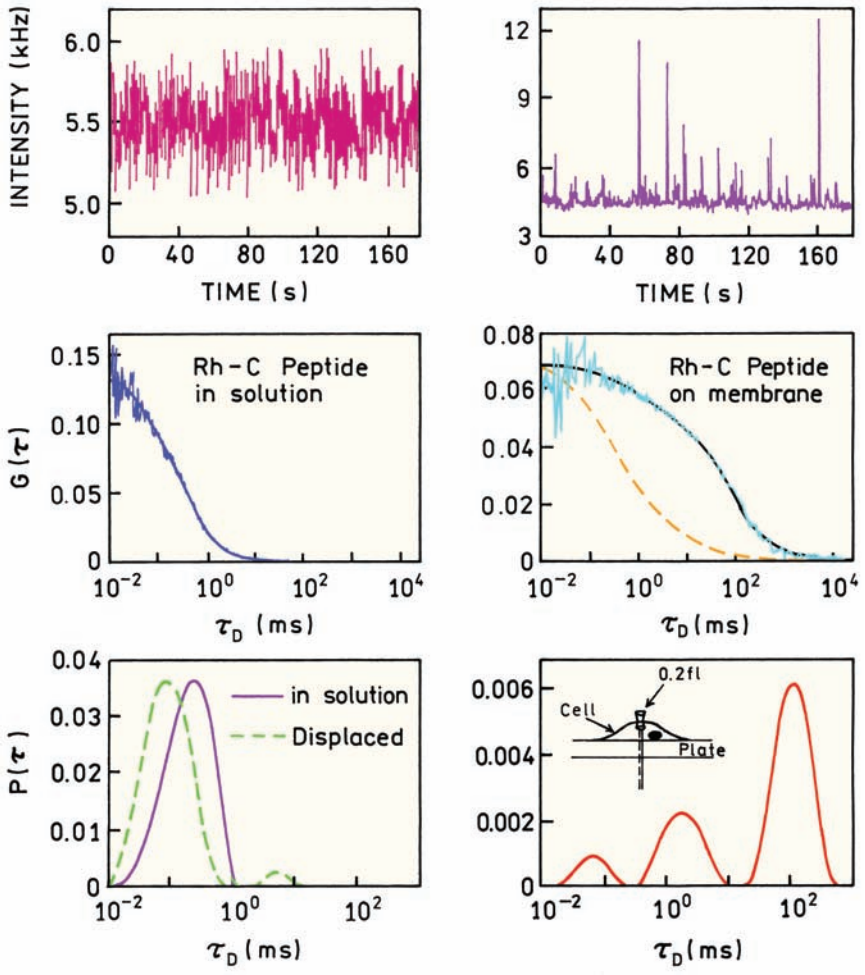

Figure 24.22. FCS studies of insulin C-peptide binding to human renal tubular cells using rhodamine-labeled (Rh) C-peptide. The dashed lines show $G(\tau)$ and $P(\tau)$ after addition of a 1000-fold excess of unlabeled C-peptide. Revised from [71].

$$G(\tau) = \frac{1}{N}\int_0^\infty \frac{P(\tau_D)}{(1 + \tau/\tau_D)} d\tau_D \qquad (24.36)$$

In the absence of the receptor the diffusion time is near 0.5 ms (lower left panel). In the presence of the receptor there is a dramatic increase in τ_D to 100 ms, with some fraction of the peptide diffusing more rapidly (lower right panel). There is nearly complete reversal of binding upon addition of an excess of unlabeled C-peptide, showing the specificity of C-peptide binding (dashed line, lower left).

FCS measurements of membranes provides information that is different from fluorescence measurements in bulk solution or fluorescence microscopy. It would not be possible to detect lateral diffusion of the insulin receptor using steady-state measurements because the nanosecond decay times are short relative to the long times needed for diffusion. Receptor diffusion would also be undetectable by fluorescence microscopy because the system is roughly stationary. The receptors are diffusing but the average distribution is constant. FCS can detect receptor motion because diffusion affects the number of fluorophores in the observed volume, even under conditions when the average distribution of receptors is not changing. The results shown in Figure 24.22 also indicate that the rate at which labeled C-peptide dissociates from its receptor is slow relative to the longest time, near one second, in the autocorrelation function.

It is instructive to compare FCS and fluorescence recovery after photobleaching (FRAP) for studies of mobil-

ity in membranes. When performing FRAP a laser is focused on the region of interest in the membrane.[74–76] The laser is transiently brought to high intensity to photobleach the fluorophores in the focal region. The laser intensity is then decreased to allow continuous monitoring of the emission from this same region of the membrane. The intensity increases as the unbleached probes diffuse into the bleached area, and the rate of recovery is used to determine the diffusion coefficients. In this FRAP measurement the experimental system was synchronized with the bleaching pulse and the system studied as it returned to equilibrium. The system is not stationary during the experiment. In contrast to FRAP, FCS measurements are performed under stationary conditions. The system is hopefully not perturbed by the illumination needed for FCS. Information about mobility in the membrane is obtained by diffusion of the probe molecules under equilibrium conditions.

24.6. EFFECTS OF INTERSYSTEM CROSSING

In the preceding sections we described the effects of translational diffusion on the autocorrelation functions of labeled molecules. Diffusion is just one of several mechanisms that can cause intensity fluctuations, and such processes can be studied by FCS. Because of the high illumination intensities in FCS, intersystem crossing from the first excited singlet state (S_1) to the triplet state (T) is frequently observed. A Jablonski diagram for intersystem crossing is shown in Figure 24.23. The excitation intensities used in FCS can result in a significant fraction of the fluorophores in the triplet state. The fluorophores in the triplet state are not observed, resulting in an apparent decrease in the number of fluorophores in the effective volume. If the fluorophores do not return to S_0 within the diffusion time then only the amplitude of the correlation function will be changed. If the triplet fluorophores can return to S_0 within the diffusion time then this is a mechanism that can cause fluctuations or blinking of the fluorophores,[77–80] as is also observed in single-molecule experiments.

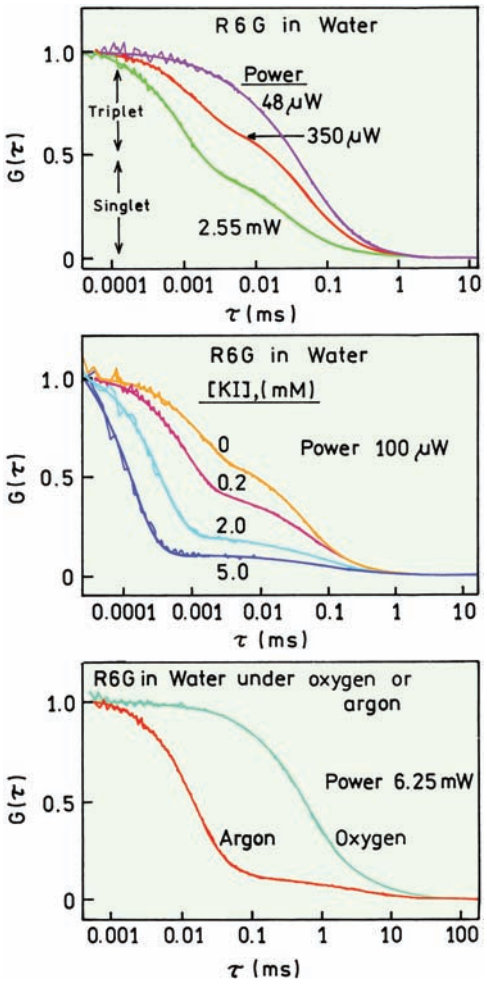

Figure 24.24. Effect of illumination intensity, iodide, and oxygen on the normalized autocorrelation function of rhodamine 6G in water. Revised and reprinted with permission from [78]. Copyright © 1995, American Chemical Society.

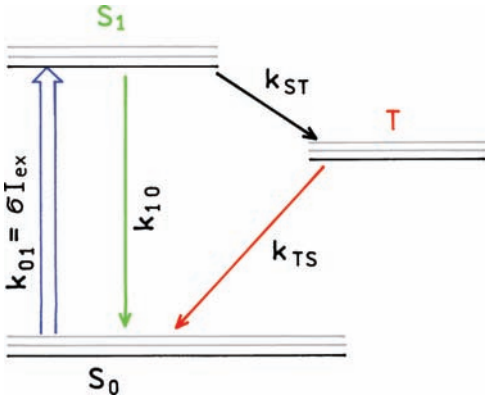

Figure 24.23. Jablonski diagram with intersystem crossing from the singlet (S) to the triplet (T) state. k_{10} is the sum of the radiative and non-radiative decay rates.

Prior to describing the theory for blinking in FCS it is informative to examine some examples. The top panel in Figure 24.24 shows autocorrelation functions for rhodamine 6G (R6G) in water, using different illumination intensities. At low incident power of 48 μW, $G(\tau)$ appears normal with a diffusion time near 0.03 ms (top panel). As the incident power increases a new component appears in

$G(\tau)$ with a new characteristic time (τ_T), which, depending on intensity, ranged from 0.5 to 1 μs. We do not call this a diffusion time since the origin of the component is not diffusion, but rather the rate of transition and return from the triplet state. The relative amplitude of the short τ_T component represents the fraction of the fluorophore in the triplet state.

24.6.1. Theory for FCS and Intersystem Crossing

The presence of an additional fluctuation mechanism requires a different correlation function. In general the theory for such systems can be complex. Some simplification is possible if the reaction is faster than the diffusion time and if there is no change in diffusion coefficient due to the reaction.[17] In this case the overall correlation function can be written as the product

$$G(\tau) = G_D(\tau)G_T(\tau) \tag{24.37}$$

where $G_D(\tau)$ is the term due to translational diffusion and $GT(\tau)$ is the term due to the additional mechanism, in this case transition to the triplet state. For the system shown in Figure 24.23 the correlation function is given by[81]

$$G_T(\tau) = \left[1 + \frac{\overline{T}}{1-\overline{T}}\exp(-\tau/\tau_T)\right] \tag{24.38}$$

where T is the fraction of the molecules in the triplet state and τ_T is the relaxation time for the singlet–triplet relaxation. This equation accounts for the decrease in the average number of singlet molecules in the observed volume by increasing the amplitude of $\tau = 0$. Increased amplitudes are not seen in Figure 24.24 because the autocorrelation functions are normalized. The relaxation time for the triplet path shown in Figure 24.23 is given by

$$\frac{1}{\tau_T} = k_{TS} + \frac{\sigma I_{ex} k_{ST}}{\sigma I_{ex} + k_{10}} \tag{24.39}$$

where σ is the cross-section for absorption, I_{ex} is the illumination intensity, k_{ST} is the rate of intersystem crossing, and k_{10} is the rate of return to the ground state from the excited singlet state. The fraction of fluorophores present in the triplet state is given by

$$\overline{T} = \frac{\sigma I_{ex} k_{ST}}{\sigma I_{ex}(k_{ST} + k_{TS}) + k_{TS}(k_{ST} + k_{10})} \tag{24.40}$$

Fitting the data in Figure 24.24 to the full correlation function allows determination of the value of T and τ_T. These values then need to be interpreted with consideration of the system being studied, because other chemical mechanisms can yield similar effects.

This theory can be used to account for the effects of different solution conditions on the autocorrelation function for R6G. The middle panel in Figure 24.24 shows the effect of iodide on the autocorrelation. As the iodide concentration increases the amplitude of the triplet portion of $G(\tau)$ increases. This is the result of iodide increasing the rate of intersystem crossing so that k_{ST} becomes

$$k_{ST} = k_{ST}^0 + k[\mathrm{KI}] \tag{24.41}$$

where k_{ST}^0 is the rate in the absence of iodide and k is the bimolecular rate constant for intersystem crossing due to iodide. By examination of eq. 24.40 one can see that an increase in k_{ST} will result in an increase in the fraction of fluorophores in the triplet state.

It is surprising to find that the effect of oxygen was opposite of the effect of iodide. To study this effect the sample was strongly illuminated to obtain a large fractional population in the triplet state (Figure 24.24, lower panel). For this 6.25-mW intensity, in the absence of oxygen, most of the fluorophores are in the triplet state. Equilibration of the water solution with oxygen resulted in almost complete recovery of the correlation function due to diffusion alone. This effect occurred because oxygen increased the rate of return to the singlet state (k_{TS}) more than it increased the rate of crossing to the triplet (k_{ST}). The net result was a decrease in the triplet population.

24.7. EFFECTS OF CHEMICAL REACTIONS

Kinetics processes other than intersystem crossing can be detectable by FCS. FCS has been used to study conformational transitions of fluorophores,[82] association reactions of fluorescent indicators,[83] and kinetic processes in GFP.[84–86] One example is shown in Figure 24.25 for EGFP. In this case the $G(\tau)$ function shows an increasing amplitude of a short-time component as the pH is decreased.[86] The longer characteristic time is due to translational diffusion of EGFP. It is known that the emission intensity of EGFP is strongly quenched at low pH (insert). This quenching is due to protonation of an ionized hydroxyl group, because EGFP is only fluorescent when the tyrosine is ionized. As the pH is decreased a new short-time component appears in $G(\tau)$,

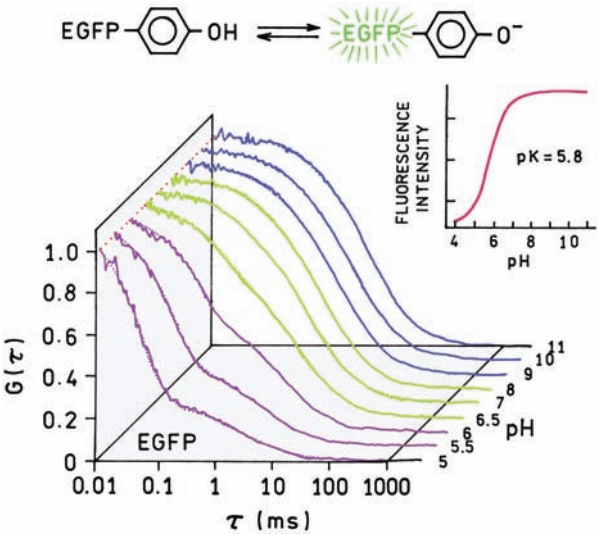

Figure 24.25. Normalized autocorrelation function for EGFP at various pH values. Revised from [86].

which is assigned to pH-dependent protonation of the tyrosine residue. The rate of protonation increases at lower pH values, resulting in the increased amplitude at short times. The proton may come from the bulk solution or from the protein itself.

24.8. FLUORESCENCE INTENSITY DISTRIBUTION ANALYSIS

In the preceding sections we considered processes that result in intensity and/or concentration fluctuations in the observed volume. The relative contributions of different brightness fluorophores to the correlation function was given in eq. 24.19, but we did not describe any approach to resolve the different fluorophores from each other. The presence of different brightness fluorophores changes the apparent number of observed molecules (eq. 24.20), but the information about their individual brightness values is lost during collection of $G(\tau)$, as can be seen by examining eq. 24.10. The amplitude of the correlation function is due to the same fluorophore emitting more than a single photon during the binning time. During a particular time interval the signal from the same dim fluorophores correlate with each other, as will the signal from the bright fluorophores. When the diffusion coefficients are the same the brightness of each fluorophore cannot be resolved and the correlation function will have the usual shape for a single diffusion species.

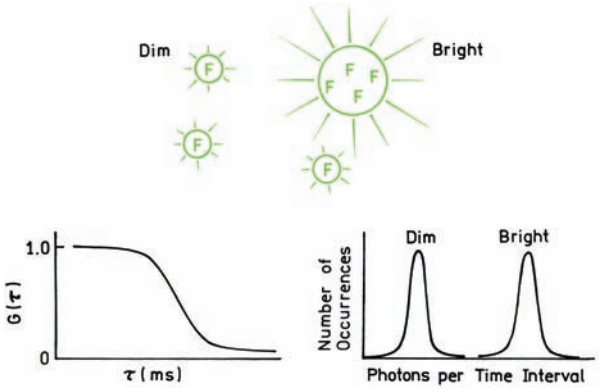

Figure 24.26. Comparison of correlation function and photon-count histogram for a mixture of dim and bright particles.

Suppose the sample contains two types of molecules with the same diffusion coefficient (Figure 24.26). This could be the same protein labeled with one or several fluorophores. If $G(\tau)$ were measured for this mixture one would see the usual correlation function for a single diffusion coefficient (lower left). Suppose now that the entire time course of intensities was available instead of the correlation functions. There would be lower and higher intensity fluctuations due to the dimmer and brighter particles, respectively. One can count the number of times a fluctuation has a dim or bright amplitude, and create a histogram of the results (lower right). For the mixture there will be two populations of fluorophores, which will be seen from the intensity distributions. If the particles display very different brightness it is possible to count the number of times dim and bright particles pass through the observed volume. One example is shown in Figure 24.27 for coumarin-labeled

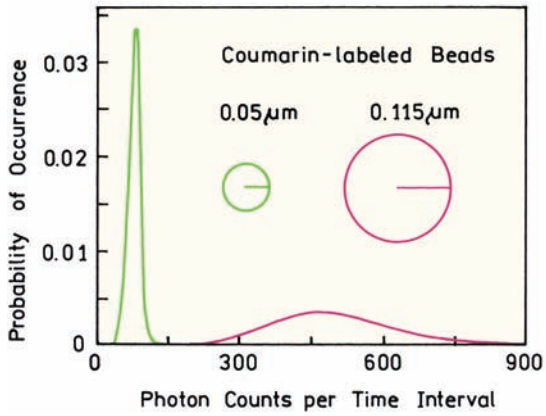

Figure 24.27. Photon-count histogram for a mixture of 0.05 and 0.115 μm coumarin-labeled beads. Revised from [87].

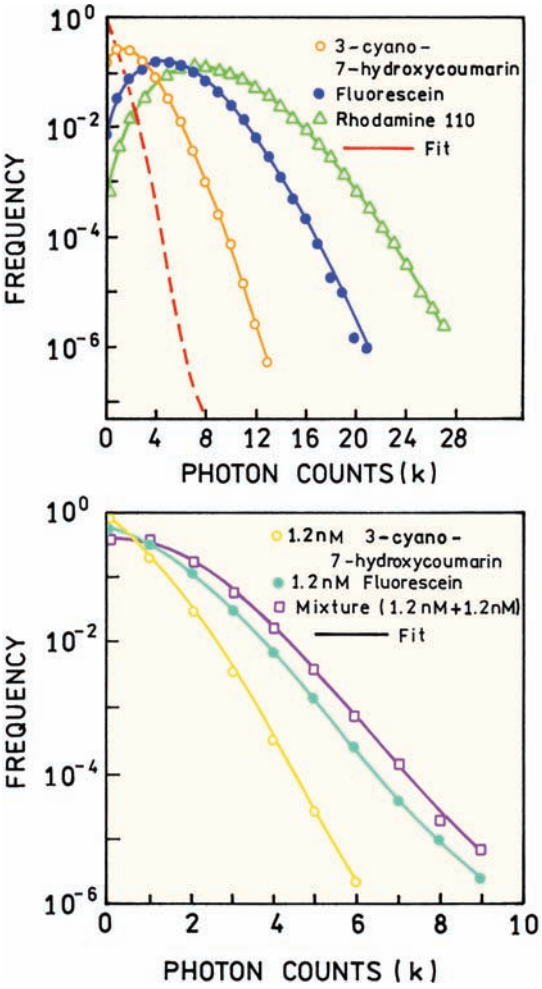

Figure 24.28. Photon counting histogram for three fluorophores (top) and for a fluorophore mixture. Also shown as a dashed line is the distribution for fluorescein at a lower concentration. Revised from [91].

beads with radii of 0.05 and 0.115 μm.[87] Two populations are already visible in the photon-count histogram.

Until recently the correlation functions were obtained with dedicated circuit boards that calculate $G(\tau)$ in real time. This was necessary because of the need to rapidly sample the fluctuating signal on a timescale short enough to characterize the process of interest. With modern electronics and computers it is possible to record the intensities for each time interval during the measurement. This allows the data to be analyzed in a different way, which is called fluorescence intensity distribution analysis (FIDA) or photon-counting histograms (PCH) by different authors.[88–97]

Unfortunately, actual use of this concept with fluorophores rather than beads is not as clear as in Figures 24.26 and 24.27. This is because there are multiple Poisson distributions that need to be considered.[91–92] The number of photons observed during a given time interval shows a Poisson distribution, as does the number of fluorophores in the volume. Additionally, a given fluorophore will display a different brightness in each region of the observed volume. As a result the distribution of the number of photon counts is broad even for a single fluorophore. These effects were less important in Figure 24.27 because of the brightness of the labeled beads and/or the mutual exclusion of the beads from being in the laser beams at the same time. The theory of FIDA/PCH is complex and not yet used in a standardized way. Hence we will present just a few examples to illustrate the nature of the data and the possible resolution.

Figure 24.28 (top) shows an example of FIDA data.[91] The top panel shows the photon-count histograms for three individual fluorophores. The data represent the probability a bin contained k photon counts. A different distribution was observed for each fluorophore. While the histograms appear distinct for each fluorophore this appearance is somewhat misleading because the shapes of the distributions depend on fluorophore concentration, as shown for a lower concentration of fluorescein (dashed line). The lower panel shows the use of these histograms to resolve a mixture of fluorophores. Curves are shown for fluorescein, a coumarin derivative, and a mixture of both fluorophores, 1.2 nM each. The PCH for the mixture was different from each fluorophore alone, but the difference is due in part to the overall higher photon counts when the two fluorophores are present in the solution. The relative concentration and brightness of each fluorophore to the PCH are determined by fitting the data to simulated histograms. In this example the difference in brightness was about twofold. It may be difficult to use this approach if there is only a modest difference in fluorophore brightness.

The resolution of FIDA increases as the fluorophores display larger differences in brightness. Figure 24.29 shows the photon-count histograms for TMR and R6G, and for a mixture (top).[89] These data were used to recover two populations of particles: one with a brightness of 36.6 kHz per molecule (TMR) and the second about threefold brighter—107 kHz per molecule (R6G). In this case the two populations are well resolved. The dashed lines show the distributions observed for the individual fluorophores, which are already wide. This intrinsic width must be taken into account when using the measured distributions to resolve the underlying populations.

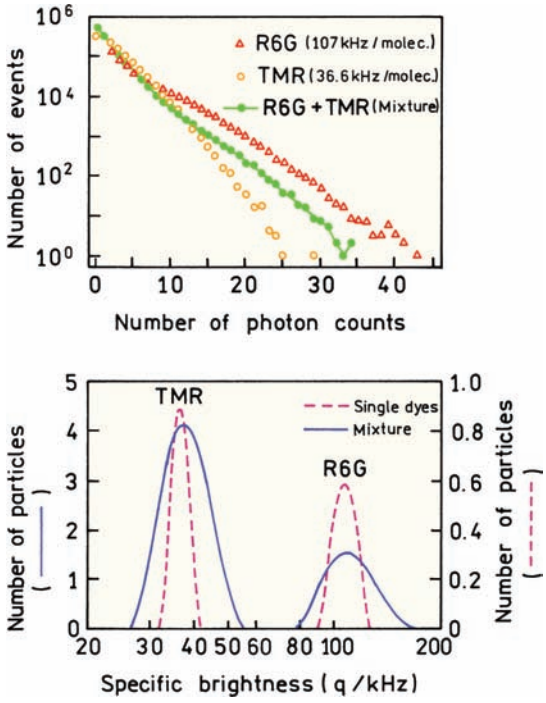

Figure 24.29. Fluorescence-intensity distribution and analysis for a mixture of TMR and R6G. The dashed line shows the results for separate solutions of each fluorophore. Revised from [89].

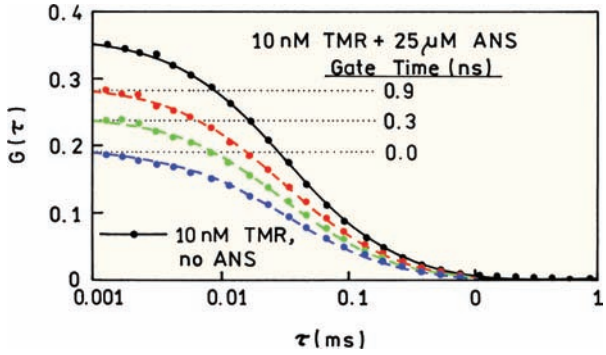

Figure 24.30. Background suppression in FCS using gated detection. The top line shows 10-nM TMR with no ANS. Two-photon excitation at 790 nm. Revised from [98].

24.9. TIME-RESOLVED FCS Advanced Topic

Nanosecond time-resolved measurements are now being combined with FCS.[98–100] This is accomplished using high-repetition-rate pulse lasers and time-domain detection. It is possible to recover correlation data using a pulse train because the fluorophore in the observed volume can be excited by many light pulses during the millisecond timescale diffusion times. Lifetimes on the nanosecond timescale are also shorter than the diffusion time. For example, suppose the laser repetition rate is 40 MHz, so the pulses are 25 ns apart. This time interval is 4 x 10^3-fold shorter than a diffusion time of 0.1 ms. Hence there is time for the same fluorophore to be excited many times while in the laser beam, which allows the correlation curves to be measured.

Time-resolved methods can use off gating at short times to suppress unwanted autofluorescence from the samples.[98] Figure 24.30 shows the correlation curves for a pure solution of 10-nM TMR (top curve) and for 10-nM TMR containing ANS as the mock impurity (lower 3 curves). The presence of ANS decreases the amplitude of the autocorrelation curves and increases the apparent number of observed molecules. The lifetimes of TMR and ANS were 2.2 ns and less than 100 ps, respectively. Because of the short lifetimes the emission from ANS could be suppressed by off gating the detection during the excitation pulse and turning the detector on after a time delay. The correlation curves were measured with three delay times: 0.0, 0.3, and 0.9 ns. As the delay time increased the amplitude of the curves increased, demonstrating a decreased contribution from the short-lived ANS impurity. For a delay time of 1.4 ns the correlation curves become almost the same as for TMR alone (not shown). Gating is likely to become useful for FCS because the small number of observed molecules makes FCS sensitive to impurities, particularly in studies of intracellular fluorophores.

As described above, FIDA can be used to determine the presence and brightness of two or more species in an FCS sample. Another approach is to resolve the FCS data from a mixture using the decay times of the two species.[100] Figure 24.31 (top) shows autocorrelation curves for pure Cy5, pure FR662, and a mixture of both fluorophores. Apparently these fluorophores have somewhat different diffusion coefficients even though their molecular weights are similar. The lifetime of FR662 near 3.5 ns is almost threefold longer than that of Cy5, which is near 1 ns. This difference was used with a fast-fitting algorithm[101] to determine the amplitude of each decay time and to resolve the autocorrelation function for each fluorophore (lower panel). Since probe lifetimes frequently change upon binding to macromolecules it seems likely that time-resolved measurements will become widely used in FCS.

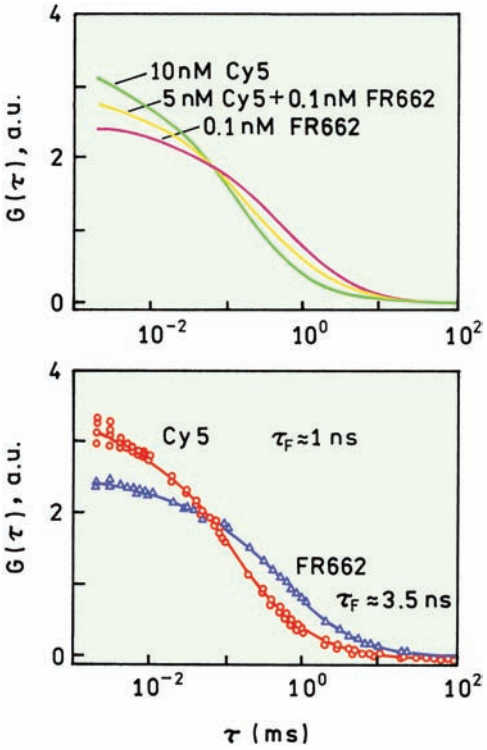

Figure 24.31. **Top**: Autocorrelation curves for pure Cy5, pure FR662, and a mixture. **Bottom**: $G(\tau)$ resolved from the mixture using the time-resolved decays. Revised from [100].

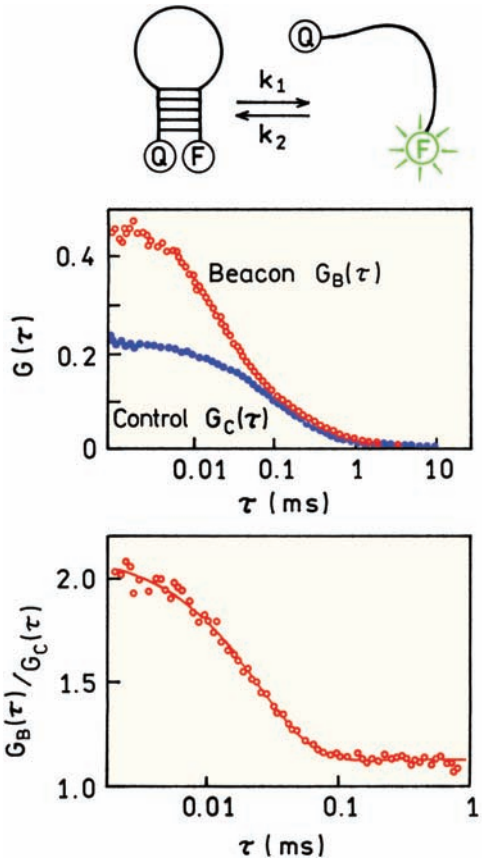

Figure 24.32. Folding kinetics of a molecular beacon at 45°C. Revised from [108].

24.10. DETECTION OF CONFORMATIONAL DYNAMICS IN MACROMOLECULES

Since FCS can detect blinking and chemical reactions that change the intensity, it seems natural to use FCS to study the conformational dynamics of macromolecules.[102–108] Given the ms timescale of FCS, and the possibility of increasing the diffusion time by increasing the size of the volume, FCS should be able to detect conformational changes that occur during the diffusion time. Since the observed volume is limited by background emission, the observed volume cannot be made too large, so the events will probably need to occur on the microsecond timescale or faster to be detectable by FCS. One example of measuring macromolecular dynamics is shown in Figure 24.32. This shows a molecular beacon that is opening and closing with rate constants k_1 and k_2. The open state is fluorescent and the closed state quenched.

The correlation functions were measured for the beacon $G_B(\tau)$ and for a control oligonucleotide $G_C(\tau)$ that did not have the quencher (Figure 24.32, middle panel). While the difference between $G_B(\tau)$ and $G_C(\tau)$ seems substantial, the difference in amplitude may be the result of about 65% the beacon being in the closed state at the experimental temperature of 45°C, thus reducing the effective fluorophore concentration. If the timescales are very different, the overall correlation function is the product of the functions due to the different processes. In this case the control molecule reveals the portion of $G(\tau)$ due to translational diffusion:

$$G_C(\tau) = \frac{1}{N}\left(1 + \frac{\tau}{\tau_D}\right)^{-1} \tag{24.42}$$

The overall correlation function is given by

$$G_B(\tau) = G_C(\tau)\left[1 + \frac{1-p}{p}\exp\left(-\frac{\tau}{\tau_R}\right)\right] \tag{24.43}$$

where p is the fraction of the beacons in the open conformation and $1/\tau_R = k_1 + k_2$ is the relaxation time for the reaction. The functional form of eq. 24.43 is the same as eq. 24.38 because both equations account for fluorophore blinking, but due to different mechanisms. Division of $G_B(\tau)$ by $G_C(\tau)$ reveals the part of the correlation function that is due to opening and closing of the molecular beacon (lower panel). Note the time axes on the panels are different, and the ratio is greater than unity only for delay times less than 0.1 ms. This ratio of correlation function is consistent with a relaxation time near 24 μs. By examination of a range of DNA sequences the authors were able to show that the opening rate k_1 was mostly independent of sequence, but the closing rate k_2 was strongly dependent on sequence.[108]

The FCS measurements provided a measure of the sum of the forward and reverse reaction rates for the molecular beacon. Additional information is needed to determine both rates individually. The equilibrium constant K for folding of the beacon is given by $K = k_1/k_2$ and can be measured in a steady-state experiment. One can show that the forward and reverse reaction rates are related to the equilibrium constant by

$$k_1 = \frac{1}{\tau_R} \frac{K}{1 + K} \tag{24.44}$$

$$k_2 = \frac{1}{\tau_R} \frac{1}{1 + K} \tag{24.45}$$

The FCS measurements only provide information on the reaction rates if the relaxation time is comparable to the correlation time, irrespective of the fraction of the fluorophore in either form. This can be seen by examination of eq. 24.43. The exponential term approaches unity when $\tau_R > \tau$.

24.11. FCS WITH TOTAL INTERNAL REFLECTION

Measurement of the correlation functions requires observation of a small number of fluorophores in a restricted volume. This can be accomplished by focused illumination and confocal detection. Another approach to FCS is to obtain the small volume using total internal reflection (TIR). Recall from Chapter 23 on Single-Molecule Fluorescence that TIR occurs from light incident on an interface when the index of refraction is lower in the distal region and the angle of incidence, measured from the normal, exceeds the critical angle θ_C. Under these conditions there is an evanescent field in the distal region. The intensity of this field decays according to

$$I(z) = I(0) \exp(-z/d) \tag{24.46}$$

where $I(0)$ is the intensity at the interface and z is the distance above the interface. The decay constant for the intensity of the evanescent field is given by

$$d = \frac{\lambda_0}{4\pi} (n_2^2 \sin\theta_C - n_1^2)^{-1/2} \tag{24.47}$$

where λ_0 is the wavelength in a vacuum, and n_1 and n_2 are the refractive indices of the distal (water) and local (glass) regions, respectively. The evanescent field typically penetrates a distance $d = 200$ nm. As a result the volume can be restricted by localized excitation of fluorophores near the interface.

Figure 24.33 shows a typical configuration of FCS using TIR. The observed volume is a thin circle or elliptical disk 100–200 nm thick and about 5 μm in diameter. In this configuration fluorophores that are free in solution can enter or exit the volume by diffusion to and away from the glass surface. Diffusion out of the observed volume along

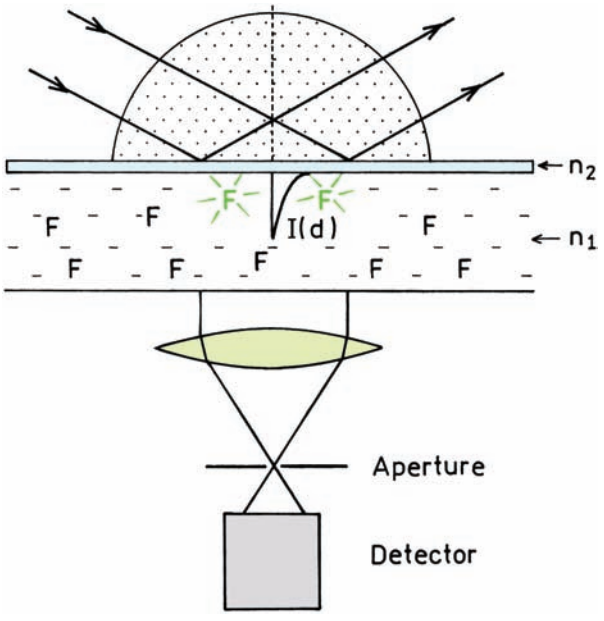

Figure 24.33. Experimental configuration for FCS using total internal reflection.

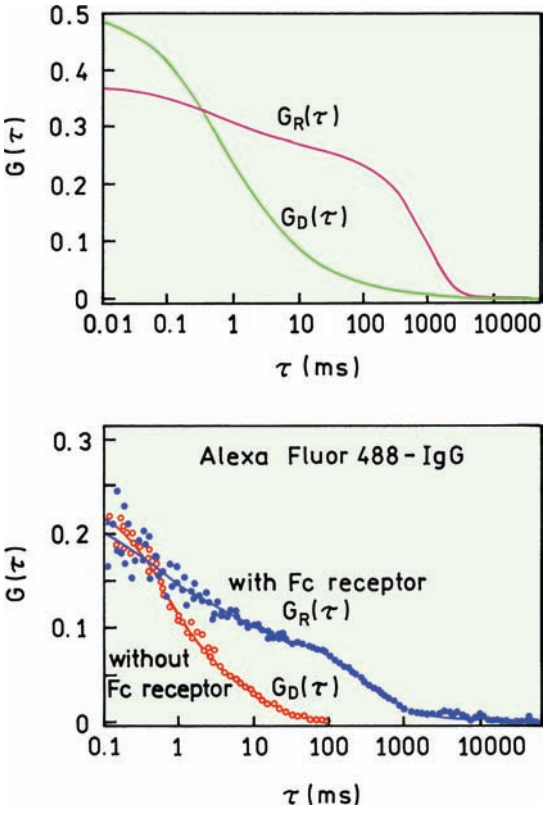

Figure 24.34. FCS with TIR. **Top**: Simulated correlation functions near a planar surface, without ($G_D(\tau)$) and with ($G_R(\tau)$) binding sites for the diffusing species. **Bottom**: Experimental data for labeled IgG near a lipid surface, without and with receptors for the Fc region. Revised from [111].

the interface is slow due to the large diameter of the spot. If the fluorophores are bound to the surface then they can only leave the volume by lateral diffusion along the surface or dissociation from the surface. Because of the difference in geometry and diffusion paths the correlation functions have a different functional form. This theory has been developed[109–111] and TIR-FCS has been used to study diffusion and binding near glass or membrane interfaces. The equations are rather complex and can be found elsewhere.[112–115] However, we will present an experimental example.

The correlation function for diffusion with TIR geometry has a characteristic shape (Figure 24.34). The shape depends strongly on whether the labeled molecules simply diffuses near the surface $G_D(\tau)$ or, if there are receptor sites on the surface, $G_R(\tau)$. The presence of binding sites results in a long time component in the correlation function that can be used to detect binding to the surface. The lower panel in Figure 24.34 shows experimental data for Alexa Fluor 488-labeled IgG. The correlation function was measured near a lipid-coated surface, or near a lipid-coated surface that contained a receptor for the Fc region. The presence of binding sites results in a dramatic shift in $G(\tau)$. One can imagine such measurements being used to measure binding to cells to screen for drug–receptor interactions.

24.12. FCS WITH TWO-PHOTON EXCITATION

Two-photon (TPE) or multiphoton excitation (MPE) is very useful in FCS. When using MPE the excited volume is small because of the quadratic dependence on light intensity. Importantly, the z-axis resolution is improved because the excited volume is less elongated. Sensitivity is also improved because the emission can be observed without a confocal aperture. The theory for FCS using MPE is very similar to that for one-photon excitation. The molecules can still enter and exit the observed volume from three directions. However, the shape of the volume is changed due to the quadratic dependence on intensity. For two-photon excitation diffusion time is related to the volume diameter:

$$\tau_D = \frac{s^2}{8D} \tag{24.48}$$

where s is the distance at which the intensity is $1/e^2$ of its maximum value. Equation 24.48 for two-photon excitation is different than eq. 24.14 because the intensity profile is squared to provide the two-photon excitation profile.[62] That is, the dimensions of the excited volume are described in terms of the original long-wavelength intensity profile rather than the square of the intensity profile. For two-photon excitation the correlation function for diffusion becomes[116–117]

$$G_D(\tau) = G(0)\left(1 + \frac{8D\tau}{s^2}\right)^{-1}\left(1 + \frac{8D\tau}{u^2}\right)^{-1/2} \tag{24.49}$$

For the same diameter beam the diffusion times are smaller with TPE even if the diffusion coefficient is not changed because of the quadratic dependence on intensity and the smaller excited volume. Some authors assume the excitation intensity is Gaussian in the focal plane and Lorentzian along the z-axis. This assumption results in an expression for $G_D(\tau)$ that is different from eq. 24.49 and more complex, but the visual shape of $G_D(\tau)$ is similar. A significant fraction of the publications on FCS[118–121] use two-photon excitation because of its experimental advantages. When using

two-photon excitation there is no need for a confocal aperture and the beam profile is shorter along the z-axis.

24.12.1. Diffusion of an Intracellular Kinase Using FCS with Two-Photon Excitation

Localized excitation using TPE has made it possible to study labeled intracellular proteins in selected regions of a cell. One example is studies of the ubiquitous enzyme adenylate kinase in HeLa cells.[122] Adenylate kinase (AK) occurs in two forms: a cytoplasmic form AKC and a membrane-bound form AKM. The membrane-bound form contains an additional 18-amino-acid chain that appears to bind AKM to membranes. These two forms of AK from murine cells were fused with EGFP and expressed in HeLa cells. Figure 24.35 shows a microscope image of cells expressing these proteins. The cells containing AKC-EGFP are bright in the cytoplasm and the cells containing AKM-EGFP show a line of fluorescence at the plasma membrane, showing that the two forms of AK are localized differently in the cells. The bottom panel shows the correlation functions recovered for both proteins. The autocorrelation functions for the cytoplasmic form (○) shows the protein diffuses freely, as can be seen by comparison with the autocorrelation function for EGFP alone in the cells (▲). The membrane-bound protein shows a large long τ component centered near 100 ms. The middle panel in Figure 24.35 shows the diffusion coefficients of AKM-EGFP on or near the plasma membrane. At the plasma membrane two diffusion coefficients are found, one being about tenfold smaller than in the cytoplasm. This component is thought to be due to membrane-bound AKM. These separate measurements on each form of AK were facilitated by the use of localized two-photon excitation.

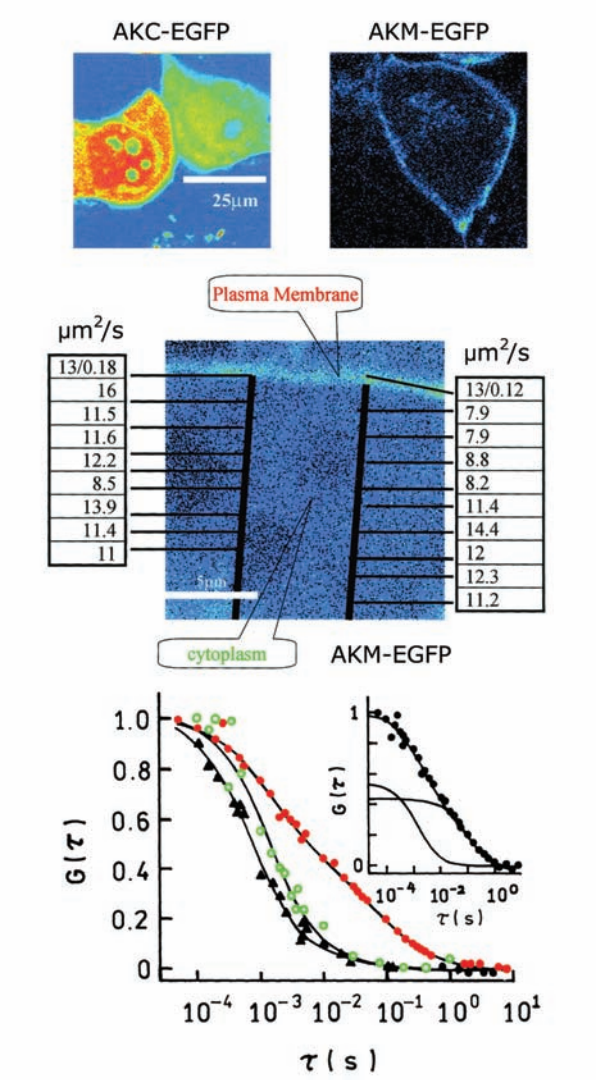

Figure 24.35. **Top**: Image of an HeLa cell containing AKC-EGFP (left) or AKM-EGFP (right). **Middle**: Image of the cell membrane with AKM-EGFP with the recovered diffusion coefficients. **Bottom**: Normalized autocorrelation function for cytoplasmic AKC-EGFP (○), membrane-bound AKM-EGFP (●), and EGFP in the cytoplasm (▲). The solid lines in the insert show the components due to each diffusion coefficient. Revised from [122].

24.13. DUAL-COLOR FLUORESCENCE CROSS-CORRELATION SPECTROSCOPY

We have seen that the fluorescent fluctuation autocorrelation functions are sensitive to the rate of diffusion and to chemical or photophysical processes that occur during observation. The weak dependence of the diffusion coefficients on molecular weight makes it difficult to use FCS to measure binding reactions unless there is a large change in molecular weight. Formation of dimers is near the resolution limit for FCS using the diffusion time to distinguish two species. The addition of two-color excitation and detection to FCS changes the form of the correlation functions and provides new applications of FCS. Figure 24.36 shows a schematic of a dual-color FCS experiment. Suppose the sample contains three types of molecules, labeled with green (G), red (R), or both green and red (RG) fluorophores. Such a sample could be observed with an FCS instrument configured for two-color measurements and separate detectors for the R and G signals. Different time-dependent fluctuations will be observed in each channel (Figure 24.36). If a G fluorophore diffuses into the volume

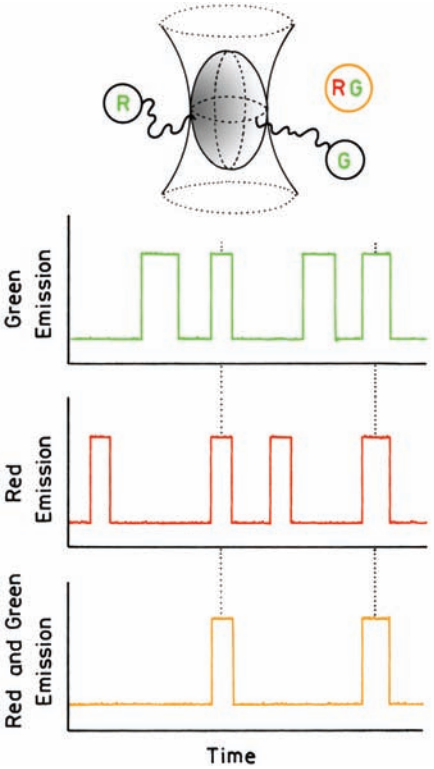

Figure 24.36. Dual-color fluorescence cross-correlation spectroscopy.

there is a burst of photons in the G channel, and similarly for an R fluorophore. If the RG fluorophore diffuses into the volume then a burst of photons is observed in both channels. This shows that doubly labeled molecule can be detected by cross-correlation between the two channels. The method is called fluorescence cross-correlation spectroscopy (FCCS).

24.13.1. Instrumentation for Dual-Color FCCS

Before describing the theory for FCCS it is instructive to examine the instrumentation (Figure 24.37). We have assumed a red and a green channel since these wavelengths have been used in FCCS.[123–131] Two lasers are used typically: an argon laser for 488 nm and an HeNe laser for 633 nm. Additionally, a single laser has been used with two-photon excitation to excite two fluorophores.[132] In order to obtain a cross-correlation signal the observed volumes for both colors must overlap in space. For this reason it is convenient to bring the excitation to the microscope using an optical fiber, which provides the same point source for both wavelengths and overlap the excitation volumes, assuming the objective is corrected for color aberration. The emission wavelengths are separated by a dichroic filter and sent to separate detectors.

The optics used to separate the green and red signals are sophisticated. The emission spectra of rhodamine green (RhG) and Cy5 are shown in Figure 24.38. It is necessary to excite both fluorophores and to separate their emissions. The double dichroic filter is a specialized component. It reflects both 488 and 633 nm and transmits the emission from both RhG and Cy5. The emission from these fluorophores is then sent to different detectors using additional dichroic filters. There is always some overlap or crosstalk between the channels. Excitation at 488 nm excites mostly RhG but will weakly excite Cy5. The emission of RhG extends to the region of Cy5 emission. Excitation at 633 nm excites only Cy5. Analysis of the cross-correlation signals requires correction for crosstalk. The actual equation becomes complex, so we will only describe the theory assuming no crosstalk between the channels.

24.13.2. Theory of Dual-Color FCCS

The theory of dual-color FCCS has been described in detail.[123–124] The sample will contain some average concentrations of each species— C_B , C_R , and C_{GR} —and each species will have an autocorrelation function—$G_G(\tau)$, $G_R(\tau)$, and $G_{GR}(\tau)$. The observed autocorrelation or cross-correlation function will depend on which detector is observed and the crosstalk between the detectors, which we assume to be zero. The green fluorophore is excited with the green excitation source, and the red fluorophore with the red source. For simplicity we assume the brightness of all species are the same. In this case the correlation functions for the three species are given by

$$G_G(\tau) = \frac{\overline{C}_G D_G(\tau) + \overline{C}_{GR} D_{GR}(\tau)}{V_{eff}(\overline{C}_G + \overline{C}_{GR})^2} \quad (24.50)$$

$$G_R(\tau) = \frac{\overline{C}_R D_R(\tau) + \overline{C}_{GR} D_{GR}(\tau)}{V_{eff}(\overline{C}_R + \overline{C}_{GR})^2} \quad (24.51)$$

$$G_{GR}(\tau) = \frac{\overline{C}_{GR} D_{GR}(\tau)}{V_{eff}(\overline{C}_G + \overline{C}_{GR})(\overline{C}_R + \overline{C}_{GR})} \quad (24.52)$$

where $D_i(\tau)$ are the portion of the correlation functions that contain the diffusion coefficients. These expressions can be

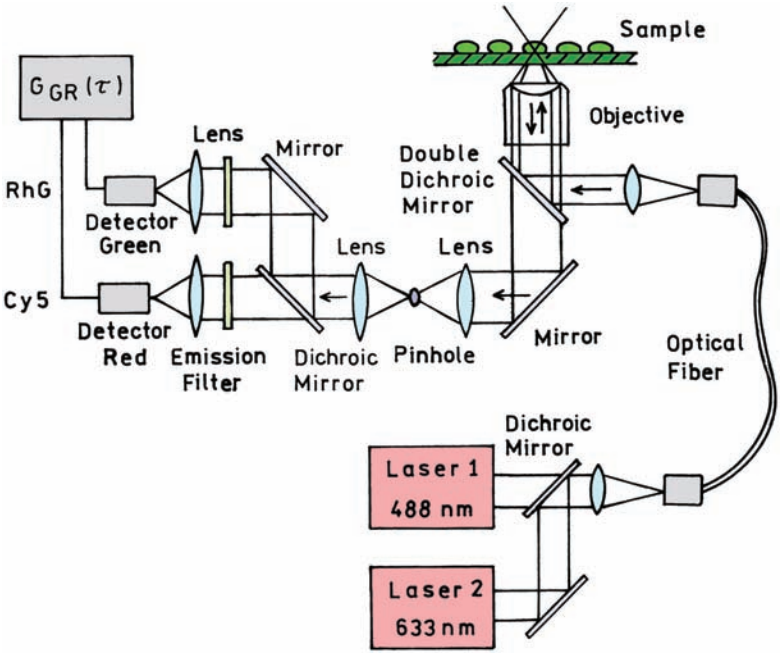

Figure 24.37. Instrumentation for dual-color FCS. Revised from [125].

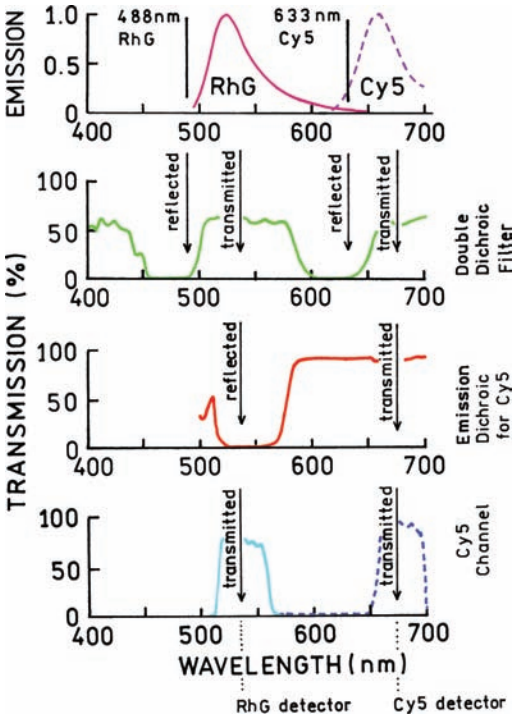

Figure 24.38. Optical filters for FCCS using RhG and Cy5. In the bottom panel the solid line is the dichroic mirror and the dashed line is the emission filter. Revised from [125].

understood as each autocorrelation function being the weighted sum for each species (G and R) as seen through one of the channels. For instance, the G fluorophore is detected in the G channel if it is present on the G or GR particle. It is important to notice that the amplitude of the cross-correlation function is proportional to the concentration of the doubly labeled species C_{GR}.

Because of the different excitation wavelengths the dimension of the observed volume will be different for each color, and different for the cross-correlation function. For each channel

$$V_{\text{eff}}^{\text{G}} = \pi^{3/2} s_{\text{G}}^2 u_{\text{G}}, \quad \tau_{\text{D}}^{\text{G}} = \frac{s_{\text{G}}^2}{4D} \tag{24.53}$$

$$V_{\text{eff}}^{\text{R}} = \pi^{3/2} s_{\text{R}}^2 u_{\text{R}}, \quad \tau_{\text{D}}^{\text{R}} = \frac{s_{\text{R}}^2}{4D} \tag{24.54}$$

For the cross-correlation measurement

$$V_{\text{eff}}^{\text{GR}} = \frac{\pi^{3/2}}{2^{3/2}} \left[(s_{\text{G}}^2 + s_{\text{R}}^2)(u_G^2 + u_{\text{R}}^2) \right]^{1/2} \tag{24.55}$$

$$\tau_{\text{GR}} = \frac{s_{\text{G}}^2 + s_{\text{R}}^2}{8D} \tag{24.56}$$

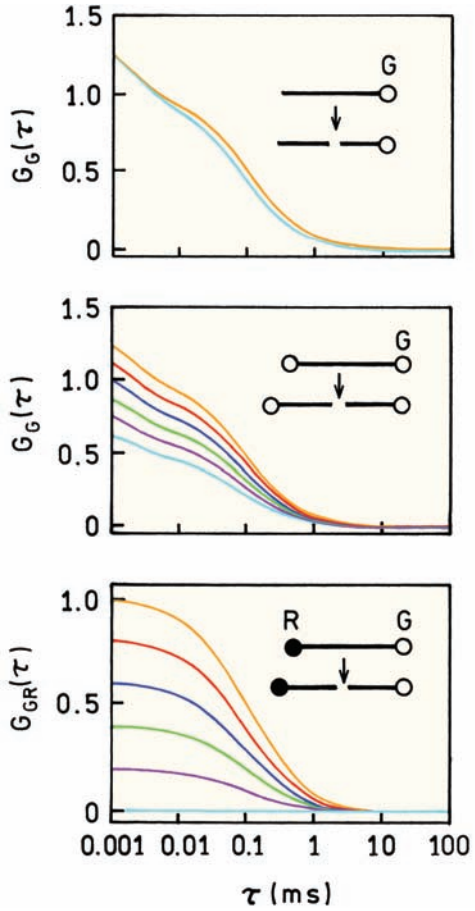

Figure 24.39. Autocorrelation and cross-correlation function for cleaving of labeled DNA. Revised from [125].

It is informative to visualize how the cross-correlation function is different from autocorrelation functions. Assume a DNA strand is labeled and cleaved by an enzyme (Figure 24.39). If the strand contains one green fluorophore and the strand is cut in half, then $G_G(\tau)$ shifts slightly to shorter diffusion times due to slightly faster diffusion: $2^{1/3}$ = 1.26-fold. The intercept $G_G(0)$ is not changed because the number of diffusing fluorophores remains the same. Now assume the DNA contains two green fluorophores, one on each end. Cleavage of the strand again results in an increase in the diffusion coefficient, but also a decrease in $G_G(0)$ because the number of independent diffusing species is doubled. In practice it may be difficult to quantify the $G(0)$ value since it depends on the bulk concentration and the extent of triplet formation.

A remarkably different and useful result is obtained if the fluorophore is labeled on each end, but with a different-color fluorophore (Figure 24.39 bottom). In the intact strand the G and R fluorophores diffuse together and yield a cross-correlation function $G_{GR}(\tau)$ that is proportional to the concentration of the intact strand. As the DNA is cleaved the amplitude of the cross-correlation function decreases dramatically to zero when all the DNA is cleaved. The cross-correlation measurement detects only the doubly labeled species. Notice that the amplitude of $G_{GR}(\tau)$ is proportional to C_{GR}, rather than the inverse, C_G^{-1} or C_R^{-1}, as for the autocorrelation functions.

While dual-color FCCS is very powerful it does have some intrinsic limitations. Examination of eq. 24.52 reveals that the cross-correlation amplitude is inversely proportional to the concentration of the singly labeled species. Hence FCCS is not useful for detection of trace amounts of doubly labeled species in the presence of excess amounts of singly labeled species.

24.13.3. DNA Cleavage by a Restriction Enzyme

The unique information provided by FCCS is illustrated by the cleavage of a 66-bp long double-stranded DNA oligomer.[125] This DNA is labeled on one end with rhodamine green (RhG) and on the other end Cy5. The cleavage site for the restrictive enzyme EcoRI is near the middle of the strand (Figure 24.40). The cross-correlation was measured for various times following addition of EcoRI, and its amplitude decreased progressively to near zero. The residual amplitude at long times is probably due to crosstalk between the channels.

At first glance one may think that the cross-correlation signal is dependent on RET between RhG and Cy5 (Figure 24.38), since these probes would be a good donor–acceptor pair for Förster transfer. However, the distance between RhG and Cy5 in the 66-mer is too long for RET. The appearance of cross-correlation does not depend on energy transfer, but instead on the two probes being linked so both appear in the observed volume at the same time.

24.13.4. Applications of Dual-Color FCCS

Applications of FCCS have already been published.[133–142] One example is the stoichiometry of binding of RNA oligomers to transcription activator protein NtrC.[136] This protein controls part of the nitrogen metabolism pathway in bacteria. It was thought that the octameric NtrC complex may bind two DNA oligomers, which could be tested by dual-color FCS. The oligomers were labeled with either

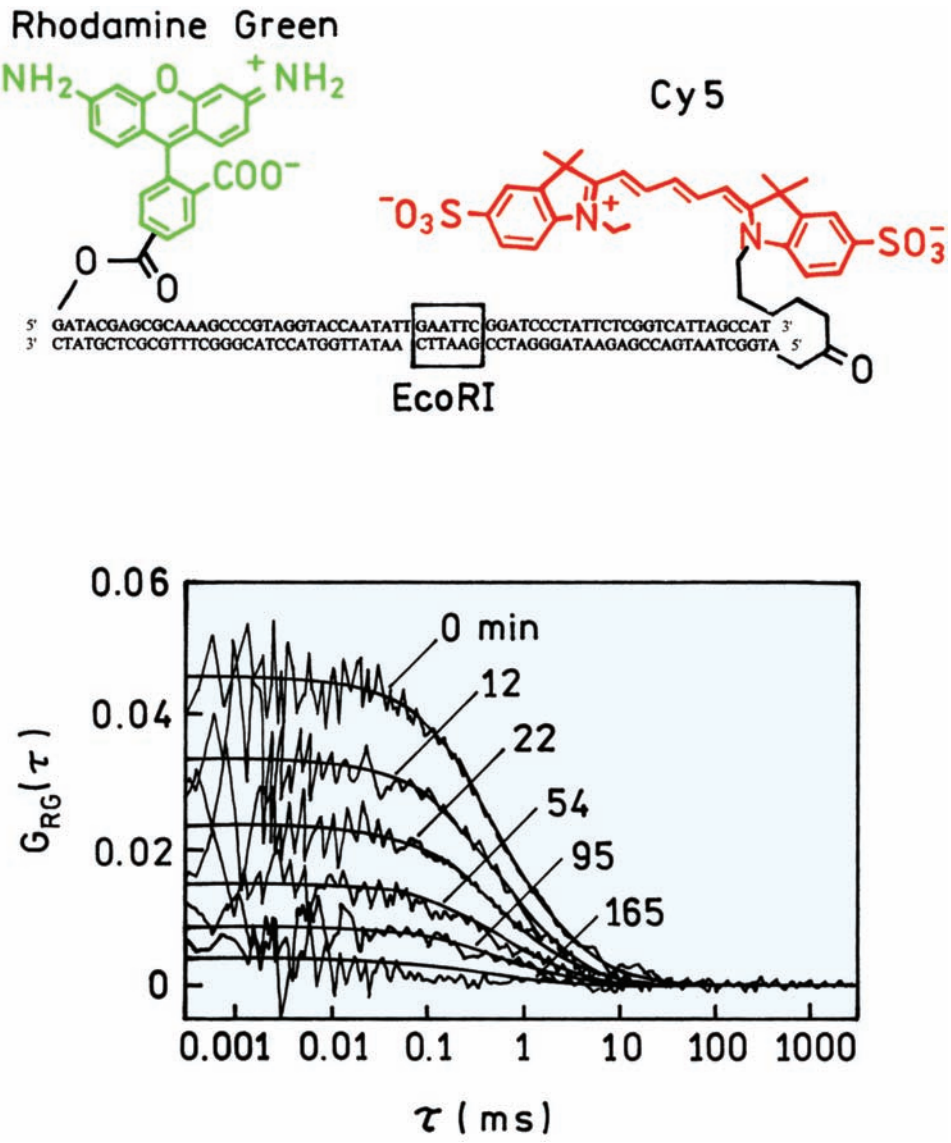

Figure 24.40. Sequence of DNA labeled with both RhG and Cy5. The lower panel shows the cross-correlation function during incubation of the labeled DNA with the restriction enzyme EcoRI. Revised from [125].

FAM or ROX (Figure 24.41). Detection of binding of both labeled oligomers was demonstrated by the cross-correlation signal. If NtrC bound only one oligomer then the cross-correlation amplitude would be zero.

Dual-color FCCS is likely to find widespread use in studies of gene expression. This can be accomplished by synthesis of two oligonucleotides, each labeled with a different fluorophore and each specific for a different region of the same gene. The concept of the experiment is shown in Figure 24.42.[137] The RNA from the cells of interest is extracted and converted to cDNA using reverse transcriptase. The cDNA is then mixed with the two labeled probes, which are specific for nearby regions of the same gene. If the gene is present the G and R probes bind near to each other and create a cross-correlation signal. If the probes are mixed with cDNA that was depleted of this gene the cross-correlation signal is near zero.

Dual-color FCS can be used to measure protein association. Aggregation of amyloid proteins appears to be an important component of Alzheimer's disease, and aggregation of prion proteins occurs in bovine spongiform encephalopathy and Creutzfeldt-Jakob disease.[138] Dual-color FCS has been used to study aggregation of prion proteins (PrP). The isolated proteins were labeled either with

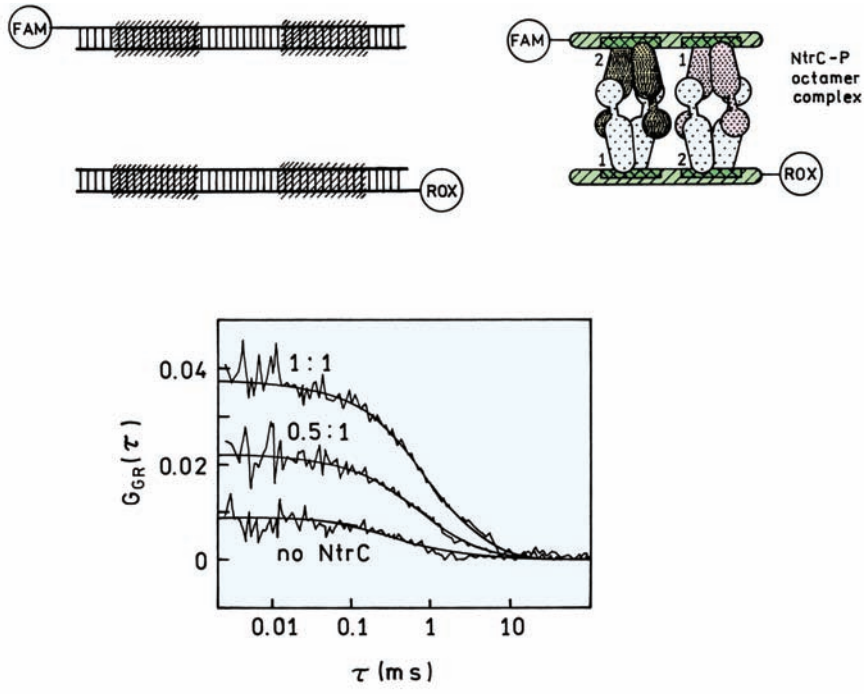

Figure 24.41. Detection of binding of two DNA oligomers to the regulatory protein NtrC by dual-color FCCS. Revised and reprinted with permission from [136]. Copyright © 2000, American Chemical Society.

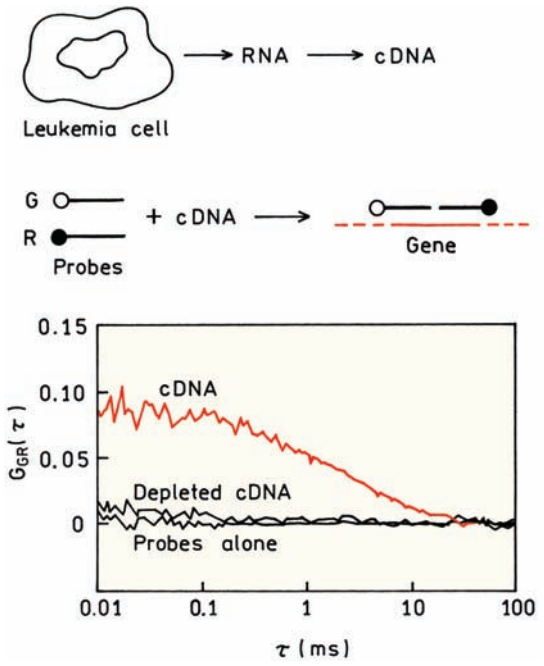

Figure 24.42. Detection of gene expression using dual-color FCCS. Revised from [137].

Cy5 or Oregon Green.[139] A cross-correlation signal appeared immediately upon mixing (Figure 24.43), showing the formation of aggregates. The use of FCCS allows kinetics to be studied, and to see if aggregate formation is spontaneous or requires seeds of aggregated proteins.

In the previous examples the needed information was contained in the amplitude of the cross-correlation function. The diffusion coefficients were not needed, and hence there was no need to calculate the cross-correlation function. Instead, the data can be analyzed by coincidence analysis.[143–147] The oligonucleotides with the desired requirements are labeled with two different probes (Figure 24.44). Instead of the correlation function one records the time-dependent intensities from each channel. The data are analyzed to count the number of events where signals appear in both channels.

24.14. ROTATIONAL DIFFUSION AND PHOTON ANTIBUNCHING Advanced Topic

Since FCS is sensitive to translational diffusion it seems logical to use FCS to measure rotational diffusion. Such measurements would be useful because rotational correlation times are directly proportional to the molecular weight, but translational diffusion coefficients are proportional to

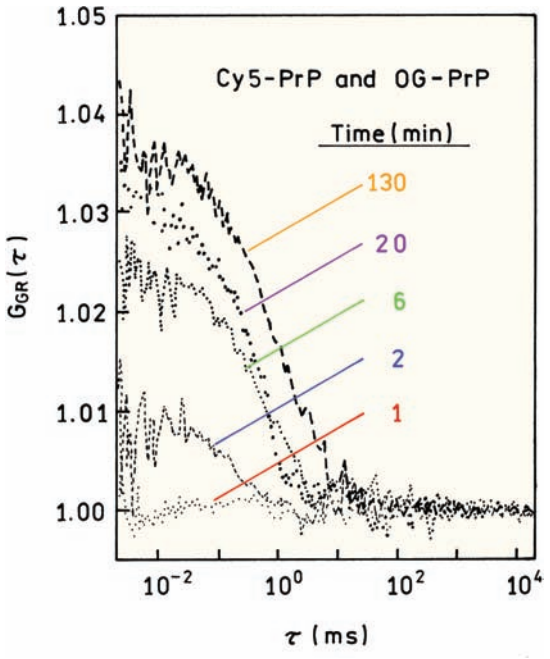

Figure 24.43. Association of prion proteins (PrP) by dual wavelength cross-correlation FCS. PrP were labeled with either Cy5 or Oregon Green (OG). Revised from [139].

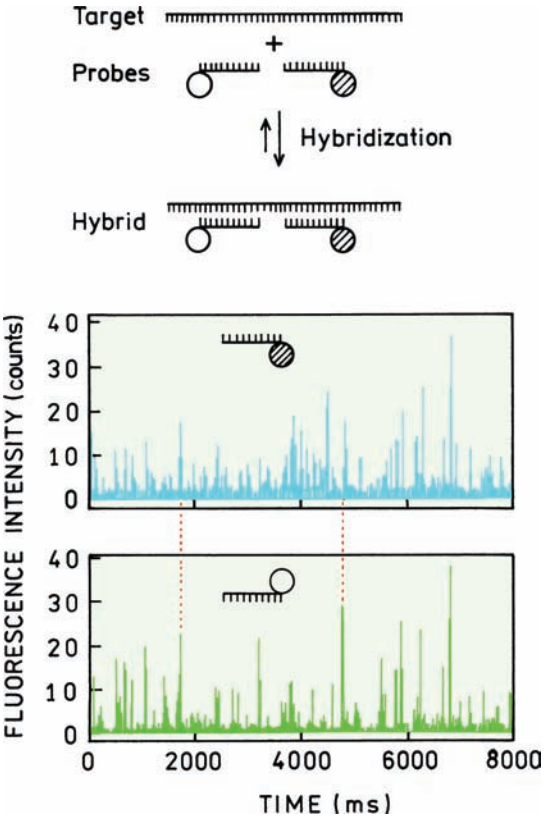

Figure 24.44. Coincidence analysis to detect λ phage DNA. Coincidence events are shown by the vertical dashed lines. Revised and reprinted with permission from [143]. Copyright © 1997, American Chemical Society.

(MW)$^{1/3}$. The use of FCS to measure the hydrodynamics and internal dynamics of macromolecules is promising because the timescale is not limited by fluorescence lifetimes. However, there have been relatively few publications on rotational diffusion[148–152] because there are a number of physical limitations and technical challenges. To measure rotational motions using FCS it is necessary to account for photon antibunching and triplet formation, which can occur on the same timescale as rotational diffusion.

In a typical FCS experiment the timescale of interest is the diffusion time τ_D, which is usually much longer than the fluorescence lifetime τ_F. Hence there is time for the fluorophore to return to the ground state to be excited again while still in the observed volume. However, rotational correlation times θ are usually comparable to the lifetimes and much shorter than the diffusion times. In order to observe a correlation it is necessary to detect more than a single photon from the molecule before its orientation is randomized by rotational diffusion. While the fluorophore is in the excited state it cannot be excited again. As a result there is always some time delay, comparable to the fluorescence lifetime, between detection of two photons from the same fluorophore. This delay is called photon antibunching, to indicate that detection of a second photon is statistically less probably as the time delay becomes smaller.[153–155]

An optical configuration for anisotropy FCS (AFCS) is shown in Figure 24.45. The sample is excited with polarized light. The emission is observed using two detectors. The emission is split by a beamsplitter that randomly transmits or reflects the photons. The detection electronics is similar to that used for TCSPC. The difference in arrival times of the emitted photons is measured with the time-domain electronics. Because the photons are randomly distributed the first photon can arrive in either channel, so the correlation function will appear to be symmetrical around $\tau = 0$. Figure 24.45 shows polarizers in the emission light paths, but they are not necessary because photoselection occurs upon excitation.

The theory for AFCS can be complex,[148–149] so we will present the simplest case. Assume that the lifetime τ_F is much shorter than the rotational correlation time θ, and that

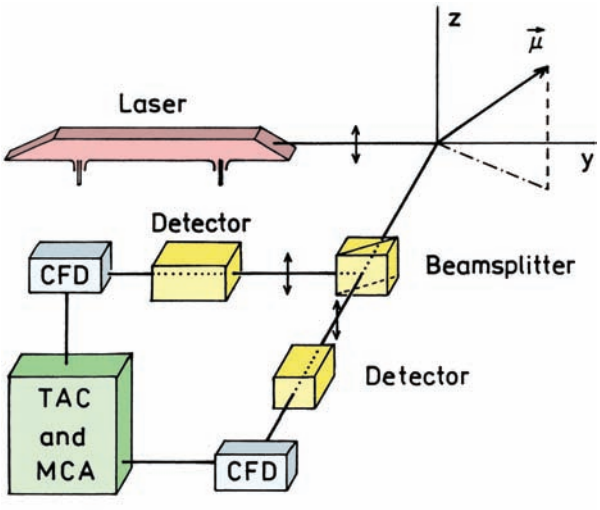

Figure 24.45. Measurement of photon antibunching and rotational diffusion by FCS. CFD, constant fraction discriminator. TAC, time-to-amplitude converter. MCA, multichannel analyses. Revised from [150].

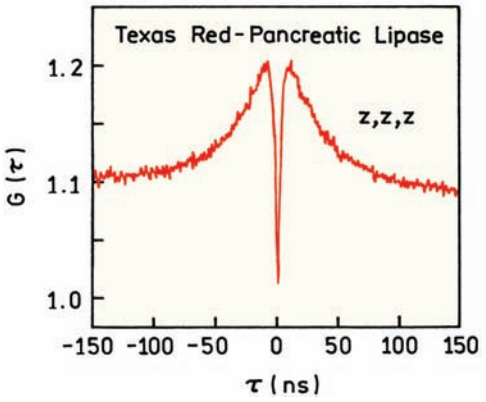

Figure 24.46. Measurement of rotational diffusion of Texas Red-labeled pancreatic lipase using FCS. Revised from [151].

both of these are shorter than the diffusion time. Also assume that the absorption and emission dipoles are parallel, and that the excitation is polarized in the z direction and the emission is observed without polarizers, the observed volume is long along the z-axis. The correlation function is then given by

$$G(\tau) = G(0)\Big[\frac{1}{1+\tau/\tau_D} + \frac{4}{5}\exp\Big(\frac{-\tau}{\theta}\Big) - \frac{9}{5}\exp\Big(\frac{-\tau}{\tau_F}\Big)\Big] \qquad (24.57)$$

The correlation time information is available without polarizers because the probability of excitation depends on the orientation of the fluorophore relative to the incident polarization. This separation of correlation time from lifetime can be seen in the middle term of eq. 24.57, where the exponential relationship depends on the ratio of the experimental correlation time τ to the rotational correlation time θ. This is different from time-resolved anisotropy decays, where the lifetime must be comparable to the rotational correlation time to obtain useful information. The last term in eq. 24.57 represents the photon antibunching, which decreases exponentially with the ratio of the experimental correlation time to the lifetime τ_F.

It is interesting to notice that eq. 24.57 contains two exponential terms plus the diffusion term. Recall that the concentration autocorrelation function is also exponential in τ (eq. 24.11). The averaging over a Gaussian volume results in the dependence shown in eq. 24.57. The photon antibunching term and the rotational diffusion terms still show the exponential dependence because they do not depend on the position of the fluorophore in the volume.

Figure 24.46 shows an AFCS experiment, in this case for pancreatic lipase labeled with Texas Red.[151] The data were collected using three parallel polarizers (Figure 24.45), so that eq. 24.57 is not appropriate for these data but requires additional geometric factors. $G(\tau)$ is symmetrical because of the random distribution of photons by the beamsplitter. Notice that the timescale is ns rather than ms because rotational diffusion occurs on this timescale. The dip in the middle is due to photon antibunching and is several ns wide, comparable to the lifetime τ_F. The decays on either side are due, at least in part, to rotational diffusion of the protein.

24.15. FLOW MEASUREMENTS USING FCS

As a final application of FCS we will describe how it can be used to detect the velocity in flowing samples. This is not a trivial problem, especially in microfluidic structures where the velocity will vary across the channel and will be different in branches of a channel. The theory of FCS with flow has been described,[156] and the interest in such measurements appears to be growing rapidly.[157–162] A typical

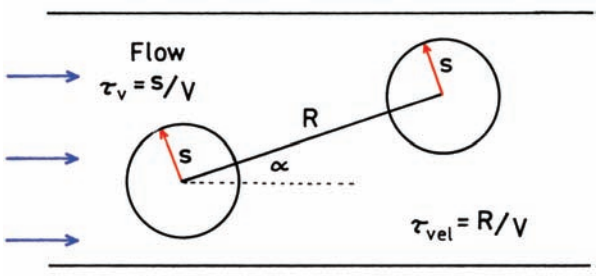

Figure 24.47. Flow velocity measurements using FCS.

arrangement for flow measurements is shown in Figure 24.47. The flowing sample is illuminated with one laser beam or with two spatially separated laser beams. Flow velocities can be measured using either the autocorrelation function from one volume or the cross-correlation signal from two spatially separated volumes.

When a single volume is observed the time a fluorophore remains in the laser beam is reduced in a flowing sample. $G(\tau)$ is expected to decay more quickly as the velocity increases. In the presence of flow, if diffusion can be neglected, the single volume autocorrelation function is given by

$$G(\tau) = \frac{1}{N} \exp\left[-\left(\frac{\tau}{\tau_V}\right)^2 \right] \qquad (24.58)$$

where τ_V is the time for a fluorophore to be swept through the volume at a velocity V:

$$\tau_V = s/V \qquad (24.59)$$

The effect of flow is shown in Figure 24.48 for rhodamine green in water.[161] In the absence of flow the usual autocorrelation function is observed. As the flow rate increases the curves shift progressively to shorter times, and begin to take on the exponential shape given by eq. 24.58. This shift is the result of the fluorophores being removed from the observed volume prior to being excited multiple times.

Another approach to measuring flow is to use cross-correlation between two spatially separate volumes (Figure 24.49). In this case the cross-correlation curves show a peak at the time needed for a fluorophore to flow from one volume to the next volume.[162] The increased amplitude below 0.1 ms is due to crosstalk between the channels. The expression for cross-correlation due to flow, neglecting diffusion, is given by

$$G(\tau) = \frac{1}{N} \exp\left[\frac{-R^2}{s^2}\left(\frac{\tau^2}{\tau_{vel} V^2} + 1 - 2\frac{\tau^2}{\tau_{vel}^2} \cos\alpha \right) \right] \qquad (24.60)$$

where $\tau_{vel} = R/V$. This last expression is complex, but the result is simple. The cross-correlation curves show a peak at

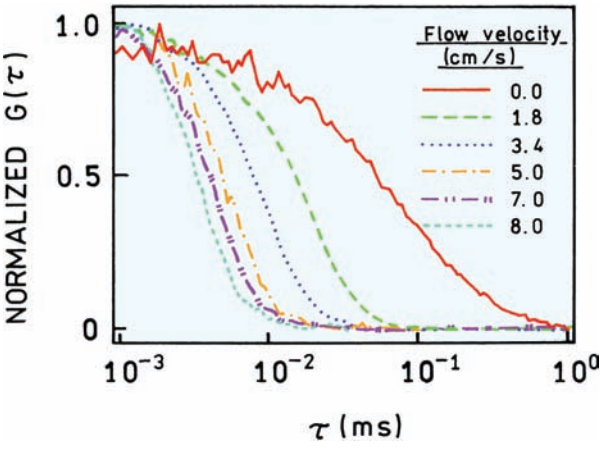

Figure 24.48. Normalized autocorrelation curves for 5-nM rhodamine green flowing in a capillary. Revised and reprinted with permission from [161]. Copyright © 2002, American Chemical Society.

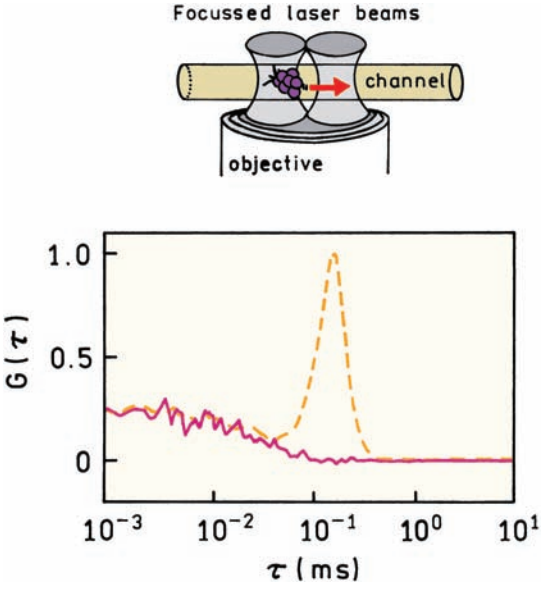

Figure 24.49. Measurement of the flow of TMR in water using cross-correlation between spatially separated channels. Revised and reprinted with permission from [162]. Copyright © 2002, American Chemical Society.

a time that corresponds to the transit time between the two volumes.

24.16. ADDITIONAL REFERENCES ON FCS

FCS is in a stage of rapid development. Additional references on various aspects of FCS are listed after the main reference section.

REFERENCES

1. Magde D, Elson E, Webb WW. 1972, Thermodynamic fluctuations in a reacting system—measurement by fluorescence correlation spectroscopy. *Phys Rev Lett* **29**(11):705–708.
2. Elson E, Magde D. 1974. Fluorescence correlation spectroscopy: conceptual basis and theory. *Biopolymers* **13**:1–27.
3. Magde D, Elson E, Webb WW. 1974. Fluorescence correlation spectroscopy. *Biopolymers* **13**:29–61.
4. Aragon SR, Pecora R. 1975. Fluorescence correlation spectroscopy and brownian rotational diffusion. *Biopolymers* **14**:119–138.
5. Rigler R. Elson ES, eds. 2001. *fluorescence correlation spectroscopy: theory and applications*. Springer, New York.
6. Webb WW. 2001. Fluorescence correlation spectroscopy: genesis, evolution, maturation and prognosis. In *Fluorescence correlation spectroscopy: theory and applications*, pp. 305–330. Ed R Rigler, ES Elson. Springer, New York.
7. Eigen M, Rigler R. 1994. Sorting single molecules: application to diagnostics and evolutionary biotechnology. *Proc Natl Acad Sci USA* **91**:5740–5747.
8. Haustein E, Schwille P. 2003. Ultrasensitive investigations of biological systems by fluorescence correlation spectroscopy. *Methods* **29**: 153–166.
9. Visser AJWG, Hink MA. 1999. New perspectives of fluorescence correlation spectroscopy. *J Fluoresc* **9**(1):81–87.
10. Thompson NL, Lieto AM, Allen NW. 2002. Recent advances in fluorescence correlation spectroscopy. *Struct Biol* **12**:634–641.
11. Hess ST, Huang S, Heikal AA, Webb WW. 2002. Biological and chemical applications of fluorescence correlation spectroscopy: a review. *Biochemistry* **41**(3):647–708.
12. Brock R, Jovin TM. 2001. Fluorescence correlation microscopy (FCM): fluorescence correlation spectroscopy (FCS) in cell biology. In *Fluorescence correlation spectroscopy: theory and applications*, pp. 133–161. Ed R Rigler, ES Elson. Springer, New York.
13. Rigler R. 1995. Fluorescence correlations, single molecule detection and large number screening: applications in biotechology. *J Biotechnol* **41**:177–186.
14. Földes-Papp Z, Demel U, Domej W, Tilz GP. 2002. A new dimension for the development of fluorescence-based assays in solution: from physical principles of FCS detection to biological applications. *Exp Biol Med* **227**(5):291–300.
15. Sterer S, Henco K. 1997. Fluorescence correlation spectroscopy (FCS)—a highly sensitive method to analyze drug/target interactions. *J Recept Signal Transduction Res* **17**(1–3):511–520.
16. Kim SA, Schwille P. 2003. Intracellular applications of fluorescence correlation spectroscopy: prospects for neuroscience. *Curr Opin Neurobiol* **13**:583–590.
17. Widengren J, Mets Ü. 2002. Conceptual basis of fluorescence correlation spectroscopy and related techniques as tools in bioscience. In *Single molecule detection in solution*, pp. 69–120. Ed CH Zander, J Enderlein, RA Keller. Wiley-VCH, Darmstadt, Germany.
18. Thompson NL. 1991. Fluorescence correlation spectroscopy. In *Topics in fluorescence spectroscopy*, Vol. 1: *Techniques*, pp. 337–378. Ed JR Lakowicz. Plenum Press, New York.
19. Rigler R, Mets Ü, Widengren J, Kask P. 1993. Fluorescence correlation spectroscopy with high count rate and low background: analysis of translational diffusion. *Eur Biophys J* **22**:169–175.
20. Rigler R, Widengren J, Mets Ü. 1993. Interactions and kinetics of single molecules as observed by fluorescence correlation spectroscopy. In *Fluorescence spectroscopy*, pp. 14–24. Ed O Wolfbeis. Springer-Verlag, New York.
21. Müller JD, Chen Y, Gratton E. 2003. Fluorescence correlation spectroscopy. *Methods Enzymol* **361**:69–92.
22. Maiti S, Haupts U, Webb WW. 1997. Fluorescence correlation spectroscopy: diagnostics for sparse molecules. *Proc Natl Acad Sci USA* **94**:11753–11757.
23. Pack CG, Nishimura G, Tamura M, Aoki K, Taguchi H, Yoshida M, Kinjo M. 1999. Analysis of interaction between chaperonin GroEL and its substrate using fluorescence correlation spectroscopy. *Cytometry* **36**:247–253.
24. Meyer-Almes FJ. 2001. Nanoparticle immunoassays: a new method for use in molecular diagnostics and high throughput pharmaceutical screening based on fluorescence correlation spectroscopy. In *Fluorescence correlation spectroscopy: theory and applications*, pp. 379–395. Ed R Rigler, ES Elson. Springer, New York.
25. Wohland T, Friedrich K, Hovius R, Vogel H. 1999. Study of ligand-receptor interactions by fluorescence correlation spectroscopy with different fluorophores: evidence that the homopentameric 5-hydroxytryptamine type 3_{As} receptor binds only one ligand. *Biochemistry* **38**:8671–8681.
26. Van Craenenbroeck E, Engelborghs Y. 1999. Quantitative characterization of the binding of fluorescently labeled colchicine to tubulin in vitro using fluorescence correlation spectroscopy. *Biochemistry* **38**: 5082–5088.
27. Larson DR, Ma YM, Vogt VM, Webb WW. 2003. Direct measurement of gag–gag interaction during retrovirus assembly with FRET and fluorescence correlation spectroscopy. *J Cell Biol* **162**(7):1233–1244.
28. Pitschke M, Prior R, Haupt M, Riesner D. 1999. Detection of single amyloid β-protein aggregates in the cerebrospinal fluid of Alzheimer's patients by fluorescence correlation spectroscopy. *Nature Med* **4**(7):832–834.
29. Schwille P, Bieschke J, Oehlenschlager F. 1997. Kinetic investigations by fluorescence correlation spectroscopy: the analytical and diagnostic potential of diffusion studies. *Biophys Chem* **66**:211–228.
30. Schwille P, Oehlenschlager F, Walter NG. 1996. Quantitative hybridization kinetics of DNA probes to RNA in solution followed by diffusional fluorescence correlation analysis. *Biochemistry* **35**: 10182–10193.

31. Bjorling S, Kinjo M, Foldes-Papp Z, Hagman E, Thyberg P, Rigler R. 1998. Fluorescence correlation spectroscopy of enzymatic DNA polymerization. *Biochemistry* **37**:12971–12978.
32. Rigler R, Foldes-Papp Z, Meyer-Almes FJ, Sammet C, Volcker M, Schnetz A. 1998. Fluorescence cross-correlation: a new concept for polymerase chain reaction. *Biotechnology* **63**:97–109.
33. Kinjo M. 1998. Detection of asymmetric PCR products in homogeneous solution by fluorescence correlation spectroscopy. *Biotechnology* **25**:706–715.
34. Schubert F, Zettl H, Hafner W, Krauss G, Krausch G. 2003. Comparative thermodynamic analysis of DNA–protein interactions using surface plasmon resonance and fluorescence correlation spectroscopy. *Biochemistry* **42**:10288–10294.
35. Wohland T, Friedrich-Benet K, Pick H, Preuss A, Hovius R, Vogel H. 2001. The characterization of a transmembrane receptor protein by fluorescence correlation spectroscopy. In *Single molecule spectroscopy*, pp. 195–210. Ed R Rigler, M Orrit, T Basche. Springer, New York.
36. Schuler J, Frank J, Trier U, Schäfer-Korting M, Saenger W. 1999. Interaction kinetics of tetramethylrhodamine transferrin with human transferrin receptor studied by fluorescence correlation spectroscopy. *Biochemistry* **38**:8402–8408.
37. Pick H, Preuss AK, Mayer M, Wohland T, Hovius R, Vogel H. 2003. Monitoring expression and clustering of the ionotropic $5HT_3$ receptor in plasma membranes of live biological cells. *Biochemistry* **42**: 877–884.
38. Boukari H, Nossal R, Sackett DL. 2003. Stability of drug-induced tubulin rings by fluorescence correlation spectroscopy. *Biochemistry* **42**:1292–1300.
39. Sevenich FW, Langowski J, Weiss V, Rippe K. 1998. DNA binding and oligomerization of ntrC studied by fluorescence anisotropy and fluorescence correlation spectroscopy. *Nucleic Acids Res* **26**(6): 1373–1381.
40. Auer M, Moore KJ, Meyer-Almes FJ, Guenther R, Pope AJ, Stoeckli KA. 1998. Fluorescence correlation spectroscopy: lead discovery by miniaturized HTS. *Drug Discovery Today* **3**(10):457–465.
41. Xu H, Frank J, Trier U, Hammer S, Schroder W, Behlke J, Schafer-Korting M, Holzwarth JF, Saenger W. 2001. Interaction of fluorescence labeled single-stranded DNA with hexameric DNA-helicase repA: a photon and fluorescence correlation spectroscopy study. *Biochemistry* **40**:7211–7218.
42. Daniel DC, Thompson M, Woodbury NW, 2002. DNA-binding interactions and conformational fluctuations of tc3 transposase DNA binding domain examined with single molecule fluorescence spectroscopy. *Biophys J* **82**:1654–1666.
43. Kral T, Langner M, Benes M, Baczynska D, Ugorski M, Hof M. 2002. The application of fluorescence correlation spectroscopy in detecting DNA condensation. *Biophys Chem* **95**:135–144.
44. Kral T, Hof M, Langner M. 2002. The effect of spermine on plasmid condensation and dye release observed by fluorescence correlation spectroscopy. *Biol Chem* **383**:331–335.
45. Schwille P, Oehlenschlager F, Walter NG. 1996. Quantitative hybridization kinetics of DNA probes to RNA in solution followed by diffusional fluorescence correlation analysis. *Biochemistry* **35**: 10182–10193.
46. Kinjo M, Rigler R. 1995. Ultrasensitive hybridization analysis using fluorescence correlation spectroscopy. *Nucleic Acids Res* **23**:1795–1799.
47. Foldes-Papp Z, Kinjo M. 2001. Fluorescence correlation spectroscopy in nucleic acid analysis. In *Fluorescence correlation spectroscopy: theory and applications*, pp. 25–64. Ed R Rigler, ES Elson. Springer, New York.
48. Nishimura G, Rigler R, Kinjo M. 1997. Number analysis of fluorescence correlation spectroscopy for the cleaving process of fluorescence labeled DNA. *Bioimaging* **5**:129–133.
49. Kovacic RT, van Holde KE. 1977. Sedimentation of homogeneous double-strand DNA molecules. *Biochemistry* **16**(7):1490–1498.
50. Eisenberg D, Crothers D, eds. 1979. *Physical chemistry with applications to the life sciences*, Benjamin Cummings, Melno Park, CA.
51. Kinjo M, Nishimura G, Koyama T, Mets Ü, Rigler R. 1998. Single-molecule analysis of restriction DNA fragments using fluorescence correlation spectroscopy. *Anal Biochem* **260**:166–172.
52. Fradin C, Abu-Arish A, Granek R, Elbaum M. 2003. Fluorescence correlation spectroscopy close to a fluctuating membrane. *Biophys J* **84**:2005–2020.
53. Benda A, Benes M, Marecek V, Lhotsky A, Hermens WTh, Hof M. 2003. How to determine diffusion coefficients in planar phospholipid systems by confocal fluorescence spectroscopy. *Langmuir* **19**:4120–4126.
54. Palmer III AG, Thompson NL. 1989. Fluorescence correlation spectroscopy for detecting submicroscopic clusters of fluorescent molecules in membranes. *Chem Phys Lipids* **50**:253–270.
55. Hegener O, Jordan R, Haberlein H. 2002. Benzodiazepine binding studies on living cells: application of small ligands for fluorescence correlation spectroscopy. *Biol Chem* **383**:1801–1807.
56. Briddon SJ, Middleton RJ, Yates AS, George MW, Kellam B, Hill SJ. 2004. Application of fluorescence correlation spectroscopy to the measurement of agonist binding to a G-protein coupled receptor at the single cell level. *Faraday Discuss* **126**:197–207.
57. Hink MA, van Hoek A, Visser AJWG. 1999. Dynamics of phospholipid molecules in micelles: characterization with fluorescence correlation spectroscopy and time-resolved fluorescence anisotropy. *Langmuir* **15**:992–997.
58. Gennerich A, Schild D. 2002. Anisotropic diffusion in mitral cell dendrites revealed by fluorescence correlation spectroscopy. *Biophys J* **83**:510–522.
59. Meissner O, Häberlein H. 2003. Lateral mobility and specific binding to $GABA_A$ receptors on hippocampal neurons monitored by fluorescence correlation spectroscopy. *Biochemistry* **42**:1667–1672.
60. Pramanik A, Thyberg P, Rigler R. 2000. Molecular interactions of peptides with phospholipid vesicle membranes as studied by fluorescence correlation spectroscopy. *Chem Phys Lipids* **104**:35–47.
61. Kahya N, Scherfeld D, Bacia K, Poolman B, Schwille P. 2003. Probing lipid mobility of raft-exhibiting model membranes by fluorescence correlation spectroscopy. *J Biol Chem* **278**(30):28109–28115.
62. Schwille P, Haupts U, Maiti S, Webb WW. 1999. Molecular dynamics in living cells observed by fluorescence correlation spectroscopy with one- and two- photon excitation. *Biophys J*, **77**:2251–2265.

63. Schwille P, Korlach J, Webb WW. 1999. Fluorescence correlation spectroscopy with single-molecule sensitivity on cell and model membranes. *Cytometry* **36**:176–182.
64. Weiss M, Hashimoto H, Nilsson T. 2003. Anomalous protein difussion in living cells as seen by fluorescence correlation spectroscopy. *Biophys J* **84**:4043–4052.
65. Wachsmuth M, Waldeck W, Langowski J. 2000. Anomalous diffusion of fluorescent probes inside living cell nuclei investigated by spatially-resolved fluorescence correlation spectroscopy. *J Mol Biol* **298**:677–689.
66. Milon S, Hovius R, Vogel H, Wohland T. 2003. Factors influencing fluorescence correlation spectroscopy measurements on membranes: simulations and experiments. *Chem Phys* **288**:171–186.
67. Korlach J, Schwille P, Webb WW, Feigenson GW. 1999. Characterization of lipid bilayer phases by confocal microscopy and fluorescence correlation spectroscopy. *Proc Natl Acad Sci USA* **96**:8461–8466.
68. Steiner DF, Cunningham D, Spigelman L, Aten B. 1967. Insulin biosynthesis: evidence for a precursor. *Science* **157**:697–700.
69. Wahren J, Johansson B-L, Wallberg-Henriksson H. 1994. Does C-peptide have a physiological role? *Diabetologia* **37**(2):S99–S107.
70. Wahren J, Ekberg K, Johansson J, Henriksson M, Pramanik A, Johansson B-L, Rigler R, Jörnvall H. 2000. Role of C-peptide in human physiology. *Am J Physiol Endocrinol Metab* **278**:E759–E768.
71. Rigler R, Pramanik A, Jonasson P, Kratz G, Jansson OT, Nygren PD, Stahl S, Ekberg K, Johansson B-L, Uhlén S, Uhlén M, Jörnvall H, Wahren J. 1999. Specific binding of proinsulin C-peptide to human cell membranes. *Proc Natl Acad Sci USA* **96**(23):13318–13323.
72. Zhong Z-H, Pramanik A, Ekberg K, Jansson OT, Jörnvall H, Wahren J, Rigler R. 2001. Insulin binding monitored by fluorescence correlation spectroscopy. *Diabetologia* **44**:1184–1188.
73. Pramanik A, Rigler R. 2001. FCS-analysis of ligand-receptor interactions in living cells. In *Fluorescence correlation spectroscopy: theory and applications*, pp. 101–131. Ed R Rigler, ES Elson. Springer, New York.
74. Wolf DE. 1992. Theory of fluorescence recovery after photobleaching measurements on cylindrical surfaces. *Biophys J* **61**:487–493.
75. Braeckmans K, Peeters L, Sanders NN, DeSmedt SC, Demeester J. 2003. Three-dimensional fluorescence recovery after photobleaching with the confocal scanning laser microscope. *Biophys J* **85**:2240–2252.
76. Lopez A, Dupou L, Altibelli A, Trotard J, Tocanne JF. 1988. Fluorescence recovery after photobleaching (FRAP) experiments under conditions of uniform disk illumination: critical comparison of anaytical solutions, and a new mathematical method for calculation of diffusion coefficient D. *Biophys J* **53**:963–970.
77. Widengren J, Rigler R, Mets Ü. 1994. Triplet-state monitoring by fluorescence correlation spectroscopy. *J Fluoresc* **4**(3):255–258.
78. Widengren J, Mets Ü, Rigler R. 1995. Fluorescence correlation spectroscopy of triplet states in solution: a theoretical and experimental study. *J Phys Chem* **99**:13368–13379.
79. Widengren J. 2001. Photophysical aspects of FCS measurements. In *Fluorescence correlation spectroscopy: theory and applications*, pp. 177–301. Ed R Rigler, ES Elson. Springer, New York.
80. Hegerfeldt GC, Seidel D. 2003. Blinking molecules: determination of photophysical parameters from the intensity correlation function. *J Chem Phys* **118**(17):7741–7746.
81. Widengren J, Mets Ü, Rigler R. 1999. Photodynamic properties of green fluorescent proteins investigated by fluorescence correlation spectroscopy. *Chem Phys* **250**:171–186.
82. Widengren J, Schwille P. 2000. Characterization of photoinduced isomerization and back-isomerization of the cyanine dye Cy5 by fluorescence correlation spectroscopy. *J Phys Chem A* **104**:6416–6428.
83. Widengren J, Rigler R. 1997. An alternative way of monitoring ion concentrations and their regulation using fluorescence correlation spectroscopy. *J Fluoresc* **7**(1):2118–2135.
84. Malvezzi-Campeggi F, Jahnz M, Heinze KG, Dittrich P, Schwille P. 2001. Light-induced flickering of DsRed provides evidence for distinct and interconvertible fluorescent states. *Biophys J* **81**:1776–1785.
85. Jung G, Mais S, Zumbusch A, Bräuchle C. 2000. The role of dark states in the photodynamics of the green fluorescent protein examined with two-color fluorescence excitation spectroscopy. *J Phys Chem* **104**(5):873–877.
86. Haupts U, Maiti S, Schwille P, Webb WW. 1998. Dynamics of fluorescence fluctuations in green fluorescent protein observed by fluorescence correlation spectroscopy. *Proc Natl Acad Sci USA* **95**:13573–13578.
87. Qian H, Elson EL. 1990. Distribution of molecular aggregation by analysis of fluctuation moments. *Proc Natl Acad Sci USA* **87**:5479–5483.
88. Müller JD, Chen Y, Gratton E. 2001. Photon counting histogram statistics. In *Fluorescence correlation spectroscopy: theory and applications*, pp. 410–437. Ed R Rigler, ES Elson. Springer, New York.
89. Kask P, Palo K, Ullmann D, Gall K. 1999. Fluorescence-intensity distribution analysis and its application in biomolecular detection technology. *Proc Natl Acad Sci USA* **96**:13756–13761.
90. Kask P, Palo K, Fay N, Brand L, Mets Ü, Ullmann D, Jungmann J, Pschorr J, Gall K. 2000. Two-dimensional fluorescence intensity distribution analysis: theory and application. *Biophys J* **78**:1703–1713.
91. Chen Y, Müller J, So PTC, Gratton E. 1999. The photon counting histogram in fluorescence fluctuation spectroscopy. *Biophys J* **77**:553–567.
92. Müller JD, Chen Y, Gratton E. 2000. Resolving heterogeneity on the single molecule level with the photon-counting histogram. *Biophys J* **78**:474–486.
93. Haupts U, Rüdiger M, Ashman S, Turconi S, Bingham R, Wharton C, Hutchinson J, Carey C, Moore KJ, Pope AJ. 2003. Single-molecule detection technologies in miniaturized high-throughput screening: fluorescence intensity distribution analysis. *J Biomol Screening* **8**(1):19–33.
94. Chen Y, Müller JD, Ruan Q-Q, Gratton E. 2002. Molecular brightness characterization of EGFP in vivo by fluorescence fluctuation spectroscopy. *Biophys J* **82**:133–144.
95. Laurence TA, Kapanidis AN, Kong X, Chemia DS, Weiss S. 2004. Photon arrival-time interval distribution (PAID): a novel tool for analyzing molecular interactions. *J Phys Chem B* **108**:3051–3067.
96. Chen Y, Wei L-N, Müller JD. 2003. Probing protein oligomerization in living cells with fluorescence fluctuation spectroscopy. *Proc Natl Acad Sci USA* **100**(26):15492–15497.
97. Kask P, Egeling C, Palo K, Mets Ü, Cole M, Gall K. 2002. Fluorescence intensity distribution analysis (FIDA) and related fluorescence fluctuation techniques: theory and practice. In *Fluorescence spectroscopy, imaging and probes. New tools in chemical, physical*

and life sciences, pp. 152–181. Ed R Kraayenhof, AJWG Visser, HC Gerritsen. Springer, New York.

98. Lamb DC, Schenk A, Rocker C, Scalfi-Happ C, Nienhaus GU. 2000. Sensitivity enhancement in fluorescence correlation spectroscopy of multiple species using time-gated detection. *Biophys J* **79**:1129–1138.
99. Palo K, Brand L, Eggeling C, Jager S, Kask P, Gall K. 2002. Fluorescence intensity and lifetime distribution analysis: toward higher accuracy in fluorescence fluctuation spectroscopy. *Biophys J* **83**: 605–618.
100. Bohmer M, Wahl M, Rahn HJ, Erdmann R, Enderlein J. 2002. Time-resolved fluorescence correlation spectroscopy. *Chem Phys Lett* **353**: 439–445.
101. Enderlein J, Erdmann R. 1997. Fast fitting of multi-exponential decay curves. *Opt Commun* **134**:371–378.
102. Chattopadhyay K, Saffarian S, Elson EL, Frieden C. 2002. Measurement of microsecond dynamic motion in the intestinal fatty acid binding protein by using fluorescence correlation spectroscopy. *Proc Natl Acad Sci USA* **99**(22):14171–14176.
103. Lumma D, Keller S, Vilgis T, Rädler JO. 2003. Dynamics of large semiflexible chains probed by fluorescence correlation spectroscopy. *Phys Rev Lett* **90**(21):218301-1–218301-4.
104. Borejdo J, Putnam S, Morales MF. 1979. Fluctuations in polarized fluorescence: evidence that muscle cross bridges rotate repetitively during contraction. *Proc Natl Acad Sci USA* **76**(12):6346–6350.
105. Altan-Bonnet G, Libchaber A, Krichevsky O. 2003. Bubble dynamics in double-stranded DNA. *Phys Rev Lett* **90**(13):138101-1–138101-4
106. Edman L, Rigler R. 2000. Memory landscapes of single-enzyme molecules. *Proc Natl Acad Sci USA* **97**(15):8266–8271.
107. Wallace MI, Ying L, Balasubramanian S, Klenerman D. 2000. FRET fluctuation spectroscopy: exploring the conformational dynamics of a DNA hairpin loop. *J Phys Chem B* **104**:11551–11555.
108. Bonnet G, Krichevsky O, Libchaber A. 1998. Kinetics of conformational fluctuations in DNA hairpin-loops. *Proc Natl Acad Sci USA* **95**:8602–8606.
109. Thompson NL, Burghardt TP, Axelrod D. 1981. Measuring surface dynamics of biomolecules by total internal reflection fluorescence with photobleaching recovery or correlation spectroscopy. *Biophys J* **33**:435–455.
110. Starr TE, Thompson NL. 2001. Total internal reflection with fluorescence correlation spectroscopy combined surface reaction and solution diffusion. *Biophys J* **80**:1575–1584.
111. Lieto AM, Cush RC, Thompson NL. 2003. Ligand-receptor kinetics measured by total internal reflection with fluorescence correlation spectroscopy. *Biophys J* **85**:3294–3302.
112. Starr TE, Thompson NL. 2002. Local diffusion and concentration of IgG near planar membranes: Measurement by total internal reflection with fluorescence correlation spectroscopy. *J Phys Chem B* **106**:2365–2371.
113. Hansen RL, Harris JM. 1998. Total internal reflection fluorescence correlation spectroscopy for counting molecules at solid/liquid interfaces. *Anal Chem* **70**:2565–2575.
114. Hansen RL, Harris JM. 1998. Measuring reversible adsorption kinetics of small molecules at solid/liquid interfaces by total internal reflection fluorescence correlation spectroscopy. *Anal Chem* **70**: 4247–4256.
115. McCain KS, Harris JM. 2003. Total internal reflection fluorescence-correlation spectroscopy study of molecular transport in thin sol-gel films. *Anal Chem* **75**:3616–3624.
116. Guiot E, Enescu M, Arrio B, Johannin G, Roger G, Tosti S, Tfibel F, Mérola F, Brun A, Georges P, Fontaine-Aupart MP. 2000. Molecular dynamics of biological probes by fluorescence correlation microscopy with two-photon excitation. *J Fluoresc* **10**(4):413–419.
117. Chen Y, Müller JD, Eid JS, Gratton E. 2001. Two-photon fluorescence fluctuation spectroscopy. In *New trends in fluorescence spectroscopy: applications to chemical and life sciences*, pp. 277–296. Ed B Valeur, JC Brochon. Springer, New York.
118. Chirico G, Fumagalli C, Baldini G. 2002. Trapped brownian motion in single- and two-photon excitation fluorescence correlation experiments. *J Phys Chem B* **106**:2508–2519.
119. Heinze KG, Koltermann A, Schwille P. 2000. Simultaneous two-photon excitation of distinct labels for dual-color fluorescence crosscorrelation analysis. *Proc Natl Acad Sci USA* **97**(19):10377–10382.
120. Alexandrakis G, Brown EB, Tong RT, McKee TD, Campbell RB, Boucher Y, Jain RK. 2004. Two-photon fluorescence correlation microscopy reveals the two-phase nature of transport in tumors. *Nature Med* **10**(2):203–207.
121. Clamme JP, Azoulay J, Mely Y. 2003. Monitoring of the formation and dissociation of polyethylenimine/DNA complexes by two photon fluorescence correlation spectroscopy. *Biophys J* **84**:1960–1968.
122. Ruan Q, Chen Y, Gratton E, Glaser M, Mantulin WM. 2002. Cellular characterization of adenylate kinase and its isoform: Two-photon excitation fluorescence imaging and fluorescence correlation spectroscopy. *Biophys J* **83**:3177–3187.
123. Rigler R, Foldes-Papp Z, Franz-Josef MA, Sammet C, Volcker M, Schnetz A. 1998. Fluorescence cross-correlation: a new concept for polymerase chain reaction. *J Biotechnol* **63**:97–109.
124. Schwille P, Franz-Josef MA, Rigler R. 1997. Dual-color fluorescence cross-correlation spectroscopy for multicomponent diffusional analysis in solution. *Biophys J* **72**:1878–1886.
125. Rarbach M, Kettling U, Koltermann A, Eigen M. 2001. Dual-color fluorescence cross-correlation spectroscopy for monitoring the kinetics of enzyme-catalyzed reactions. *Methods* **24**:104–116.
126. Kettling U, Koltermann A, Schwille P, Eigen M. 1998. Real-time enzyme kinetics monitored by dual-color fluorescence cross-correlation spectroscopy. *Proc Natl Acad Sci USA* **95**:1416–1420.
127. Koltermann A, Kettling U, Stephan J, Winkler T, Eigen M. 2001. Dual-color confocal fluorescence spectroscopy and its application in biotechnology. In *Fluorescence correlation spectroscopy: theory and applications*, pp. 187–203. Ed R Rigler, ES Elson. Springer, New York.
128. Bacia K, Schwille P. 2003. A dynamic view of cellular processes by in vivo fluorescence auto- and cross-correlation spectroscopy. *Methods* **29**:74–85.
129. Jankowski T, Janka R. 2001. ConfoCor 2—the second generation of fluorescence correlation microscopes. In *Fluorescence correlation spectroscopy: theory and applications*, pp. 331–345. Ed R Rigler, ES Elson. Springer, New York.

130. Qian H, Elson EL. 2004. Fluorescence correlation spectroscopy with high-order and dual color correlation to probe nonequilibrium steady states. *Proc Natl Acad Sci USA* **101**(9):2828–2833.
131. Schwille P. 2001. Cross-correlation analysis in FCS. In *Fluorescence correlation spectroscopy: theory and applications*, pp. 360–378. Ed R Rigler, ES Elson. Springer, New York.
132. Heinze KG, Koltermann A, Schwille P. 2000. Simultaneous two-photon excitation of distinct labels for dual-color fluorescence crosscorrelation analysis. *Proc Natl Acad Sci USA* **97**(19):10377–10382.
133. Koltermann A, Kettling U, Bieschke J, Winkler T, Eigen M. 1998. Rapid assay processing by integration of dual-color fluorescence cross-correlation spectroscpy: high-throughput screening for enzyme activity. *Proc Natl Acad Sci USA* **95**:1421–1426.
134. Lucas B, Van Rompaey E, De Smedt SC, Demeester J. 2002. Dual-color fluorescence fluctuation spectroscopy to study the complexation between poly-L-lysine and oligonucleotides. *Macromolecules* **35**:8152–8160.
135. Bieschke J, Schwille P. 1998. Aggregation of prion protein investigated by dual-color fluorescence cross-correlation spectroscopy. In *Fluorescence microscopy and fluorescent probes*, Vol. 2, pp. 81–86. Ed J Slavik. Plenum Press, New York.
136. Rippe K. 2000. Simultaneous binding of two DNA duplexes to the NtrC-enhancer complex studied by two-color fluorescence cross-correlation spectroscopy. *Biochemistry* **39**(9):2131–2139.
137. Korn K, Gardellin P, Liao B, Amacker M, Bergstrom A, Bjorkman H, Camacho A, Dorhofer S, Dorre K, Enstrom J, Ericson T, Favez T, Gosch M, Honegger A, Jaccoud S, Lapczyna M, Litborn E, Thyberg P, Winter H, Rigler R. 2003. Gene expression analysis using single molecule detection. *Nucleic Acids Res* **31**(16):e89.
138. Riesner D. 2001. Protein aggregation associated with Alzheimer and prion diseases. In *Fluorescence correlation spectroscopy: theory and applications*, pp. 225–247. Ed R Rigler, ES Elson. Springer, New York.
139. Bieschke J, Schwille P. 1998. Aggregation of prion protein investigated by dual-color fluorescence cross-correlation spectroscopy. In *Fluorescence microscopy and fluorescent probes*, Vol. 2. Ed J Slavik. Plenum Press, New York, 27.
140. Berland KM. 2004. Detection of specific DNA sequences using dual-color two-photon fluorescence correlation spectroscopy. *J Biotechnol* **108**(2):127–136.
141. Winter H, Korn K, Rigler R. 2004. Direct gene expression analysis. *Curr Pharm Biotechnol* **5**(2):191–197.
142. Foldes-Papp Z, Kinjo M, Saito K, Kii H, Takagi T, Tamura M, Costa JM, Birch-Hirschfeld E, Demel U, Thyberg P, Tilz GP. 2003. C677T single nucleotide polymorphisms of the human methylene tetrahydrofolate reductase and specific identification: a novel strategy using two-color cross-correlation fluorescence spectroscopy. *Mol Diagn* **7**(2):99–111.
143. Castro A, Williams JGK. 1997. Single-molecule detection of specific nucleic acid sequences in unamplified genomic DNA. *Anal Chem* **69**:3915–3920.
144. Winkler T, Kettling U, Koltermann A, Eigen M. 1999. Confocal fluorescence coincidence analysis: an approach to ultra high-throughput screening. *Proc Natl Acad Sci USA* **96**:1375–1378.
145. Heinze KG, Rarbach M, Jahnz M, Schwille P. 2002. Two-photon fluorescence coincidence analysis: rapid measurements of enzyme kinetics. *Biophys J* **83**:1671–1681.
146. Li H, Ying L, Green JJ, Balasubramanian S, Klenerman D. 2003. Ultrasensitive coincidence fluorescence detection of single DNA molecules. *Anal Chem* **75**:1664–1670.
147. Weston KD, Dyck M, Tinnefeld P, Müller C, Herten DP, Sauer M. 2002. Measuring the number of independent emitters in single-molecule fluorescence images and trajectories using coincident photons. *Anal Chem* **74**:5342–5349.
148. Ehrenberg M, Rigler R. 1974. Rotational brownian motion and fluorescence intensity fluctuations. *Chem Phys* **4**:390–401.
149. Kask P, Piksarv P, Pooga M, Mets Ü, Lippmaa E. 1989. Separation of the rotational contribution in fluorescence correlation experiments. *Biophys J* **55**:213–220.
150. Ehrenberg M, Rigler R. 1976. Fluorescence correlation spectroscopy applied to rotational diffusion of macromolecules. *Q Rev Biophys* **9**(1):69–81.
151. Mets Ü. 2001. Antibunching and rotational diffusion in FCS. In *Fluorescence correlation spectroscopy: theory and applications*, pp. 346–359. Ed R Rigler, ES Elson. Springer, New York.
152. Kask P, Piksarv P, Mets Ü, Pooga M, Lippmaa E. 1987. Fluorescence correlation spectroscopy in the nanosecond time range: rotational diffusion of bovine carbonic anhydrase B. *Eur Biophys J* **14**:257–261.
153. Davidovich L. 1996. Sub-poissonian processes in quantum optics. *Rev Mod Phys* **68**(1):127–173.
154. Kask P, Piksarv P, Mets Ü. 1985. Fluorescence correlation spectroscopy in the nanosecond time range: photon antibunching in dye fluorescence. *Eur Biophys J* **12**:163–166.
155. Basché Th, Moerner WE. 1992. Photon antibunching in the fluorescence of a single dye molecule trapped in a solid. *Phys Rev Lett* **69**(10):1516–1519.
156. Magde D, Webb WW, Elson EL. 1978. Fluorescence correlation spectroscopy: uniform translation and laminar flow. *Biopolymers* **17**: 361–376.
157. Van Orden A, Keller RA. 1998. Fluorescence correlation spectroscopy for rapid multicomponent analysis in a capillary electrophoresis system. *Anal Chem* **70**(21):4463–4471.
158. Brinkmeier M, Dorre K, Stephan J, Eigen M. 1999. Two-beam cross-correlation: a method to characterize transport phenomena in micrometer-sized structures. *Anal Chem* **71**:609–616.
159. Gosch M, Blom H, Holm J, Heino T, Rigler R. 2000. Hydrodynamic flow profiling in microchannel structures by single molecule fluorescence correlation spectroscopy. *Anal Chem* **72**:3260–3265.
160. Lenne PF, Colombo D, Giovannini H, Rigneault H. 2002. Flow profiles and directionality in microcapillaries measured by fluorescence correlation spectroscopy. *Single Mol* **3**:194–200.
161. Kunst BH, Schots. A, Visser AJWG. 2002. Detection of flowing fluorescent particles in a microcapillary using fluorescence correlation spectroscopy. *Anal Chem* **74**:5350–5357.
162. Dittrich PS, Schwille P. 2002. Spatial two-photon fluorescence cross-correlation spectroscopy for controlling molecular transport in microfluidic structures. *Anal Chem* **74**:4472–4479.

ADDITIONAL REFERENCES TO FCS AND ITS APPLICATIONS

Binding Reactions

Daniel DC, Thompson M, Woodbury NW. 2002. DNA-binding interactions and conformational fluctuations with single molecule fluorescence spectroscopy. *Biophys J* **82**:1654–1666.

Foldes-Papp Z, Demel U, Tilz GP. 2002. Detection of single molecules: solution-phase single-molecule fluorescence correlation spectroscopy as an ultrasensitive, rapid and reliable system for immunological investigation. *J Immunol Methods* **260**:117–124.

Kral T, Langner M, Benes M, Baczynska D, Ugorski M, Hof M. 2002. The application of fluorescence correlation spectroscopy in detecting DNA condensation. *Biophys Chem* **95**:135–144.

Krouglova T, Amayed P, Engelborghs Y, Carlier M-F. 2003. Fluorescence correlation spectroscopy analysis of the dynamics of tubulin interaction with RB3. a stathmin family protein. *FEBS Lett* **546**:365–368.

Nishimura G, Kinjo M. 2004. Systematic error in fluorescence correlation measurements identified by a simple saturation model of fluorescence. *Anal Chem* **76**:1963–1970.

Sanchez SA, Brunet JE, Jameson DM, Lagos R, Monasterio O. 2004. Tubulin equilibrium unfolding followed by time-resolved fluorescence correlation spectroscopy. *Protein Sci* **13**:81–88.

Schubert F, Zettl H, Hafner W, Krauss G, Krausch G. 2003. Comparative thermodynamic analysis of DNA-protein interactions using surface plasmon resonance and fluorescence correlation spectroscopy. *Biochemistry* **42**:10288–10294.

Vercammen J, Maertens G, Gerard M, Clercq ED, Debyser Z, Endelborghs Y. 2002. DNA-induced polymerization of HIV-1 integrase analyzed with fluorescence fluctuation spectroscopy. *J Biol Chem* **277**(41): 38045–38052.

Wolcke J, Reimann M, Klumpp M, Gohler T, Kim E, Deppert W. 2003. Analysis of p53 "latency" and "activation" by fluorescence correlation spectroscopy. *J Biol Chem* **278**(35):32587–32595.

Zettl H, Hafner W, Boker A, Schmalz H, Lanzendorfer M, Muller AHE, Krausch G. 2004. Fluorescence correlation spectroscopy of single dye-labeled polymers in organic solvents. *Macromolecules* **37**:1917–1920.

Classics

Aragón SR, Pecora R. 1976. Fluorescence correlation spectroscopy as a probe of molecular dynamics. *J Chem Phys* **64**:1791–1803.

Koppel DE, Axelrod D, Schléssinger J, Elson EL, Webb WW. 1976. Dynamics of fluorescence marker concentration as a probe of mobility. *Biophys J* **16**:1315–1329.

Data Analysis

Brock R, Hink MA, Jovin TM. 1998. Fluorescence correlation microscopy of cells in the presence of autofluorescence. *Biophys J* **75**:2547–2557.

Koppel DE. 1974. Statistical accuracy in fluorescence correlation spectroscopy. *Phys Rev A* **10**(6):1938–1945.

Meseth U, Wohland T, Rigler R, Vogel H. 1999. Resolution of fluorescence correlation measurements. *Biophys J* **76**:1619–1631.

Nishimura G, Kinjo M. 2004. Systematic error in fluorescence correlation measurements identified by a simple saturation model of fluorescence. *Anal Chem* **76**:1963–1970.

Perroud TD, Huang B, Wallace MI, Zare RN. 2003. Photon counting histogram for one-photon excitation. *ChemPhysChem* **4**:1121–1123.

Saffarian S, Elson EL. 2003. Statistical analysis of fluorescence correlation spectroscopy: the standard deviation and bias. *Biophys J* **84**: 2030–2042.

Sengupta P, Garai K, Balaji J, Periasamy N, Maiti S. 2003. Measuring size distribution in highly heterogeneous systems with fluorescence correlation spectroscopy. *Biophys J* **84**:1977–1984.

Van Craenenbroeck E, Matthys G, Beirlant J, Engelborghs Y. 1999. A statistical analysis of fluorescence correlation data. *J Fluoresc* **9**(4): 325–331.

Wahl M, Gregor I, Patting M, Enderlein J. 2003. Fast calculation of fluorescence correlation data with asynchronous time-correlated single-photon counting. *Opt Express* **11**(26):3583–3591

DNA Applications

Scalettar BA, Hearst JE, Klein MP. 1989. FRAP and FCS studies of self-diffusion and mutual diffusion in entangled DNA solutions. *Macromolecules* **22**:4550–4559.

Lucas B, Remaut K, Braeckmans K, Haustraete J, Smedt SC, Demeester J. 2004. Studying pegylated DNA complexes by dual color fluorescence fluctuation spectroscopy. *Macromolecules* **37**:3832–3840.

Dual Color

Berland KM. 2004. Detection of specific DNA sequences using dual-color two-photon fluorescence correlation spectroscopy. *J Biotechnol* **108**: 127–136.

Koltermann A, Kettling U, Stephan J, Rarbach M, Winkler T, Eigen M. 2001. Applications of dual-color confocal fluorescence spectroscopy in biotechnology. In *Single molecule spectroscopy*. Ed R Rigler, M Orrit, T Basché. Springer, New York.

Image Correlation Spectroscopy

Huang Z, Thompson NL. 1996. Imaging fluorescence correlation spectroscopy: nonuniform IgE distributions on planar membranes. *Biophys J* **70**:2001–2007.

Palmer AG, Thompson NL. 1989. Optical spatial intensity profiles for high order autocorrelation in fluorescence spectroscopy. *Appl Opt* **28**(6): 1214–1220.

Petersen NO, Brown C, Kaminski A, Rocheleau J, Srivastava M, Wiseman PW. 1998. Analysis of membrane protein cluster densities and sizes in situ by image correlation spectroscopy. *Faraday Discuss* **111**: 289–305.

Petersen NO, Hoddelius PL, Wiseman PW, Seger O, Magnusson KE. 1993. Quantitation of membrane receptor distributions by image correlation spectroscopy: concept and application. *Biophys J* **65**:1135–1146.

Vanden Broek W, Huang Z, Thompson NL. 1999. High-order autocorrelation with imaging fluorescence correlation spectroscopy: application to IgE on supported planar membranes. *J Fluoresc* **9**(4):313–324.

Wiseman PW, Petersen NO. 1999. Image correlation spectroscopy: optimization for ultrasensitive detection of preexisting platelet-derived

growth factor-β receptor oligomers on intact cells. *Biophys J* **76**: 963–977.

Instrumentation

Lamb DC, Schenk A, Rocker C, Scalfi-Happ C, Nienhaus GU. 2000. Sensitivity enhancement in fluorescence correlation spectroscopy of multiple species using time-gated detection. *Biophys J* **79**:1129–1138.

Mukhopadhyay A, Zhao J, Bae SC, Granick S. 2003. An integrated platform for surface forces measurements and fluorescence correlation spectroscopy. *Rev Sci Instrum* **74**(6):3067–3072.

Ruckstuhl T, Seeger S. 2004. Attoliter detection volumes by confocal total-internal-reflection fluorescence microscopy. *Opt Lett* **29**(6):569–571.

Sorscher SM, Klein MP. 1980. Profile of a focused collimated laser beam near the focal minimum characterized by fluorescence correlation spectroscopy. *Rev Sci Instrum* **51**(1):98–102.

Intracellular

Braun K, Peschke P, Pipkorn R, Lampel S, Wachsmuth M, Waldeck W, Friedrich E, Debus J. 2002. A biological transporter for the delivery of peptide nucleic acids (PNAs) to the nuclear compartment of living cells. *J Mol Biol* **318**:237–343.

Brock R, Jovin TM. 1998. Fluorescence correlation microscopy (FCM)–fluorescence correlation spectroscopy (FCS) taken into the cell. *Cell Mol Biol* **44**(5):847–856.

Brock R, Vamosi G, Vereb G, Jovin TM. 1999. Rapid characterization of green fluorescent protein fusion proteins on the molecular and cellular level by fluorescence correlation spectroscopy. *Proc Natl Acad Sci USA* **96**:10123–10128.

Politz JC, Browne ES, Wolf DE, Pederson T. 1998. Intranuclear diffusion and hybridization state of oligonucleotides measured by fluorescence correlation spectroscopy. *Proc Natl Acad Sci USA* **95**:6043–6048.

Wachsmith M, Weidemann T, Muller G, Hoffmann-Rohrer UW, Knoch TA, Waldeck W, Langowski J. 2003. Analyzing intracellular binding and diffusion with continuous fluorescence photobleaching. *Biophys J* **84**:3353–3363.

Wang Z, Shah JV, Chen Z, Sun C, Berns MW. 2004. Fluorescence correlation spectroscopy investigation of a GFP mutant-enhanced cyan fluorescent protein and its tubulin fusion in living cells with two-photon excitation. *J Biomed Opt* **9**(2):395–403.

Kinetics

Bismuto E, Gratton E, Lamb DC. 2001. Dynamics of ANS binding to tuna apomyoglobin measured with fluorescence correlation spectroscopy. *Biophys J* **81**:3510–3521.

Rigler R, Edman L, Földes-Papp Z, Wennmalm S. 2001. Fluorescence correlation spectroscopy in single-molecule analysis: enzymatic catalysis at the single molecule level in *Single molecule spectroscopy*. Ed R Rigler, M Orrit, T Basché. Springer, New York.

Widengren J, Dapprich J, Rigler R. 1997. Fast interactions between Rh6G and dGtTP in water studied by fluorescence correlation spectroscopy. *Chem Phys* **216**:417–426.

Membranes

Briddon SJ, Middleton RJ, Yates AS, George MW, Kellam B, Hill SJ. 2004. Application of fluorescence correlation spectroscopy to the measurement of agonist binding to a G-protein coupled receptor at the single cell level. *Faraday Discuss* **126**:197–207.

Fahey PF, Koppel DE, Barak LS, Wolf DE, Elson EL, Webb WW. 1977. Lateral diffusion in planar lipid bilayers. *Science* **195**:305–306.

Fahey PF, Webb WW. 1978. Lateral diffusion in phospholipid bilayer membranes and multilamellar liquid crystals. *Biochemistry* **17**: 3046–3053.

Palmer III AG, Thompson NL. 1989. Fluorescence correlation spectroscopy for detecting submicroscopic clusters of fluorescent molecules in membranes. *Chem Phys Lipids* **50**:253–270.

Moments and Higher Orders

Palmer III AG, Thompson NL. 1987. Molecular aggregation characterized by high order autocorrelation in fluorescence correlation spectroscopy. *Biophys J* **52**:257–270.

Palmer III AG, Thompson NL. 1989. Optical spatial intensity profiles for high-order autocorrelation in fluorescence spectroscopy. *Appl Opt* **28**(6):1214–1220.

Palmer III AG, Thompson NL. 1989. High-order fluorescence fluctuation analysis of model protein clusters. *Proc Natl Acad Sci USA* **86**: 6148–6152.

Palmer III AG, Thompson NL. 1989. Intensity dependence of high-order autocorrelation functions in fluorescence correlation spectroscopy. *Rev Sci Instrum* **60**(4):624–633.

Qian H, Elson EL. 2004. Fluorescence correlation spectroscopy with high-order and dual-color correlation to probe nonequilibrium steady states. *Proc Natl Acad Sci USA* **101**(9):2828–2833.

Qian H, Elson EL. 1990. On the analysis of high order moments of fluorescence fluctuations. *Biophys J* **57**:375–380.

Novel Methods

Eggeling C, Berger S, Brand L, Fries JR, Schaffer J, Volkmer A, Seidel CAM. 2001. Data registration and selective single-molecule analysis using multi-parameter fluorescence detection. *J Biotechnol* **86**:163–180.

Hansen RL, Zhu XR, Harris JM. 1998. Fluorescence correlation spectroscopy with patterned photoexcitation for measuring solution diffusion coefficients of robust fluorophores. *Anal Chem* **70**:1281–1287.

Lenne P-F, Etienne E, Rigneault H. 2003. Subwavelength patterns and high detection efficiency in fluorescence correlation spectroscopy using photonic structures. *Appl Phys Lett* **80**(22):4106–4108.

Levene MJ, Korlach J, Turner SW, Foquet M, Craighead HG, Webb WW. 2003. Zero-mode waveguides for single-molecule analysis at high concentrations. *Science* **299**:682–686.

Muller JD, Gratton E. 2003. High-pressure fluorescence spectroscopy. *Biophys J* **85**:2711–2719.

Rigneault H, Lenne P-F. 2003. Fluorescence correlation spectroscopy on a mirror. *J Opt Soc Am B* **20**(10):2203–2214.

Sonehara T, Kojima K, Irie T. 2002. Fluorescence correlation spectroscopy excited with a stationary interference pattern for capillary electrophoresis. *Anal Chem* **74**:5121–5131.

Photon Counting Histograms

Chirico G, Olivini F, Beretta S. 2000. Fluorescence excitation volume in two-photon microscopy by autocorrelation spectroscopy and photon counting histogram. *Appl Spectrosc* **54**(7):1084–1090.

Hillesheim LN, Müller JD. 2003. The photon counting histogram in fluorescence fluctuation spectroscopy with non-ideal photodetectors. *Biophys J* **85**:1948–1958.

Proteins and FCS

Chattopadhyay K, Saffarian S, Elson EL, Frieden C. 2002. Measurement of microsecond dynamic motion in the intestinal fatty acid binding protein by using fluorescence correlation spectroscopy. *Proc Natl Acad Sci USA* **99**(22):14171–14176.

Lippitz M, Erker W, Decker H, Van Holde KE, Basché T. 2002. Two-photon excitation microscopy of tryptophan-containing proteins. *Proc Natl Acad Sci USA* **99**:2772–2777.

Polymers and FCS

Sukhishvili SA, Chen Y, Müller JD, Gratton E, Schweizer KS, Granick S. 2000. Diffusion of a polymer "pancake." *Nature* **406**:146.

Resonance Energy Transfer

Hom EFY, Verkman AS. 2002. Analysis of coupled bimolecular reaction kinetics and diffusion by two-color fluorescence correlation spectroscopy: enhanced resolution of kinetics by resonance energy transfer. *Biophys J* **83**:533–545.

Katiliene Z, Katilius E, Woodbury NW. 2003. Single molecule detection of DNA looping by *Ngo*MIV restriction endonuclease. *Biophys J* **84**: 4053–4061.

Margittai M, Widengren J, Schweinberger E, Schroder GF, Felekyan S, Haustein E, Konig M, Fasshauer D, Grubmuller H, Jahn R, Seidel CAM. 2003. Single-molecule fluorescence resonance energy transfer reveals a dynamic equilibrium between closed and open conformations of syntaxin. *Proc Natl Acad Sci USA* **100**(26):15516–15521.

Talaga DS, Leung Lau W, Roder H, Tang J, Jia Y, DeGrado WF, Hochstrasser RM. 2000. Dynamics and folding of single two-stranded coiled-coil peptides studied by fluorescent energy transfer confocal microscopy. *Proc Natl Acad Sci USA* **97**(24):13021–13026.

Widengren J, Schweinberger E, Berger S, Seidel CAM. 2001. Two new concepts to measure fluorescence resonance energy transfer via fluorescence correlation spectroscopy: theory and experimental realizations. *J Phys Chem A* **105**:6851–6866.

Scanning FCS

Koppel DE, Morgan F, Cowan AE, Carson JH. 1994. Scanning concentration correlation spectroscopy using the confocal laser microscope. *Biophys J* **66**:502–507.

Palmer III AG, Thompson NL. 1987. Theory of sample translation in fluorescence correlation spectroscopy. *Biophys J* **51**:339–343.

Petersen NO. 1986. Scanning fluorescence correlation spectroscopy: theory and simulation of aggregation measurements. *Biophys J* **49**:809–815.

Petersen NO, Johnson DC, Schlesinger MJ. 1986. Scanning fluorescence correlation spectroscopy: application to virus glycoprotein aggregation. *Biophys J* **49**:817–820.

Reviews

Valeur B, Brochon J-C., ed. 2001. *New trends in fluorescence spectroscopy: applications to chemical and life sciences*. Springer, New York.

Webb WW. 2001. Fluorescence correlation spectroscopy: inception, biophysical experimentations, and prospectus. *Appl Opt* **40**(24):3969–3983.

Theory of FCS

Edman L. 2000. Theory of fluorescence correlation spectroscopy on single molecules. *J Phys Chem A* **104**:6165–6170.

Enderlein J. 1996. Path integral approach to fluorescence correlation experiments. *Phys Lett A* **221**:427–433.

Enderlein J, Gregor I, Patra D, Fitter J. 2004. Art and artifacts of fluorescence correlation spectroscopy. *Curr Pharm Biotechnol* **5**:155–161.

Generich A, Schild D. 2000. Fluorescence correlation spectroscopy in small cytosolic compartments depends critically on the diffusion model used. *Biophys J* **79**:3294–3306.

Hess ST, Webb WW. 2002. Focal volume optics and experimental artifacts in confocal fluorescence correlation spectroscopy. *Biophys J* **83**: 2300–2317.

Hoshikawa H, Asai H. 1985. On the rotational Brownian motion of a bacterial idle motor, II: theory of fluorescence correlation spectroscopy. *Biophys Chem* **22**:167–172.

Qian H, Elson EL. 1991. Analysis of confocal laser-microscopy optics for 3-D fluorescence correlation spectroscopy. *Appl Opt* **30**(10): 1185–1195.

Scalettar BA, Klein MP, Hearst JE. 1987. A theoretical study of the effects of driven motion on rotational correlations of biological systems. *Biopolymers* **26**:1287–1299.

Starchev K, Zhang J, Buffle J. 1998. Applications of fluorescence correlation spectroscopy-particle size effect. *J Colloid Interface Sci* **203**: 189–196.

Total Internal Reflection

Thompson NL, Axelrod D. 1983. Immunoglobulin surface-binding kinetics studied by total internal reflection with fluorescence correlation spectroscopy. *Biophys J* **43**:103–114.

Thompson NL, Pearce KH, Hsieh HV. 1993. Total internal reflection fluorescence microscopy: application to substrate-supported planar membranes. *Eur Biophys J* 22:367–378.

Thompson NL, Lagerholm BC. 1997. Total internal reflection fluorescence: applications in cellular biophysics. *Curr Opin Biotechnol* **8**: 58–64.

PROBLEMS

P24.1. Figure 24.8 shows autocorrelation curves for several concentrations of R6G. Assume these concentrations are correct. What is the effective volume (V_{eff}) of the sample? Assume the ratio for the ellipsoidal volume is $\mu/s = 4.0$. What are the dimensions of the ellipsoid?

P24.2. Figure 24.10 shows the autocorrelation function for labeled α-lactalbumin (14,000 daltons) in the absence and presence of GroEL (840,000 daltons). Is the change in diffusion time consistent with complete binding of α-lactalbumin to GroEL?

P24.3. Figure 24.21 shows autocorrelation functions for GUVs composed of DLPC or DLPC/DPFC (0.2/0.8). Assume the laser beam diameter is 1 μm. Using the same diffusion coefficient, calculate the time it takes a Dil-C_{20} molecule to diffuse 10 μm. Suppose the beam diameter is increased to 2 μm. How long does it take the molecule to diffuse 10 μm?

P24.4. Figure 24.32 shows a correlation function for the opening and closing of a molecular beacon. Assume you have access to a steady-state fluorometer with control of the sample temperature. Suggest a way to separately determine the values of k_1 and k_2.

P24.5. Figure 24.33 shows a typical configuration for FCS using TIR. Suppose you wanted to measure diffusion coefficients near the interface, and the illuminated spot had a diameter of 5.0 μm. Calculate the volume of the observed solution assuming $d = 100$ nm. What concentration of fluorophore is needed to obtain approximately 10 fluorophores in the volume?

Assume the volume contains a single phospholipid bilayer that contains all the probe molecules. What fraction of the lipids need to be labeled to obtain 10 fluorophores in the volume? The area occupied by a single phospholipid molecule is about 70 Å^2.

P24.6. Figure 24.50 shows autocorrelation curves for tubulin with cryptophycin as the sample was diluted. Explain how these data can be used to determine if the complex dissociates upon dilution. Assume all the tubulin substrates contain the TMR label.

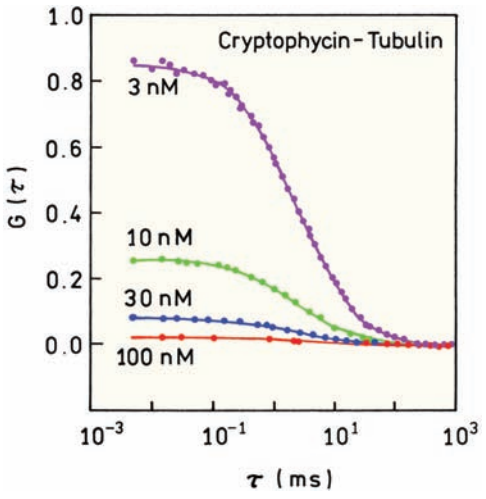

Figure 24.50. Effect of increasing concentrations of cryptophycin on labeled tubulin dimers. Revised and reprinted with permission from [38]. Copyright © 2003, American Chemical Society.